DETERMINING DURATIONS OF TRANSIENT, TRANSITION, AND BOUNDARY-DOMINATED FLOW REGIMES FOR RECTANGULAR-SHAPED DRAINAGE AREAS

A Thesis

by

HAFIZ MUSTAFA UD DIN SHEIKH

Submitted to the Office of Graduate and Professional Studies of
Texas A&M University
in partial fulfillment of the requirements for the degree of

MASTER OF SCIENCE

Chair of Committee,   William John Lee
Committee Members, Thomas Blasingame
                                  George Voneiff
Head of Department,   Jeff Spath

December 2020

Major Subject: Petroleum Engineering

ABSTRACT

The primary objective of this work is to investigate the times at the end of transient flow period and the start of boundary dominated flow using Bourdet pressure derivative for various combinations of well types and reservoir geometries and compare them with existing definitions of the radius and depth on investigation for constant rate production and constant pressure production cases. Empirical methods are applied on synthetic production data obtained from numerical simulator to estimate these times. The scope of this work includes vertical wells and horizontal wells with vertical fractures in various rectangular shaped drainage areas.

This work also presents analytically derived shape factors which are used in pseudo steady state equation for horizontal wells with vertical fractures in rectangular-shaped drainage areas. Shape factors previously presented by other authors were used to validate the method and apply it to some new drainage area configurations.

To account for noisy production data which leads to uninterpretable pressure derivatives, an outlier's detection method i.e. Angle Based Outlier Detection (or ABOD) has been evaluated. Although this method was proposed by Kriegel et al. (2008) for outliers' detection in high-dimensional data, it has been found to be equally useful in our case of two-dimensional production data. This method has the advantage of having no user-defined parameters i.e. it is unaffected by the personal bias and it provides justification for objective identification and removal of outliers from production data based on divergence of angles that a point makes with other surrounding points in the data. Synthetic production data with random addition of gaussian noise is used to evaluate this method based on mean absolute error (MAE) and true negative, true positive, false positive and false negative responses.

DEDICATION

I dedicate this work to my family.

ACKNOWLEDGEMENTS

I am thankful to Dr. W. J. Lee, the chair of my graduate committee, for his continuous guidance and untiring support throughout the course of this work. This work would not have been possible without his supervision and dedication. I am also thankful to Dr. Thomas Blasingame and Prof. George Voneiff for serving as my graduate committee members and providing their due and timely support whenever requested. I am also thankful to Dr. J. P. Spivey for his support and providing a kick-start for this work.

I am also thankful to The Fulbright Program, Institute of International Education (IIE) and United States Educational Foundation in Pakistan (USEFP) for providing me this excellent educational opportunity and exceptional experience to do my master's degree from the United States and for providing administrative and financial support during my stay in the US.

Above all, I am thankful to GOD for giving me strength to complete this work and my family for their love, support and prayers.

TABLE OF CONTENTS

LIST OF FIGURES

x

LIST OF TABLES

CHAPTER I

INTRODUCTION

1.1. Background

Pressure transient tests have been an important well testing technique in petroleum engineering. Their applications are widespread from estimating wellbore skin and reservoir permeability to reservoir pressure and in-place volumes. Different techniques are used for interpretation of pressure data obtained from well tests which includes methods suggested by Horner (1951), Gringarten et al. (1979) and Bourdet (1989). Bourdet's pressure derivative when plotted against logarithmic time on log-log plot provides useful information regarding the existing flow regime in the reservoir. In radial flow systems, pressure derivatives follow a horizontal line. Similarly, a half-slope line can be seen in case of linear flow in the reservoir whereas boundary dominated flow can be identified by a unit slope line on Bourdet's pressure derivative plot. These diagnostic characteristics of the pressure derivative plot are discussed in detail below.

Transient radial flow is typically observed in vertical wells fully penetrating into the reservoir. During transient radial flow, the pressure response at the wellbore is a linear function of the logarithm of time. It can be represented in dimensionless units as:

$$p_{wD} = \frac{1}{2}[\ln(1.781t_D) + s] \tag{I.1}$$

The derivative of equation (I.1) with respect to logarithmic time can be obtained as:

$$\frac{\partial p_{wD}}{\partial \ln t_D} = t_D \frac{\partial p_{wD}}{\partial t_D} \qquad (I.2)$$

Or,

$$\frac{\partial p_{wD}}{\partial \ln t_D} = t_D \frac{\partial \left(\frac{1}{2}[\ln(t_D) + 0.809 + 2s]\right)}{\partial t_D} \qquad (I.3)$$

Or,

$$\frac{\partial p_{wD}}{\partial \ln t_D} = \frac{1}{2} \qquad (I.4)$$

Hence, during transient radial flow, pressure derivative when plotted in dimensionless units will fall on a horizontal line at 0.5 on a log-log plot.

Similarly, transient linear flow is typically observed in horizontal wells with infinite conductivity vertical fractures. During transient linear flow, pressure at the wellbore is a linear function of the square root of time. In dimensionless units, it can be represented as:

$$p_{wD} = 2\sqrt{\frac{t_D}{\pi}} \qquad (I.5)$$

Equation (I.5) can be differentiated with respect to logarithm of time as:

$$\frac{\partial p_{wD}}{\partial \ln t_D} = t_D \frac{\partial p_{wD}}{\partial t_D} \qquad (I.6)$$

Or,

$$\frac{\partial p_{wD}}{\partial \ln t_D} = t_D \frac{\partial \left(2\sqrt{\frac{t_D}{\pi}}\right)}{\partial t_D} \tag{I.7}$$

Or,

$$\frac{\partial p_{wD}}{\partial \ln t_D} = \left(\frac{t_D}{\pi}\right)^{1/2} \tag{I.8}$$

Therefore, linear flow can be recognized by a straight line of half-slope on the pressure derivative plot.

When pressure transients reach the reservoir boundary, we start seeing boundary effects on the wellbore pressure response. For a well producing at constant rate production in a bounded reservoir, these boundary effects end up into pseudo steady flow. The dimensionless form of the pseudo steady state equation can be defined as:

$$p_{wD} = 2\pi t_D + \frac{1}{2} \ln \frac{4A_d}{e^\gamma C_A r_W^2} \tag{I.9}$$

where, $\gamma = 0.5772156649 \dots$ is the Euler's constant, A_d is the area of arbitrary-shaped reservoir and C_A is the shape factor of the reservoir. It can be seen from equation (I.9) that pressure at the wellbore is a linear function of time during pseudo steady state flow. Equation (I.9) can differentiated with respect to logarithm of time as:

$$\frac{\partial p_{wD}}{\partial \ln t_D} = t_D \frac{\partial p_{wD}}{\partial t_D} \tag{I.10}$$

Or,

3

$$\frac{\partial p_{wD}}{\partial \ln t_D} = t_D \frac{\partial \left(2\pi t_D + \frac{1}{2}\ln \frac{4A_d}{e^{\gamma}C_A r_W^2}\right)}{\partial t_D} \tag{I.11}$$

Or,

$$\frac{\partial p_{wD}}{\partial \ln t_D} = t_D \tag{I.12}$$

Equation (I.12) shows that during pseudo steady state flow, the pressure derivative will fall on a unit slope line on the log-log plot.

These characteristics of the pressure derivative plot can be used to identify times at the end of the transient flow regime and the start of boundary dominated flow regime. The primary goal of this work is to estimate these times from pressure derivative plots using empirical methods and compare them with the time required for a pressure transient to reach the boundary obtained from existing definitions of radius and depth of investigation. A summary of the cases considered for this exercise can be found in CHAPTER V and relevant derivative plots in APPENDIX C.

To establish the existing definitions of the radius and depth of investigation, we have rederived these equations from instantaneous source solutions for radial, linear and spherical sources. The resulting expressions were found to be identical to those derived from the solutions of the diffusivity equation. The details of these derivations can be found in CHAPTER III.

Shape factor, C_A, as it appears in equation (I.9) was first presented by Dietz (1965) for different shapes of reservoir boundaries. Later, Earlougher (1977) recalculated these shape factors and included some more shapes considering flow into vertical fractures. However, these shape factors are limited to square-shaped bounded reservoirs. In this work, we have presented shape factors for wells with vertical fractures centered in rectangular shaped reservoirs of different configurations. The method of images proposed by Earlougher (1968) to produce the pressure response of wells in rectangular bounded reservoirs to calculate shape factors from equation (I.9). Details of this work can be found in CHAPTER IV and the relevant figures in APPENDIX B.

Noise in production data cause many problems in their analyses. In the case of production modeling and forecasts, presence of outliers can cause false fitting of the decline models and can result in underestimation or overestimation of reserves. On the other hand, analysis of pressure data using Bourdet's pressure derivative also suffer due to presence of noise in the data. The smoothening parameter, if used inappropriately for very noisy data, can disrupt the signal to noise ratio which can lead to misinterpretation of the curve. Therefore, it is necessary to *clean* data before using Bourdet's algorithm. In this work, we have evaluated an outlier detection method which is lesser known to petroleum industry i.e. Angle Based Outlier Detection (ABOD). Although this method was presented by Kriegel et al. (2008) for objective identification of outliers in high-dimensional data, we have used this method for our case of two-dimensional production data and have found the results to be quite promising. The basic idea behind this method is that, for a point to be considered as an outlier, the angles it will make with its neighboring points will have a

greater variance than those points which are theoretically inliers. To accomplish this in a systematic manner, an angle-based outlier factor is calculated for each point which is used to categorize data point in increasing order of their *outlierness*. Details of the steps of this method and the results obtained are summarized in CHAPTER VI.

1.2. Objectives

Objectives for this work can be summarized as follows:

1. To derive expressions for radius or depth of investigation for radial, linear and spherical flow using instantaneous source functions.
2. To estimate shape factors for the pseudo steady state equation of linear flow for different configurations of rectangular-shaped drainage areas.
3. To estimate times at the end of transient flow and the start of boundary dominated flow for vertical and horizontal wells with vertical fractures centered in rectangular-shaped drainage areas and compare them with the existing definitions of radius or depth of investigation.
4. To estimate and compare corresponding volumes of investigation using Spivey's method at these times.
5. To evaluate the applicability of Angle Based Outlier Detection (ABOD) method for the detection and removal of outliers from noisy pressure derivatives.

CHAPTER II

LITERATURE REVIEW

2.1. Radius of Investigation

The radius of investigation or depth of investigation is one of the most used yet least understood terms in the petroleum industry. Estimation of reservoir parameters from pressure transient tests often requires information of the reservoir volume that has been tested in the test. This is commonly done by incorporating the concept of the radius of investigation for radial flow or depth of investigation for linear flow.

Various definitions for the radius of investigation has been proposed in the past. Van Poolen (1964), Daungkaew et al (2000), and Kuchuk (2009) have provided a comprehensive summary of these definitions. The most common mathematical form presented in these works, in dimensionless form, is shown as:

$$r_D = A\sqrt{t_D} \qquad\qquad (\text{II.1})$$

where $r_D = r/r_w$ (dimensionless radius of investigation), $t_D = kt/\phi\mu c_t r_w^2$ (dimensionless time) and A is constant.

The coefficient of the equation (II.16), A, depends on the definition of the radius of investigation we use. Jones (1962) defined radius of drainage as the point at which pressure drawdown is 1% of that at the wellbore and used field data from reservoir limit test on gas wells to estimate the value of $A = 4$. Tek et al. (1957) defined the radius of

7

investigation as the point in the reservoir where 1% of the fluid is flowing compared with that flowing at the wellbore and arrived at a value of A=4.29.

Park Jones (1956, 1957) defined a parameter Y as the rate of decrease in bottomhole flowing pressure with time in $psi/days$, divided by the producing rate in reservoir B/D, or:

$$Y = \frac{1}{qB}\left|\frac{dp_w}{dt}\right| \qquad \text{(II.2)}$$

Jones used this function in conjunction with the coefficient of gas expansion to estimate explored and proved gas in-place. This Y function is inversely proportional to the investigated pore volume and gives negative unit slope for infinite-acting radial systems when plotted against time (in days) on a log-log scale ($Y_{infinite}$), while a horizontal line on the plot indicates stabilized flow (Y_{finte}). Van Poolen noted that, by assuming $Y_{infinite} = Y_{finite}$, the radius of investigation for radial flow can be defined as:

$$r_i = 2\sqrt{\frac{kt}{\phi \mu c_t}} \qquad \text{(II.3)}$$

which is the conventional form of the radius of investigation. Later, this expression was also presented by ERCB (1975), Lee (1982), Stewart (2011), and Spivey and Lee (2013) using various approaches.

Lee (1982) discussed the concepts of radius of investigation and the time required to reach stabilized flow. He defined the radius of investigation as a point in the reservoir where

8

pressure disturbance is maximum and derived its expression by differentiating the line source solution of the diffusivity equation and equating it with zero. Kutasov and Hejri (1984) presented an expression for drainage area of well producing at constant bottom hole pressure in an infinite acting reservoir and a relationship between dimensionless cumulative production and dimensionless time.

Oliver (1990) proposed a solution to radially composite reservoirs with small permeability variations in the reservoir which included a weighting function for permeability and a dimensionless arbitrary permeability distribution function. He used his solution to define the radius of investigation as a point where the weighting function becomes so small the permeabilities at greater distances do not contribute to the slope of semi-log plot. Mathematically, permeability beyond dimensionless radius, $r_D = 2.34 \sqrt{t_D}$ cannot be detected because it is excluded from the averaging. Economides (1992) discussed the effect of boundaries on pressure derivative plot in nonradial geometries and presented analytical methods to estimate the radius of investigation for those different boundaries. Sobbi (1994) presented mathematical form for radius of investigation in dual porosity reservoirs. He discussed the times at which properties of fractures or the whole system should be used, and he compared the behavior of radius of investigation propagation for different values of interporosity flow coefficient (λ) and storativity ratio (ω).

Wattenbarger (1998) presented typical linear flow behavior in multi-fractured wells in tight wells. He presented solutions to constant rate and constant pressure flow problems. He extended his solutions to depth of investigation calculation using the time at which

9

deviation of the production trend become observable from ½ slope line indicating linear flow. He then used the depth of investigation to estimate pore volume and hydrocarbon in place.

Aguilera (2006) presented derivations for radius of investigation and pore volume calculation for radial and linear flow geometries in homogenous and dual porosity reservoirs. He used Y function developed by Jones (1962) to support his calculations and identify flow regimes by plotting it against flow time. Also, the main assumption in his work is that there is a sudden change in the flow behavior of reservoir from infinite acting flow to finite acting flow without any consideration of transition period. Drainage radius equations were also presented for radial and linear geometries by considering time as stabilization time in radius of investigation equations.

Hseih et al. (2007) studied the relationship between dimensionless radius of investigation and dimensionless time using analytical and numerical methods. They used dimensionless solution of the diffusivity equation for infinite acting homogeneous radial flow system and used different values of dimensionless pressure (minimum pressure drop) as a criterion to establish linear relationship between dimensionless radius of investigation and dimensionless time.

Anderson and Mattar (2007) discussed problems related to use of pseudo time in gas reservoirs when reservoir is in transient flow. These problems arise by use of average pressure of total reservoir area when the reservoir is still in transient phase for calculation of pseudo time and, using bulk gas properties at a single value of average reservoir

pressure in the presence of large pressure gradients in the system. The authors have proposed a solution to the first problem, that the average pressure of the area of influence only (instead of total reservoir area) can be used for gas properties and pseudo time calculations. To delineate the area of influence, the authors have mentioned two methods. The first one is by calculating pressure distribution in the reservoir and define the area of influence based on some minimum percentage of pressure drop. This method, although analytically correct, would require significant computational time. Alternatively, well established concept of radius of investigation can be used to delineate the area of influence which is independent of the reservoir geometry and the pressure drop at the wellbore. This area is generally πr^2 in an unbounded system, but in the presence of one or more boundaries, the circular area of investigation can be transformed into rectangular area of investigation with similar results. Assuming the dominant geometry factor and accordingly approximating the area of influence can further simplify the problem.

Datta-Gupta (2011) built on the definition of radius of investigation presented by Lee (1982) to propose a generalized method for computation of radius of investigation using fast marching methods (FMM). This technique is suitable for any arbitrary reservoir and assumes an analogy between a propagating pressure front and propagating wave front i.e. Eikonal equation.

Xie et al (2015) presented a method for estimating radius of investigation in spatially heterogeneous and fractured unconventional reservoirs. They presented the asymptotic solution to the diffusivity equation considering the spatial heterogeneity and used it

calculate the propagation front. They solved the pressure front equation using front tracking methods called fast marching methods (FMM). They validated their approach for homogeneous reservoirs by comparing the FMM with the analytical solution given by Lee (1982).

Tabatabaie et al. (2017) discussed the application of the concept of radius of investigation and the inconsistencies observed when this concept is extended to linear flow systems. Specifically stating, when the concept of radius of investigation is used to estimate distance to the boundaries in unconventional wells by observing from the production data of a well, significant depletion has already occurred at the boundary. To explain this, he introduced the concepts of time of arrival (i.e. time at which the pressure diffusion reaches the boundary) and time of detection (i.e. the time at which the effect of reservoir boundary is observed at the wellbore). In case of radial flow – constant rate condition, there is no significant difference between time of arrival of the pressure perturbation at the boundary and its time of detection at the wellbore. Whereas, for linear flow – constant rate production case, the time of detection of the boundary is almost four times the time of arrival. However, time of arrival for linear flow is much smaller when compared with that of radial flow. Equations for time of arrival can be used for estimation of distance of investigation whereas distance to the boundaries can be estimated using time of detection equations.

Ravikumar (2018) presented proof of mathematical expressions earlier presented by Wattenbarger (1998) for depth of investigation for multi-fractured horizontal wells

depicting linear flow behavior using maximum pressure disturbance method. He presented solutions for different flow conditions including constant rate, constant bottom hole pressure, linear bottom hole pressure and logarithmic bottom hole pressure. Ramakrishnan et al. (2020) discussed the effects of gauge resolution, background noise and the model on radius of investigation and proposed that the radius of investigation can only be defined with the specification of model description and pressure transducer characterization.

However, all these definitions are based on analytical models that assume radial flow of fluid into the wellbore. Identification of flow regimes and fluid flow geometry is difficult especially at the early stages of production. Moreover, the wrong identification of flow geometry can also lead to erroneous results. For wider applicability of the concept to linear and spherical flow geometries, we need to define depth of investigation for linear flow and radius of investigation for spherical flow separately.

Spivey (2020) has recently proposed the concept of investigated pore volume. This concept is simple and general and does not require any specific flow regimes for its application. The concept is based on fundamental properties common to all constant-terminal-rate solutions to the diffusivity equation. The investigated pore volume, V_{pi}, is defined as the minimum reservoir volume necessary to provide sufficient pressure support to produce the observed rate of change of sand face pressure as a function of time. Equation (II.4) represents the volume of investigation expression for a constant terminal rate flow problem where porosity and compressibility are assumed to be constant.

$$V_{bi} = \frac{0.234qB_i}{\phi c_t \left| \frac{dp_w}{dt} \right|}$$
(II.4)

2.2. Analytical Solutions to Bounded Systems

Matthews, Brons and Hazebroek (1954) presented a method based on the principle of superposition to estimate average reservoir pressure in bounded reservoirs. In their work, the authors presented a generalized approach that can be used to estimate pressure for any polygon-shaped bounded reservoir. Their focus was to present correction in pressure obtained by extrapolating straight-line part of the shut-in pressure versus $log[\Delta t/(t + \Delta t)]$, but their generalized approach to incorporate the effect of boundaries using superposition can also be applied for drawdown tests.

Earlougher et al. (1968) used the method of superposition presented by Matthews, Brons and Hazebroek (1954) to estimate pressure distribution within bounded rectangular-shaped reservoirs. He calculated dimensionless pressure drop versus dimensionless time values for a bounded square-shaped reservoir by using the method of images to include boundary effects. For this, he assumed an infinite number of image wells surrounding the original well centered on the grid as shown in Fig. 2.2.1 and used equation (II.5) to calculate dimensionless pressure drop at specific locations throughout the reservoir. He suggested that these values can be used to develop solutions of a rectangular shaped reservoir of any shape.

$$p_D = -\frac{1}{2}\left[\ln\left[\frac{r_w^2}{4A_d t_{DA}}\right] + 0.5772 + \sum_{i=2}^{\infty} \text{Ei}\left[-\frac{a_{iD}^2}{4t_{DA}}\right]\right] \quad \text{(II.5)}$$

Here,

$$p_D = \frac{2\pi kh(p_i - p)}{q\mu} \quad \text{(II.6)}$$

$$t_{DA} = \frac{kt}{\phi\mu c_t A_d} \quad \text{(II.7)}$$

$$r_D = r/\sqrt{A_d} \quad \text{(II.8)}$$

In his example, he considered a well in the center of a rectangular reservoir with sides in a ratio of 2:1. He then modified the shape of the original square grid by overlaying a copy of the same grid with the actual well moved from its initial position of $(0,0)$ to the new location of $(1,0)$. This resulted in an infinite array of wells with rectangular drainage areas in a 2:1 ratio as shown in Fig. 2.2.2. The magnitude of the area was, however, half of the original square-shaped area. He then used tabulated values of the dimensionless time and dimensionless pressures from the square-shaped reservoir to calculate pressure solutions for the 2:1 rectangular-shaped reservoir. From the square drainage area solution, he added dimensionless pressure values at the previous location of the original well i.e. $(0,0)$, and the new location of the well in the old grid system i.e. $(1,0)$ to calculate wellbore pressure of the well centered in a 2:1 rectangle. However, the location of the well in the new grid of 2:1 is $(0,0)$.

Although he presented the example for a bounded reservoir, this method can also be extended for constant pressure boundary reservoirs by assuming alternate injection and production image wells. He also showed that the dimensionless pressure and dimensionless time values he presented can be used to obtain shape factors for the pseudo-steady-state flow condition of various bounded reservoirs.

Although this method applies to vertical wells in rectangular bounded reservoirs, it can also be used to generate solutions of elongated rectangular reservoirs which depict flow behavior similar to that of linear flow from fractures.
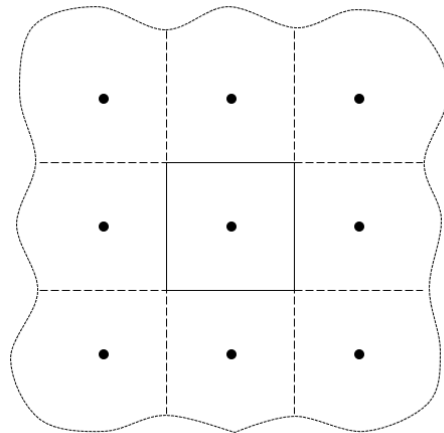
Fig. 2.2.1 – Square drainage system with infinite number of image wells (Earlougher et al. 1968, reprinted)
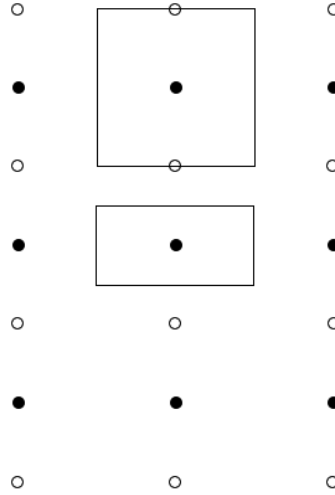
Fig. 2.2.2 – Rectangular drainage system (2:1) with infinite number of image wells (Earlougher et al. 1968, reprinted)

Wattenbarger et al. (1998) presented solutions for linear flow of liquid into fractured wells for constant rate production and constant pressure production cases. These solutions assumed infinite conductivity hydraulic fractures and no flow outside of simulated rock volume. Equation (II.9) shows the constant rate production solution for linear flow of liquid into infinite conductivity fractured well.

$$p_{wD} = \frac{\pi}{2}\left(\frac{y_e}{x_f}\right)\left[\frac{1}{3} + \left(\frac{x_f}{y_e}\right)^2 t_{Dxf}\right]$$
$$-\frac{2}{\pi^2}\left(\frac{y_e}{x_f}\right)\sum_{n=1}^{\infty}\left(\frac{1}{n^2}\right)\exp\left[-n^2\pi^2\left(\frac{x_f}{y_e}\right)^2 t_{Dxf}\right]$$

(II.9)

And, the constant bottomhole pressure solution from a closed reservoir with linear flow is presented by equation (II.10).

$$\frac{1}{q_D} = \frac{\frac{\pi}{4}\left(\frac{y_e}{x_f}\right)}{\sum_{n_{odd}}^{\infty} \exp\left[-\frac{n^2\pi^2}{4}\left(\frac{x_f}{y_e}\right)^2 t_{Dxf}\right]} \qquad (II.10)$$

Here dimensionless variables are defined as:

$$p_{wD} = \frac{kh}{141.2qB\mu}(p_i - p_{wf}) \qquad (II.11)$$

$$\frac{1}{q_D} = \frac{kh}{141.2qB\mu}(p_i - p_{wf}) \qquad (II.12)$$

$$t_{Dxf} = \frac{0.002633kt}{\phi\mu t x_f^2} \qquad (II.13)$$

Here, expressions for dimensionless pressure (p_{wd}) and inverse of dimensionless rate ($1/q_D$) appear to be identical. However, for p_{wD} bottomhole pressure (p_{wf}) varies with time and rate (q) remains constant, whereas in $1/q_D$ definition, p_{wf} remains constant and q changes with time.

The generalized form of dimensionless time, t_{Dye}, can be used to define dimensionless time for any type of reservoir geometry and were used to plot the type curves for constant rate and constant pressure solutions. Although these solutions were presented for liquid

flow, they can be extended to transient flow of gas into vertical fractured by using real gas

pseudo pressure instead of pressure and pseudo time instead of time.

The type curves plotted were used to estimate the end of linear flow for constant rate and

constant pressure production cases by visual identification of the point where half-slope

line ends. In terms of t_{Dye}, the end of half-slope for the constant rate case is 0.5 whereas

for constant pressure case it is 0.25. These values can be used to estimate minimum

drainage area from field data.

2.3. Shape Factors

Matthews, Brons, and Hazebroek (1954) presented a pressure function (p_{DMBH}) for

correcting extrapolated pressure buildup data to average drainage area pressure. This

pressure function is shown by (II.16)

$$p_{DMBH}(r_{wD}, t_{DA}) = \frac{2\pi k h(p^* - \bar{p})}{q\mu} = 4\pi t_{DA} + \sum_{i=2}^{\infty} \text{Ei}\left(-\frac{a_{iD}^2}{4t_{DA}}\right) \qquad \text{(II.14)}$$

Here, p^* is the shut-in pressure linearly extrapolated to infinite shut-in time on a semi-log

plot of pressure vs. $[\Delta t/(t + \Delta t)]$. They used method of images and plotted

$(p^* - \bar{p})/(q\mu/4\pi kh)$ against $kt/\phi\mu c_t A$ to determine average pressure $(\bar{p})$ for different

reservoirs which have polygons of simple shape. In their work, they presented these plots

for various drainage shapes which were later referenced by other authors to determine

shape factors.

Brons and Miller (1961) discussed a method to correct spot pressure readings obtained by shutting-in all the wells simultaneously and taking bottom hole pressure readings form each successive well in a field after some time. He used two separate equations correlating bottom hole pressure (p_{wf}) to static pressure of the drainage area of the well (p_s) and to the shut-in pressure $(p_{\Delta t})$, i.e., the pressure reached after shut-in time (Δt) to estimate the correction factor. He used build-up plots from Matthews, Brons, and Hazebroek (1954) and presented shape factors for a limited number of drainage configurations.

Dietz (1965) presented tabulated shape factor values for a variety of drainage shapes while he discussed a method to determine average reservoir pressure in bounded reservoirs. He suggested an expression, shown by equation (II.16), for the straight-line portions of the pressure build up plots presented by Matthews, Brons, and Hazebroek (1954).

$$\frac{2\pi kh(p^* - \bar{p})}{q\mu} = \frac{1}{2}\ln\frac{C_A kt}{\phi\mu c_t A} \qquad (\text{II}.15)$$

where C_A is a constant dependent on the shape of the drainage area and on the well location, commonly known as Dietz' shape factor. Equation (II.16) can reduce to equation (II.16) for $kt/\phi\mu c_t A = 1$.

$$\frac{2\pi kh(p^* - \bar{p})}{q\mu} = \frac{1}{2}\ln C_A \qquad (\text{II}.16)$$

Therefore, $\ln C_A$ can be read from the straight line parts of the pressure build up plots or from their extrapolations, at the abscissa value of $kt/\phi\mu c_t A = 1$.
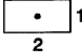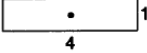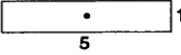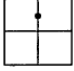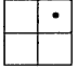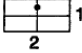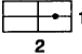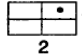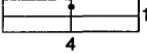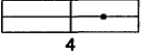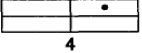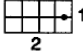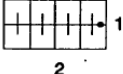
Earlougher et al. (1968) presented tabular solutions of a square bounded reservoir as described in Section 2.2. One of the applications of his tabulated values of pressure function (p_{MBH}) is determination of shape factors for pseudo-steady state flow condition for a variety of drainage shapes. Earlier, this was done graphically by Dietz (1965) using figures presented by Matthews, Brons, and Hazebroek (1954) and, hence, was not much accurate. Use of tabulated pressure values (p_{DMBH}) at dimensionless time of unity ($t_{DA} = 1$) provided more accurate shape factors using simplified form of equation (II.16) for the pseudo-steady state condition as presented below.

$$p_{DMBH} = \ln(C_A t_{DA}) \qquad \text{(II.17)}$$

Earlougher (1968) presented interpolation curves for shape factors for various rectangular reservoir configurations containing vertical wells at different well locations. These curves could be used to estimate shape factors for rectangular reservoirs with any aspect ratio and any well location. He concluded that shape factors become very small as the well location approaches the reservoir boundary and as the length to width ratio of the reservoir becomes very large.

Peaceman (1990) used closed form solution of a finite difference system presented by Babu et al. (1990) to calculate shape factors. He used to successive refinement of the grid block to calculate bottom hole pressure from the well block pressure which was used to converge reservoir shape factors up to six decimal places. He compared his results to the previously presented shape factors by Dietz (1965) and Earlougher (1977) which are summarized in Table II.1.

21

Table II.1 – Shape Factors, C_A (Peaceman 1990)

Shape	C_A this paper	C_A by Dietz	C_A Earlougher, et al
□ (well centered in square)	30.881092	30.9	30.8828
well in 2:1 rectangle (1×2)	21.836230	22.6	21.8369
well in 4:1 rectangle (1×4)	5.378107	5.38	5.3790
well in 5:1 rectangle (1×5)	2.359106	2.36	2.3606
quartered square, well at top	12.983900	12.9	12.9851
quartered square, well upper right	4.522431	4.57	4.5132
2:1 rect, well centered top	10.836863	10.8	10.8374
2:1 rect, well right center	4.522431	4.86	4.5141
2:1 rect, well upper right	2.081274	2.07	2.0769
4:1 rect, well top center	2.689016	2.72	2.6896
4:1 rect, well center right	0.232407	0.232	0.2318
4:1 rect, well upper right	0.115771	0.115	0.1155
vertical rect, well top	3.334612	3.39	3.3351
2:1 rect, well top center	3.157269	3.13	3.1573
2:1 rect grid, well right	0.583297	0.607	0.5813
long 2:1 rect, well right	0.111574	0.111	0.1109

2.4. Pressure Derivatives

The use of pressure derivatives in pressure transient test analysis was introduced by Bourdet (1989). He suggested the use of pressure derivative with respect to logarithm of time or superposition time function to identify reservoir flow regimes. Reservoir features that are hard to recognize using Horner plot or Gringarten plot due to similarity of curves for different reservoir systems can be uniquely identified by the derivative curves.

Ehlig-Economides (1988) presented a comparison of the semi-log Horner plot and log-log derivative plot for five frequently encountered reservoir systems. She presented cases for a homogeneous reservoir, a homogeneous reservoir with one sealing fault, a homogeneous reservoir with closed outer boundary, and a dual-porosity system with the pseudo-steady-state flow from the matrix to fractures all with wellbore storage and skin. She also presented a case for infinite conductivity vertical fracture in a homogeneous reservoir. She noted that transient patterns on the log-log plot have a standard appearance, hence, easier to identify when the data is plotted on square log cycles. But some derivative patterns presented can also represent other reservoir models. For example, doubling of slope representing a fault can also be due to transient inter-porosity flow in a dual-porosity system. Similarly, the valley in the pressure derivative due to the dual-porosity system with the pseudo-steady-state flow from the matrix to fractures could also represent a layered system instead of dual porosity. Therefore, in such cases, reservoir engineers should consult geologic, seismic, and core-analysis data to decide which model to use in an interpretation.

However, the presence of noise in the data is amplified in the derivative response, hence, making the analysis difficult. The obvious solution is to remove noisy data. But this option is limited as it is hard to separate noise from the actual signal.

Bourdet suggested an algorithm for pressure derivative to reduce noise effects. Equation (II.16) is the generalized form of Bourdet's pressure derivative algorithm.

$$\frac{dp}{dX} = \frac{\left(\frac{\Delta p_1}{\Delta X_1}\right)\Delta X_2 + \left(\frac{\Delta p_2}{\Delta X_2}\right)\Delta X_1}{\Delta X_1 + \Delta X_2} \tag{II.18}$$

where 1 represent the point before i, 2 represent the point after i, and X is the time function ($\ln \Delta t$ for drawdown, modified Horner, or superposition times expressed in natural logarithm for buildups).

2.5. Outliers Detection Methods

Presence of noise in production data can adversely affect the engineering data analysis. During production modeling and forecast, outliers present in the data can cause miscalculation of model parameters, thus, resulting in overestimation or underestimation of reserves. Alternatively, outliers can also cause problems during pressure transient analysis. Presence of noise aggregates in the calculation of Bourdet's pressure derivative which is a fundamental tool in the analysis of pressure data. To put things in perspective, we will first discuss the definition of an outlier followed by the methods for their detection.

There is no mathematically correct definition for an outlier, rather, declaring a point as outlier in a data set is always subjective. An apparently abnormal point in the data set

24

which can easily be declared an outlier might be the outcome of some unique response of the data generating mechanism. Hawkins (1980) defines outlier as an observation which deviates so much from other observations as to arouse suspicions that it was generated by a different mechanism. He further notes that an inspection of a sample containing outliers would show up such characteristics as large gaps between 'outlying' and 'inlying' observations and the deviation between the outliers and the group of inliers, as measured on some suitably standardized scale.

Identification of outliers can be classified in several ways. One of them classifies outlier identification methods into global and local outlier identification models. Global model is the one which leads to a binary decision of whether a point is an outlier or not. Whereas, local model assigns a factor to each data point which can be used to rank data in increasing chance of being an outlier. Another classification for outlier identification methods divides them into supervised and unsupervised approaches. A supervised approach is the one where status of a point being an inlier, or an outlier is known, and we train our model to differentiate between those two sets of data points. This makes it a global approach for outlier identification. In other words, a training data set is available in supervised models with correctly identified inliers and outliers and we use this data set to train our data model which can be used to predict future data points as inliers and outliers. This kind of problem is usually unbalanced classification problem because outliers class usually has relatively less number of observations than inliers. Alternatively, unsupervised models

This method has the advantage of having no user-defined parameters and it provides justification for declaring a point as an outlier i.e. based on the divergence of the angles. However, it requires for each point in the data that we consider all possible pairs of points in the data which makes its time-complexity in $O(n^3)$ which is relatively high compared to other methods. Therefore, to reduce the time complexity of this method, the authors suggested a FastABOD approach which uses a sample of points from the data set to calculate ABOF instead of using all pairs. This approach can reduce the time complexity of this method from $O(n^3)$ to $O(n^2 + n \cdot k^2)$ without affecting the performance of the method. A sample from the data can be collected using points with the strongest weight in the variance, i.e., pairs between k nearest neighbors. We have used the FastABOD approach in our study as it has low time-complexity and is a good approximation for low dimensionality data due to the consideration of distance weighted points in the variance.

CHAPTER III

RADIUS AND DEPTH OF INVESTIGATION

3.1. Introduction

The flow of fluids through porous media is primarily described by a partial differential equation known as the diffusivity equation. It is a combined representation of the Darcy's law, fluid's compressibility equation and the continuity equation. The partial differential diffusivity equation to model flow of a slightly compressible liquid through a homogeneous anisotropic medium can be written as:

$$\eta_X \frac{\partial^2 p}{\partial x^2} + \eta_Y \frac{\partial^2 p}{\partial y^2} + \eta_Z \frac{\partial^2 p}{\partial z^2} - \frac{\partial p}{\partial t} = 0 \qquad \text{(III.1)}$$

Here, x, y, and z are principal axes of permeability and the coefficients η_X, η_Y, and η_Z are principal diffusivities. Diffusivity constant can be defined in consistent units as:

$$\eta_j = \frac{k_j}{\phi \mu c_t}, \quad j = x, y, or\ z \qquad \text{(III.2)}$$

Most common solutions presented for equation (III.1) use Laplace or Fourier transforms which assume certain initial and boundary conditions. These solutions were first used in problems of heat flow though solids (i.e. heat conduction) and then applied for petroleum engineering problems for flow of fluid through porous media. Another useful yet less popular solution is instantaneous point source solution presented by Kelvin (1884). Instantaneous source solutions are discussed in detail by Carslaw and Jaeger (1959) for

27

different source geometries. A corresponding point source solution for petroleum engineering problems was introduced by Nisle (1958) as:

$$\Delta p = \frac{Q}{8\phi c_t (\pi\eta t)^{\frac{3}{2}}} \exp\left(-\frac{r^2}{4\eta t}\right) \tag{III.3}$$

Equation (III.3) represents the pressure drop at a point which is r distance away from a source (or sink) in an infinite reservoir, when a finite quantity of liquid, Q, is instantaneously withdrawn (or injected) from the source (or into the sink). For practical purposes, this condition is similar to an impulse or slug test where flow period is extremely short compared to the duration of shut-in period.

Ayoub (1988) discussed the principal of analysis for such tests. He noted that when an instantaneous source of unit strength or Dirac function is introduced into an infinite reservoir, the resultant pressure variations in the reservoir are given by Green's function which is, mathematically, the time derivative of the classic dimensionless pressure solution represented as type curves. In other words, if a formation is subjected to an instantaneous source of unit strength, the resulting pressure variations will directly match the appropriate pressure derivative curve. Clarkson (2014) discussed unit impulse method for defining radius of investigation. When a unit impulse is introduced into the reservoir by flowing or injecting the well source (or sink) for very short duration, the time of arrival of the impulse can be observed at an observation well at a distance d from the source (or sink). Therefore, the distance at which the maximum pressure response occurs at a particular time can be defined as the the radius of investigation.

Mattar, et al. (1975) also discussed similar concept. If an impulse is applied at a well, the transient thus created will travel throughout the formation. At any time, the point at which the maximum effect of the impulse is experienced is known as the radius of investigation. To derive radius (or depth) of investigation equation for radial, linear, and spherical flow geometries, we will use solutions for instantaneous line source, plane source and point source respectively. We will consider the instantaneous source solutions of unit strength and will equate its derivative to zero to find the radius at which the effect of impulse is maximum. Derivation steps for the radius of investigation equation from instantaneous line source solution can be illustrated as follows.

3.2. Radial Flow

Instantaneous line source equation given by Carslaw and Jaeger is:

$$S(r,t) = \exp\left[-\frac{r^2}{4\eta t}\right] / 4\pi\eta t \tag{III.4}$$

Differentiating equation (III.4) with respect to time and equating it to zero.

$$\frac{r^2 \exp\left[-\frac{r^2}{4\eta t}\right]}{16\pi\eta^2 t^3} - \frac{\exp\left[-\frac{r^2}{4\eta t}\right]}{4\pi\eta t^2} = 0 \tag{III.5}$$

Simplifying,

$$\frac{\exp\left[-\frac{r^2}{4\eta t}\right]}{4\pi\eta t^2}\left(\frac{r^2}{4\eta t} - 1\right) = 0 \qquad \text{(III.6)}$$

Or,

$$\left(\frac{r^2}{4\eta t} - 1\right) = 0 \qquad \text{(III.7)}$$

Or,

$$r^2 = 4\eta t \qquad \text{(III.8)}$$

Substituting η by $\frac{0.0002637k}{\phi\mu c_t}$ and replacing r by r_i, equation (III.8) can be written as:

$$r_i^2 = 4 * \frac{0.0002637k}{\phi\mu c_t} * t \qquad \text{(III.9)}$$

Or,

$$r_i^2 = \frac{kt}{948\phi\mu c_t} \qquad \text{(III.10)}$$

Or,

$$r_i = \sqrt{\frac{kt}{948\phi\mu c_t}} \qquad \text{(III.11)}$$

Equation (III.11) is the conventional radius of investigation equation for radial flow. We will use the same approach to derive equations for the depth of investigation for linear

30

flow and radius of investigation for spherical flow using instantaneous plane source and instantaneous spherical source solutions respectively.

3.3. Linear Flow

The instantaneous plane source solution given by Carslaw and Jaeger (p.358) is:

$$S(r,t) = \exp\left[-\frac{r^2}{4\eta t}\right] \bigg/ 2\sqrt{\pi \eta t} \qquad \text{(III.12)}$$

Differentiating equation (III.12) with respect to time and equating it to zero.

$$\frac{r^2 \exp\left[-\frac{r^2}{4\eta t}\right]}{8\eta t^2 \sqrt{\pi \eta t}} - \frac{\pi \eta \exp\left[-\frac{r^2}{4\eta t}\right]}{4\pi \eta t \sqrt{\pi \eta t}} = 0 \qquad \text{(III.13)}$$

Simplifying,

$$\frac{\exp\left[-\frac{r^2}{4\eta t}\right]}{4t\sqrt{\pi \eta t}} \left(\frac{r^2}{2\eta t} - 1\right) = 0 \qquad \text{(III.14)}$$

Or,

$$\left(\frac{r^2}{2\eta t} - 1\right) = 0 \qquad \text{(III.15)}$$

Or,

$$r^2 = 2\eta t \qquad \text{(III.16)}$$

Substituting η by $\frac{0.0002637k}{\phi\mu c_t}$ and replacing r by l_i, equation (III.16) can be written as:

$$l_i^2 = 2 * \frac{0.0002637k}{\phi\mu c_t} * t \qquad\qquad \text{(III.17)}$$

Or,

$$l_i^2 = \frac{kt}{1,896\phi\mu c_t} \qquad\qquad \text{(III.18)}$$

Or,

$$l_i = \sqrt{\frac{kt}{1,896\phi\mu c_t}} \qquad\qquad \text{(III.19)}$$

Equation (III.19) represents the depth of investigation equation for linear flow.

3.4. Spherical Flow

The instantaneous point source solution given by Carslaw and Jaeger (p.358) is:

$$S(r,t) = \exp\left[-\frac{r^2}{4\eta t}\right] / 8\sqrt{(\pi\eta t)^3} \qquad\qquad \text{(III.20)}$$

Differentiating equation (III.20) with respect to time and equating it to zero.

$$\frac{r^2 \exp\left[-\frac{r^2}{4\eta t}\right]}{32\pi\eta^2 t^3\sqrt{\pi\eta t}} - \frac{3\pi\eta \exp\left[-\frac{r^2}{4\eta t}\right]}{16\pi^2\eta^2 t^2\sqrt{\pi\eta t}} = 0 \qquad\qquad \text{(III.21)}$$

Simplifying,

32

$$\frac{3 \exp\left[-\frac{r^2}{4\eta t}\right]}{16\pi\eta t^2 \sqrt{\pi\eta t}} \left(\frac{r^2}{6\eta t} - 1\right) = 0 \qquad \text{(III.22)}$$

Or,

$$\left(\frac{r^2}{6\eta t} - 1\right) = 0 \qquad \text{(III.23)}$$

Or,

$$r^2 = 6\eta t \qquad \text{(III.24)}$$

Substituting η by $\frac{0.0002637k}{\phi\mu c_t}$ and replacing r by r_i, equation (III.24) can be written as:

$$r_i^2 = 6 * \frac{0.0002637k}{\phi\mu c_t} * t \qquad \text{(III.25)}$$

Or,

$$r_i^2 = \frac{kt}{632\phi\mu c_t} \qquad \text{(III.26)}$$

Or,

$$r_i = \sqrt{\frac{kt}{632\phi\mu c_t}} \qquad \text{(III.27)}$$

Equation (III.27) represents the radius of investigation equation for radial flow.

3.5. Discussion

In this chapter, we have derived radius and depth of investigation equations using instantaneous source solutions. Although we have started form instantaneous source functions for line, plane and point sources separately, the basic source function is that of a plane source from which line and point sources can be obtained as shown by Newman (1936). A line source function can be obtained by multiplying *two* plane source functions perpendicular to each other. Similarly, a point source function can be obtained by multiplying *three* plane source functions perpendicular to each other.

The radius and depth of investigation expressions thus obtained are comparable to the conventional definitions presented in the literature. These three equations differ by a constant factor and are similar to those presented by Datta-Gupta et al. (2011) under their diffusive time of flight concept. Datta-Gupta et al. (2011) developed their equations using *Eikonal* equation which is based on elastic and electromagnetic wave propagation. Our definitions, however, are derived from instantaneous source functions.

CHAPTER IV

DETERMINATION OF SHAPE FACTORS

4.1. Introduction

Shape factors used in the pseudo steady state equation for bounded reservoirs were first introduced by Dietz (1965) and were later tabulated by Earlougher (1977) and Lee (1982). For wells with vertical fractures, these shape factors are limited to square-shaped bounded reservoirs.

In this section, we will estimate shape factors for wells vertical fractures centered in different rectangular-shaped reservoir configurations by comparing the pseudo-steady state equation with the superimposed transient linear flow solutions of the diffusivity equation. The use of pseudo steady state equation for wells with vertical fracture can be extended to multi-fractured horizontal wells (MFHWs) by incorporating number of fractures in the equation, hence, shape factors derived for wells with vertical fracture can also be used for MFHWs.

Superimposed radial flow solutions and linear flow solution bounded reservoirs will be used to reproduce some shape factors already presented by Earlougher (1977) and Lee (1982). Therefore, the method will be validated before estimating shape factors for new reservoir configurations. Throughout this chapter, we will refer the distance between two fractures as *fracture spacing* (S_f), the length of one fracture arm as *fracture half-length* (x_f), and total length of both fracture arms as *fracture length* $(2x_f)$. We also assume that

the fracture length extends across the width of reservoir and the reservoir only produces from the simulated rock volume covered by fracture length and number of fractures (n).

4.2. Theoretical Background

The pseudo-steady-state equation for an arbitrary shaped bounded reservoir as presented by Matthews and Russell (1967) is:

$$p_i - p_{wf} = \frac{0.234qBt}{A_d h \phi c_t} + \frac{141.2qB\mu}{kh} \left[\frac{1}{2} \ln \left(\frac{4A_d}{e^\gamma C_A r_w^2} \right) \right] \qquad \text{(IV.1)}$$

Equation (IV.1) can be described for a well producing from a vertical fracture fully penetrating across and in the center of a rectangular-shaped bounded reservoir as:

$$p_i - p_{wf} = \frac{0.234q_{sc}Bt}{A_d h \phi C_t} + \frac{141.2qB\mu}{kh} \left[\frac{1}{2} \ln \left(\frac{S_f^2}{e^\gamma C_A x_f^2} \right) \right] \qquad \text{(IV.2)}$$

where, $\gamma = 0.5772156649 \ldots$ is the Euler's constant, S_f is the fracture spacing in a multiple fracture well ($S_f = 2y_e$, i.e. fracture spacing is twice of distance to the no flow boundary) and x_f is the fracture half-length. For a square-shaped reservoir with vertical fracture fully penetrating across the width of the reservoir, shape factor (C_A) takes the value of 0.7887 as presented by Earlougher (1977) and Lee (1982).

Flow from well with vertical fractures in rectangular-shaped bounded reservoirs is given by transient linear flow equation coupled with the principle of superposition in space to include effect of reservoir boundaries. Transient linear flow from an infinite plane surface can be described as:

36

$$p_D(x_D, t_D) = 2\sqrt{\frac{t_D}{\pi}} \exp\left(-\frac{x_D^2}{4t_D}\right) - x_D \, erfc\left(\frac{x_D}{2\sqrt{t_D}}\right) \qquad \text{(IV.3)}$$

where the *erfc* is the complementary error function is defined as:

$$erfc(x) = \frac{2}{\sqrt{\pi}} \int_x^\infty e^{-t^2} dt \qquad \text{(IV.4)}$$

Dimensionless variables in equation (IV.3) can be described as:

$$p_D = \frac{k\sqrt{A_f}}{887.22qB\mu}(p_i - p_{wf}) \qquad \text{(IV.5)}$$

$$t_D = \frac{0.0002637kt}{\phi\mu c_t A_f} \qquad \text{(IV.6)}$$

$$x_D = \frac{x}{\sqrt{A_f}} \qquad \text{(IV.7)}$$

Here, $A = 4x_f h$ which is the fracture flow area exposed to linear flow from reservoir into wellbore. For the special case of $x_D = 0$, equation (IV.3) can be written as:

$$p_D(0, t_D) = 2\sqrt{\frac{t_D}{\pi}} \qquad \text{(IV.8)}$$

By using superposition principle as described by Matthews, Brons and Hazebroek (1954), we can transform transient linear flow equation into bounded rectangular-shaped reservoir equation. For the case of a well with vertical fracture centered in a rectangular-shaped

reservoir, we will assume an infinite number of vertical fractures equidistant from each other on both sides of the actual well (i.e. the well is centered in the reservoir).

$$p_D(0, t_D) = 2\sqrt{\frac{t_D}{\pi}} + \sum_{i=2}^{\infty} 2\sqrt{\frac{t_D}{\pi}} exp\left(-\frac{x_{iD}^2}{4t_D}\right) - x_{iD} \, erfc\left(\frac{x_{iD}}{2\sqrt{t_D}}\right) \qquad \text{(IV.9)}$$

In equation (IV.9), x_{iD} is the distance of ith image well from actual well and i denotes the total number of vertical fractures on both sides of the actual well.

Similarly, line source solution is a good approximation to transient radial flow from vertical wells. When superposition principle is used, this solution can be used to model radial flow in bounded reservoirs.

$$p_D = -\frac{1}{2}\left[\text{Ei}\left(\frac{1}{4t_D}\right) + \sum_{i=2}^{\infty} \text{Ei}\left(\frac{a_{iD}^2}{4t_D}\right)\right] \qquad \text{(IV.10)}$$

Here, a_{iD} is the dimensionless distance of ith image well from the original well. Other dimensionless variables in equation (IV.10) are defined as:

$$p_D = \frac{kh(p_i - p)}{141.2qB\mu} \qquad \text{(IV.11)}$$

$$t_D = \frac{0.0002637kt}{\phi\mu c_t r_w^2} \qquad \text{(IV.12)}$$

$$r_D = r/r_w \qquad \text{(IV.13)}$$

At very large times when boundary dominated flow is established, results from equation (IV.1) or from equation (IV.2) will be similar to the results from equation (IV.9) or equation (IV.10) expressed in dimensions. Hence, for a pre-defined analytical model with a particular reservoir geometry, pressure drop values at sufficiently large times from equation (IV.9) or equation (IV.10) can be substituted back in equation (IV.1) or equation (IV.2) to calculate shape factor values for that reservoir geometry. If we denote the dimensionless pressure drop caused by radial flow into a vertical fracture by $p_{D(R)}$, then the equation for the shape factor for a vertical well in a rectangular shaped reservoir of area A can be written as:

$$C_A = \frac{4A}{r_w^2} \exp\left[-\gamma - \frac{2kh}{141.2qB\mu}\left(\frac{141.2qB\mu}{kh}p_{D(R)} - \frac{0.234qBt}{Ah\phi c_t}\right)\right] \qquad \text{(IV.14)}$$

Similarly, if we denote the dimensionless pressure drop caused by linear flow into a vertical fracture by $p_{D(L)}$, then the equation for the shape factor for a well with a vertical fracture can be written as:

$$C_A = \frac{S_f^2}{x_f^2} exp\left[-\gamma - \frac{2kh}{141.2qB\mu}\left(\frac{887.22qB\mu}{k\sqrt{A_f}}p_{D(L)} - \frac{0.234qBt}{A_d h\phi c_t}\right)\right] \qquad \text{(IV.15)}$$

Now, we will use equations (IV.13) and (IV.14) to calculate shape factors for different rectangular shaped reservoirs.

4.3. Validation of Method

As discussed in section (2.3), shape factors for various rectangular reservoir configurations have been previously presented by Dietz (1965), Earlougher (1977) and Peacman (1990). We will compare shape factors values calculated using the method described above with those values published by other authors. Table IV.1, Table IV.2, and Table IV.3 shows a comparison of shape factor values calculated in this work with those presented by Dietz (1965) , Earlougher (1977) and Peacman (1990), respectively. We can see that the percentage error is in acceptable range, hence the method can be used to calculate shape factor values for vertical wells in different rectangular shaped drainage area configurations.

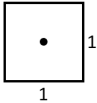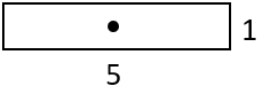Table IV.1 – Comparison of Shape Factors with Dietz (1965)

	C_A (Dietz)	C_A (Calculated)	Percentage Difference (%)
	30.9	30.88110066	0.06
	22.6	21.836239	3.38
	5.38	5.378109809	0.04
	2.36	2.359108	0.04

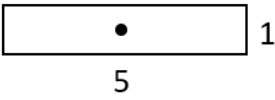Table IV.2 – Comparison of Shape Factors with Earlougher (1977)
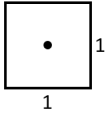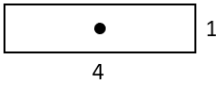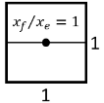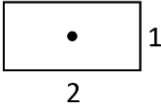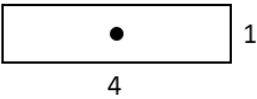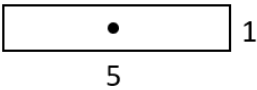
	C_A (Earlougher)	C_A (Calculated)	Percentage Difference (%)
	30.8828	30.88110066	0.006
	21.8369	21.836239	0.003
	5.379	5.378109809	0.017
	2.3606	2.359108	0.063
	0.7887	0.788109011	0.075

Table IV.3 – Comparison of Shape Factors with Peacman (1990)

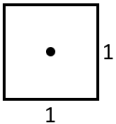|	C_A (Peacman)	C_A (Calculated)	Percentage Difference (%)
	30.881092	30.88110066	2.81E-05
	21.83623	21.836239	4.12E-05
	5.378107	5.378109809	5.22E-05
	2.359106	2.359108	8.48E-05

4.4. Application to Horizontal wells with Vertical Fractures in Rectangular Shaped Drainage Areas

Production from horizontal wells with vertical fractures is quite common these days. For the sake of simplicity, we have calculated shape factor values by considering production from a well with single vertical fracture. However, these shape factor values are equally applicable for multiple fractured horizontal wells when used with modified pseudo-steady state equation incorporating the number of fractures in the well.

Table IV.4 shows calculated values of shape factors for different combinations of fracture-length and fracture spacing. For the case of the well with single fracture, fracture spacing is defined as twice the distance to the reservoir boundary. These shape factor values obtained from equation (IV.15) were plotted against the aspect ratio of the drainage area i.e. $2x_f : S_f$, and the data was observed to follow a trend as shown in Fig. 4.4.1. We fitted a smooth curve on the data which can be used to obtain shape factor values for drainage area geometries not presented in this work. For more practical purposes, aspect ratio values are less than 0.5 (i.e. fracture spacing, S_f, is greater than the fracture length, $2x_f$). In such cases, shape factor values were found to change drastically for small changes in aspect ratio values. Therefore, care should be taken while selecting shape factor values in such cases.

Table IV.4 – Calculated Shape Factors for wells with vertical fractures centered in rectangular reservoirs of various shapes

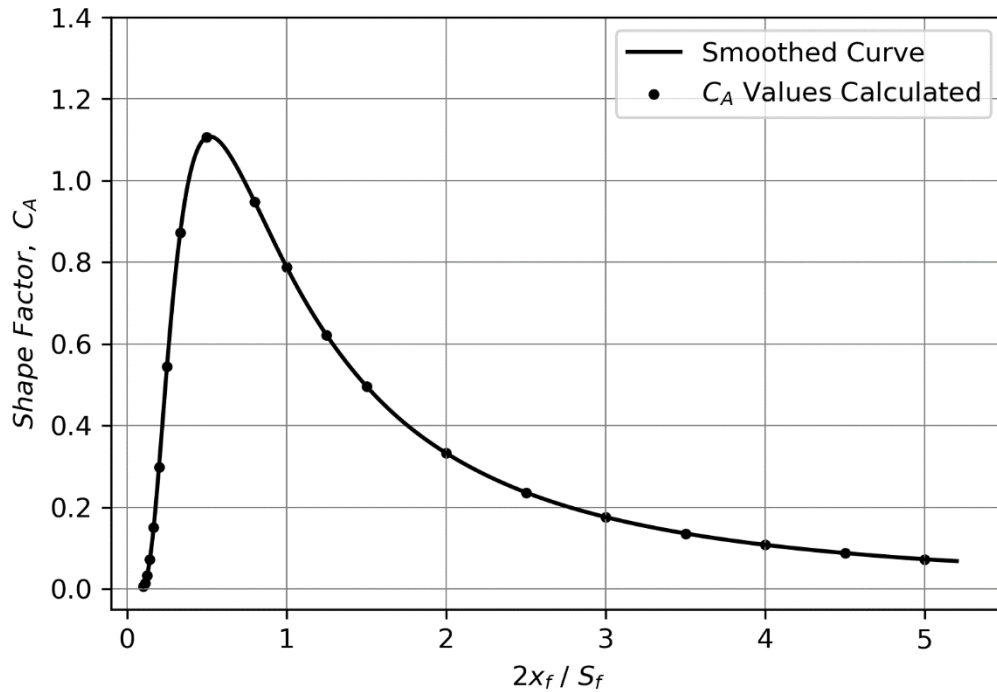| $2x_f:S_f$	Shape Factor, C_A	$2x_f:S_f$	Shape Factor, C_A
1:10	0.006364	1:1	0.788109
1:9	0.014682	1.25:1	0.621906
1:8	0.033054	1.5:1	0.496594
1:7	0.072116	2:1	0.332601
1:6	0.150983	2.5:1	0.236364
1:5	0.298784	3:1	0.176010
1:4	0.544916	3.5:1	0.135926
1:3	0.873463	4:1	0.108034
1:2	1.106252	4.5:1	0.087880
1:1.2	0.947794	5:1	0.072858

Fig. 4.4.1 – Shape Factors vs. Drainage Area Aspect Ratio $2x_f/S_f$

4.5. Discussion

In this chapter, we used method of images for vertical fractures represented by Eq. (IV.9) and conventional pseudo steady equation for linear flow represented by Eq. (IV.2) to calculate shape factors. Table IV.4 shows a list of shape factors calculated for drainage areas with various configurations. These shape factors can be applied to multiple fracture horizontal wells with various completion designs after incorporating the number of fractures in the pseudo steady state equation. Fig. 4.4.1 shows a plot of these shape factors against drainage area parameter i.e. $2x_f : S_f$ (ratios of fracture length vs. fracture spacing). Shape factors other than those presented in this work can be obtained using trend line presented in Fig. 4.4.1. For cases where fracture spacing (S_f) is more than fracture length (x_f), i.e. $2x_f : S_f < 0.5$, shape factor values change drastically with small changes in the aspect ratio (i.e. $2x_f : S_f$) as shown in Fig. 4.4.1. Hence, shape factors should be selected carefully while working for such reservoir configurations.

CHAPTER V

DETERMINATION OF THE END OF TRANSIENT FLOW (TF) AND THE START OF BOUNDARY DOMINATED FLOW (BDF)

5.1. Introduction

In this section we will present the estimated durations of transient, transition and boundary dominated flow regimes using synthetic production data obtained from rigorous numerical simulations. We have considered following two well types or flow regimes:

1. Vertical wells in rectangular shaped reservoirs (i.e. radial flow regime)
2. Horizontal wells with vertical fractures in rectangular shaped reservoirs (i.e. linear flow regime)

For each flow regime type different drainage area configurations, i.e. length to width ratios, were considered with constant rate production (CRP) and constant pressure production (CPP) schemes. We have also used production data to estimate volume of investigation as presented by Spivey (2020) at times at end of transient flow and at the start of boundary dominated flow.

5.2. Vertical Wells in Rectangular-shaped Drainage Areas

Vertical wells centered in rectangular shaped bounded reservoirs in different length to width aspect ratios are considered as shown in Fig. 5.2.1(a). Fig. 5.2.1 (b) shows that flow from such wells during transient flow period is typical transient radial flow (TRF) identified by a horizontal line on pressure derivatives plot. It is followed by a transition

period depending on the aspect ratio of the drainage area and then boundary dominated flow (BDF) starts which is indicated by unit slop line on pressure derivative plots.

For determination of the end of transient flow into vertical wells centered in rectangular drainage area, a horizontal line was fitted to the part of the data indicating transient radial flow, and a unit slope line was fitted to the part of data showing boundary dominated flow. Deviation of the pressure derivative curve from the horizontal line by 5% was used to mark the end of transient radial flow. Similarly, the point where the deviation of the pressure derivative curve become less than 5% from the unit slope line was marked as the start of boundary dominated flow period. Although the limit of 5% deviation is arbitrary, it was used to confidently identify these flow regime markers while ignoring the distortions in the pressure derivatives.

Dimensionless variables used for pressure, time and distance are defined below:

$$p_D = \frac{kh}{141.2 \, qB\mu} (p_i - p) \tag{V.1}$$

$$t_D = \frac{0.0002637kt}{\phi\mu c_t r_w^2} \tag{V.2}$$

$$r_D = \frac{r}{r_w} \tag{V.3}$$

However, plotting variable for dimensionless time axis (x-axis) was modified by multiplying it with r_w^2/A to obtain comparable values with that already mentioned in literature (such as Earlougher 1977).
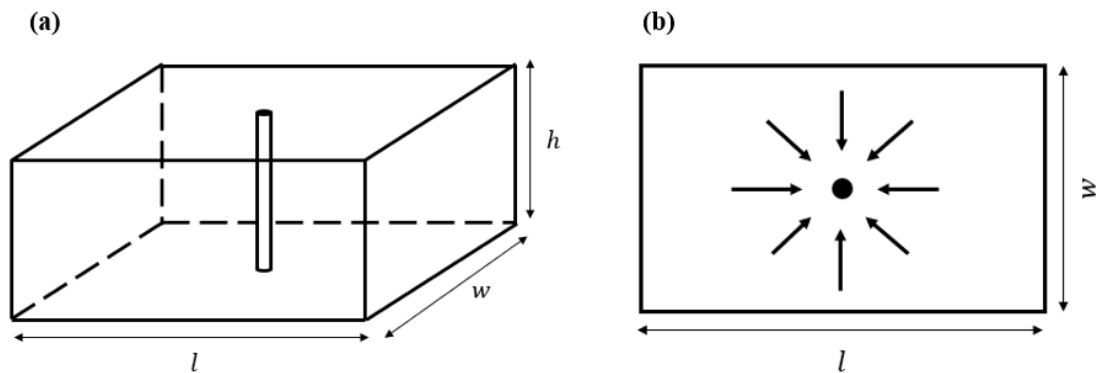

Fig. 5.2.1 – (a) Isometric view of reservoir model with vertical well (b)Top View of reservoir showing reservoir dimensions and linear flow regime

5.2.1. Constant Rate Production from Vertical Wells

For constant rate production case from vertical wells with rectangular drainage areas, four cases were considered with different drainage area configurations as shown in Table V.1. For all cases, simulation was run for an appropriate length of time to observe the boundary dominated flow (BDF) represented by a unit slope line on the log-log pressure derivative plot. Production data thus obtained was used to estimate the times at the end of transient radial flow (TRF) and the start of boundary dominated flow (BDF). Pressure derivative and volume of investigation plots for all the cases can be found in APPENDIX C section C-1.

47

Table V.1 summarizes the estimated times at the respective flow regime markers and compares them with the time to reach the boundary obtained from conventional definition of the radius of investigation presented by Lee (1982). Specific time values presented by Earlougher (1977) have been also included for similar cases for reference. When compared with the analytical definition of the radius of investigation (i.e. the time required by the pressure transient to reach the nearest boundary), the empirically estimated times at the end of transient radial flow closely matches with it. However, it is slightly more than in most cases which might be due the fact that the criteria we have chosen to mark the end of transient radial flow (i.e. 5% deviation from the horizontal line).

Table V.1 – Dimensionless time at the end of TRF and start of BDF (CRP)

CRP Cases $(l \times w)$	t_{DA} at the end of TRF	t_{DA} at the start of BDF	t_{DA} (Analytical)	Infinite Solution with <1% Error for $t_{DA}<$ (~ERF, Earlougher)	Less than 1% Error for $t_{DA}>$ (~BDF, Earlougher)	Exact PSS Solution for $t_{DA}>$ (~BDF, Earlougher)
1x1	0.0624	0.1177	0.0625	0.09	0.05	0.1
2x1	0.0373	0.1922	0.0312	0.025	0.15	0.3
4x1	0.0179	0.3830	0.0156	0.01	0.30	0.8
5x1	0.0156	0.4458	0.0125	0.025	0.4	1.0

Table V.2 – Normalized Volume of Investigation (NVOI) at the end of TRF and start of BDF (CRP)

Case ($l \times w$)	NVOI at ERF	NVOI at BDF	Fractional volume circles inscribed within rectangles
1x1 CRP	0.7168	0.9583	0.7854
2x1 CRP	0.4305	0.9562	0.3927
4x1 CRP	0.2030	0.9570	0.1964
5x1 CRP	0.1719	0.9506	0.1571

We have used simulated production data in above examples. However, in practice, we may encounter problems associated with noisy data. Derivative curves are of not much help in such cases because the derivative curves of noisy data tend to be much noisier than the drawdown curves and might be hard to interpret. Therefore, we have attempted to estimate flow regimes durations using drawdown curves which might be helpful for such real-life problems where noisy data might affect our interpretations. For this we have used superimposed analytical solutions to obtain production data for different rectangular bounded reservoirs. The results are summarized in Table V.3 and Table V.4. For each of the reservoir configurations, we estimated durations of flow regimes using difference in pressure and percentage differences. For transient radial flow (TRF), we used deviation from the straight line on the semi-log plot to estimate the time at the end of TRF. Whereas for boundary dominated flow (BDF), we used pressure difference with respect to straight line on cartesian plot and percentage deviation from the unit slope line on log-log plot to

49

identify the start of BDF. However, the pressure response of boundaries is delayed in drawdown curve than in the derivative curve (Jha and Lee 2017, Jha 2016).

Table V.3 – Dimensionless time at the end of TRF estimated using drawdown curves

Cases	Estimated Dimensionless time at the end of TRF, t_{A_dD}					Earlougher
	0.01 psi difference	0.1 psi difference	At 1% deviation	At 5% deviation	At 10% deviation	At 1% deviation
1x1	0.065	0.12	0.11	0.21	0.33	0.09
1x2	0.038	0.082	0.073	0.17	0.29	0.025
1x4	0.019	0.041	0.036	0.09	0.17	0.01
1x5	0.015	0.033	0.028	0.071	0.13	0.025

Table V.4 – Dimensionless time at the start of BDF estimated using drawdown curves

Cases	Estimated Dimensionless times at the start of BDF, t_{A_dD}					Earlougher
	0.01 psi difference	0.1 psi difference	At 1% deviation	At 5% deviation	At 10% deviation	At 1% deviation
1x1	0.11	0.049	96	21	10	0.05
1x2	0.22	0.094	98	22	11	0.15
1x4	0.5	0.26	130	25	12	0.3
1x5	0.65	0.36	200	27	13	0.4

5.2.2. Constant Pressure Production from Vertical Wells

Same reservoir models used for constant rate production scheme were used for constant pressure production cases. Unlike constant rate production case, pressure derivative plots obtained using constant pressure production data do not show the unit slope line during

boundary dominated flow. Hence, the time at the start of boundary dominated flow cannot be obtained from the log-log plots of pressure derivative and actual time.

Material balance time (MBT) was proposed by Blasingame and his students and is found to be more effective than actual time for constant pressure production case. When pressure derivative is plotted using material balance time function, it shows a horizontal line during transient radial flow and a unit slope line during boundary dominated flow. However, for identification of transient flow in real field data, a log-log plot of rate-normalized pressure vs. time works better than log-log plot of rate normalized pressure vs. material balance time (Jha & Lee 2017, Jha 2016). Equation (V.4) represents the mathematical expression for material balance time.

$$MBT = \frac{24N_p}{q} \qquad \text{(V.4)}$$

Here, N is the total oil produced in STB, and q is the rate of production at any time of interest. Therefore, in addition to the actual time used for plotting pressure derivatives, we have also used material balance time function to obtain and plot pressure derivative and normalized volume of investigation. APPENDIX C can be referred for pressure derivative and normalized volume of investigation plots obtained using actual time (section C-2) and material balance time (section C-3) for constant pressure production case.

Table V.5 summarizes the dimensionless actual time at the end of transient radial flow (TRF) for all the cases. It also shows the dimensionless actual time obtained from material balance time plot corresponding to the end of transient radial flow (TRF) and the start of

boundary dominated flow (BDF). It can be inferred that the dimensionless time values at the end of transient radial flow obtained from actual time plots for constant pressure production cases are similar to the values obtained for the corresponding constant rate production cases. From material balance time plots, dimensionless values of actual time obtained corresponding to the material balance time at the end of transient radial flow and the start of boundary dominated flow also appear to be quite similar to the values obtained from actual time plots. However, dimensionless material balance time at the end of transient radial flow and the start of boundary dominated flow are also comparable to those obtained from actual time plots and to those obtained in constant rate production case. Hence, we can conclude that for radial flow regimes, mode of production i.e. constant rate production or constant pressure production has negligible impact on the times to reach reservoir boundaries.

Table V.5 – Dimensionless actual time at the end of TRF and start of BDF (CPP)

Case $(l \times w)$	From p_D' vs. t_{DA} plot t_{DA} at the end of TRF	From p_D' vs. $(MBT)_{DA}$ plot		t_{DA} From CRP Eq.**
		t_{DA} at the end of TRF	t_{DA} at the start of BDF	
1x1 CPP	0.0638	0.0631	0.1281	0.0625
2x1 CPP	0.0353	0.0356	0.1952	0.03125
4x1 CPP	0.0179	0.0173	0.3668	0.015625
5x1 CPP	0.0135	0.0135	0.4106	0.0125

** CRP equation assumed to be correct for CPP case (Equation for ROI – CPP case is not available)

Table V.6 – Dimensionless material-balance time at the end of TRF and start of BDF (CPP)

Case	From p_D' vs. $(MBT)_{DA}$ plot		$(MBT)_{DA}$ From CRP Eq.
$(l \times w)$	$(MBT)_{DA}$ at the end of TRF	$(MBT)_{DA}$ at the start of BDF	using MBT time
1x1 CPP	0.0678	0.1389	0.0625
2x1 CPP	0.0382	0.2170	0.03125
4x1 CPP	0.0186	0.4443	0.015625
5x1 CPP	0.0147	0.5198	0.0125

Table V.7 – Normalized Volume of Investigation (NVOI) at the end of TRF and start of BDF (CPP)

Case	From $NVOI$ vs. t_{DA}	From $NVOI$ vs. $(MBT)_{DA}$	
$(l \times w)$	NVOI at the end of TRF	NVOI at the end of TRF	NVOI at the end of BDF
1x1 CPP	0.7167	0.7659	0.9897
2x1 CPP	0.4072	0.4402	0.9785
4x1 CPP	0.1999	0.2096	0.9844
5x1 CPP	0.1523	0.1662	0.9620

5.2.3. Discussion

Simulated production data obtained from a rigorous numerical simulator was used to determine times at the end of transient flow and the start of boundary dominated flow. Transient radial flow from vertical well is identified by a horizontal line on pressure derivative plot whereas boundary dominated flow is denoted by a unit slope line on the plot. A 5% deviation of the pressure derivative curve from both lines (i.e. horizontal line and unit slope line) was used to mark the end of transient flow and the start of boundary dominated flow. This 5% deviation is an arbitrary value and was chosen to confidently

53

identify flow regime markers considering the possible distortion in the derivatives of simulated pressure data. However, this 5% deviation might have slightly overestimated the time at the end of transient flow. Similarly, it might also have slightly underestimated the time at the start of boundary dominated flow as can be seen from the results shown in Table V.1 through Table V.5

5.3. Horizontal Wells in Rectangular – shaped Drainage Areas

In this section we will discuss horizontal wells with a vertical fracture of infinite conductivity centered in rectangular-shaped reservoirs with a different aspect ratio of their sides. The flow in these cases is assumed to be linear towards a single vertical fracture halfway across the length of the reservoir and occurring only in the simulated rock volume as shown in Fig. 5.3.1.

These cases can be extended to the case of a multi-fractured horizontal well with identical and equidistant fractures assuming the mid of fracture spacing as no flow boundaries for individual fractures. Flow from such wells during transient flow period is typical transient linear flow (TLF) identified by a half-slope line on the log-log plot of pressure derivatives. It is followed by a short transition period and then boundary dominated flow (BDF) starts indicated by a unit slop line. For determination of the end of transient flow into vertical fractures centered in rectangular drainage area, a half-slope line was fitted to the part of the data indicating transient linear flow, and a unit slope line was fitted to the part of data showing boundary dominated flow. Deviation of the pressure derivative curve from the half-slope line by 5% was used to mark the end of transient linear flow. Similarly, the

54

point where the deviation of the pressure derivative curve become less than 5% from the unit slope line was marked as the start of boundary dominated flow period. Although the limit of 5% deviation is arbitrary, it was used to confidently identify these flow regime markers while ignoring the distortions in the pressure derivatives.

Dimensionless variables used for pressure, time and distance are defined below:

$$p_D = \frac{k\sqrt{A_f}}{141.2 \, qB\mu}(p_i - p) \tag{V.5}$$

$$t_D = \frac{0.0002637kt}{\phi\mu c_t A_f} \tag{V.6}$$

$$x_D = \frac{x}{\sqrt{A_f}} \tag{V.7}$$

where, A_f is the fracture flow area ($= 4x_f h$) and it should be distinguished from the drainage area $A_d = 2x_f S_f$. Here x_f, h, and S_f denote the fracture half-length, reservoir height and fracture spacing, respectively. However, plotting variable for dimensionless time axis (x-axis) was modified by multiplying it with $4A_f/S_f$, hence, we can denote it by t_{DS_f}. Similarly, dimensionless pressure (y-axis) was multiplied by $2\sqrt{A_f}/S_f$ to obtain identical shaped pressure derivative for different cases (i.e. different combinations of A_d and A_f). Dimensionless variables are discussed in detail in APPENDIX A.
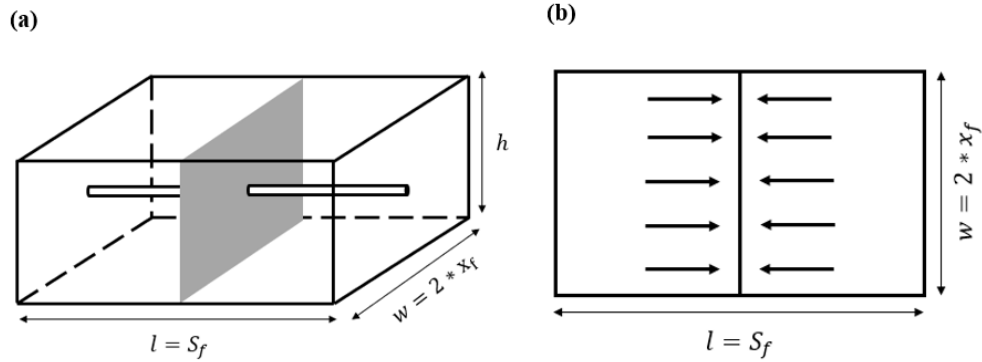
Fig. 5.3.1 – (a) Isometric view of reservoir model with horizontal well and vertical fracture, (b)Top View of reservoir showing reservoir dimensions and linear flow regime

5.3.1. Constant Rate Production from Horizontal Wells

Production data for linear flow from horizontal wells with vertical fractures under constant rate production was obtained using numerical simulations. Results were plotted using dimensionless variables to obtain comparable results for different reservoir configurations. Six different drainage area configurations (i.e. aspect ratio) were considered and the time at the end of transient linear flow (TLF) and the start of boundary dominated flow (BDF) were compared with those obtained from existing definition of the depth of investigation. Normalized volume of investigation (Spivey 2020) was also estimated for each case at these times.

Table V.8 and Table V.9 summarizes the results obtained from the synthetic production data and compares them with the standard values obtained from conventional definition of the depth of investigation (Lee 2003) and that presented by Clarkson (2014). Pressure derivative and normalized volume of investigation plots used to obtain these values for all

cases can be found in APPENDIX C, section C-4. From Table V.8, it can be seen that the conventional definition of the depth of investigation and that presented by Clarkson (2014) closely models the time at the start of boundary dominated flow. However, the estimated time at the start of boundary dominated flow might be less than the actual time because 5% limit was used to mark the star of boundary dominated flow.

Table V.8 – Dimensionless time at the end of TLF and start of BDF (CRP)

Case ($s_f \times 2x_f$)	t_{Dsf} at the end of TLF	t_{Dsf} at the start of BDF	t_{Dsf} (Analytical)	t_{Dsf} (Clarkson)
1x2 CRP	0.2827	0.3811		
1x1 CRP	0.2831	0.3987		
2x1 CRP	0.2773	0.3898	0.5	0.5
4x1 CRP	0.2854	0.3971		
5x1 CRP	0.2806	0.4053		
8x1 CRP	0.2797	0.4012		

Table V.9 – Normalized Volume of Investigation (NVOI) at the end of TLF and start of BDF (CRP)

Case ($s_f \times 2x_f$)	NVOI at the end of TLF	NVOI at the start of BDF
1x2 CRP	0.8903	0.9548
1x1 CRP	0.8895	0.9610
2x1 CRP	0.8856	0.9618
4x1 CRP	0.899	0.9708
5x1 CRP	0.8936	0.9753
8x1 CRP	0.8914	0.9704

Like vertical well cases, we have again used simulated production data in above examples. However, in practice, we may encounter problems associated with noisy data. Therefore, we have attempted to estimate flow regimes durations using drawdown curves which might be helpful for such real-life problems where noisy data might affect our interpretations. For this we have used superimposed analytical solutions for linear flow to obtain production data for different rectangular bounded reservoirs. The results are summarized in Table V.10 and Table V.11. For transient linear flow (TLF), we used deviation from the half-slope line on the log-log plot to estimate the time at the end of TLF. Whereas for boundary dominated flow (BDF), we used percentage deviation from the unit slope line on log-log plot to identify the start of BDF. We have presented results using conventional dimensionless time in terms of fracture flow area, t_{A_fD} (Table V.10) and dimensionless times in terms of fracture spacing, t_{S_fD} (Table V.11).

Table V.10 – Dimensionless time (t_{A_fD}) using drawdown curves

Cases	End of TLF, t_{A_fD}			Start of BDF, t_{A_fD}		
	At 1% deviation*	At 5% deviation*	At 10% deviation*	At 1% deviation*	At 5% deviation*	At 10% deviation*
2x1	0.12	0.21	0.29	13	2.5	1.2
1x1	0.35	0.59	0.83	37	7	3.3
1x2	0.99	1.6	2.3	110	20	9.4
1x4	2.8	4.7	6.6	300	56	27
1x5	3.9	6.6	9.3	410	78	37
1x8	7.9	13	18	830	160	75

Table V.11 – Dimensionless time (t_{S_fD}) using drawdown curves

Cases	End of TLF, t_{A_fD}			Start of BDF, t_{A_fD}		
	At 1% deviation*	At 5% deviation*	At 10% deviation*	At 1% deviation*	At 5% deviation*	At 10% deviation*
2x1	0.30855	0.53997	0.74568	33.42686	6.42824	3.08555
1x1	0.31818	0.53636	0.75455	33.63636	6.36363	3.00000
1x2	0.31819	0.51426	0.73925	35.35533	6.42824	3.02127
1x4	0.31818	0.53409	0.75000	34.09090	6.36363	3.06818
1x5	0.31711	0.53666	0.75620	33.33774	6.34230	3.00852
1x8	0.31739	0.52229	0.72317	33.34651	6.42824	3.01323

5.3.2. Constant Pressure Production from Horizontal Wells

Constant pressure production cases were run on the same reservoir models used for constant rate production. Since unit slope line is not observed in constant pressure production, pressure derivatives and normalized volumes of investigation were plotted using actual time and material balance time for each case. These plots can be found in APPENDIX C under section C-5 (actual time plots) and section C-6 (material balance time plots).

Table V.12 summarizes the dimensionless actual time at the end of transient linear flow (TLF) obtained from pressure derivatives calculated using actual dimensionless time and compares them with the values obtained from existing definitions of depth of investigation. It also shows the dimensionless actual time obtained from material balance time plots corresponding to the dimensionless material balance time at the end of transient

radial flow (TLF) and the start of boundary dominated flow (BDF). It can be inferred that the conventional definition of depth of investigation more closely models the start of boundary dominated flow whereas the definition presented by Clarkson (2014) for constant pressure production case is close to the dimensionless time at the end of transient linear flow empirically obtained from production data. However, the normalized volume of investigation values only ranges between ~0.45 – 0.46 at the time at the end of transient linear flow.

Table V.13 summarizes the results obtained pressure derivatives calculated using material balance time and compares them with the conventional depth of investigation equations for constant rate production when used with the material balance time. Both the conventional definition of depth of investigation and the definition presented by Clarkson (2014) more closely models the time at the start of boundary dominated flow. This observation is also validated by the normalized volume of investigation that ranges between ~0.97 – 0.98 at the material balance time at the start of boundary dominated flow as shown in Table 5.10.

Table V.12 – Dimensionless actual time at the end of TLF and start of BDF (CPP)

Case $(s_f \times 2x_f)$	From p'_D vs. t_{Dsf} plot	From p'_D vs. $(MBT)_{Dsf}$ plot		t_{Dsf} From CPP Eq.	t_D (Clarkson)
	t_{Dsf} at the end of TLF	t_{Dsf} at the end of TLF	t_{Dsf} at the start of BDF		
1x2 CPP	0.1636	0.1882	0.2270		
1x1 CPP	0.1657	0.1916	0.2279		
2x1 CPP	0.1612	0.1845	0.2243	0.25	1/6 (=0.1667)
4x1 CPP	0.1634	0.1867	0.2230		
5x1 CPP	0.1616	0.1992	0.2490		
8x1 CPP	0.1610	0.1841	0.2238		

Table V.13 – Dimensionless material-balance time at the end of TLF and start of BDF (CPP)

Case $(s_f \times 2x_f)$	From p'_D vs. $(MBT)_{Dsf}$ plot		$(MBT)_{Dsf}$ From CRP Eq. using MBT	t_D from Clarkson CRP Eq. using MBT
	$(MBT)_{Dsf}$ at the end of TLF	$(MBT)_{Dsf}$ at the start of BDF		
1x2 CPP	0.3746	0.4612		
1x1 CPP	0.3861	0.4648		
2x1 CPP	0.3713	0.4570	0.5	0.5
4x1 CPP	0.3724	0.4533		
5x1 CPP	0.3781	0.4578		
8x1 CPP	0.3707	0.4563		

Table V.14 – Normalized Volume of Investigation (NVOI) at the end of TLF and start of BDF (CPP)

Case $(s_f \times 2x_f)$	From $NVOI$ vs. t_{Dsf}	From $NVOI$ vs. $(MBT)_{Dsf}$	
	NVOI at the end of TLF	NVOI at the end of TLF	NVOI at the end of BDF
1x2 CPP	0.4344	0.9329	0.9785
1x1 CPP	0.4341	0.9390	0.9789
2x1 CPP	0.4343	0.9323	0.9785
4x1 CPP	0.4341	0.9310	0.9751
5x1 CPP	0.4536	0.9266	0.9659
8x1 CPP	0.4345	0.9325	0.9786

5.3.3. Discussion

The time at the end of transient linear flow and at the start of boundary dominated flow for horizontal wells under constant rate production and constant pressure production was estimated using simulated data for different reservoir configurations. These times were estimated from the deviation observed in pressure derivative curve. The time where pressure derivative deviated from half-slop line by 5% was marked as the end of the transient flow. Similarly, the point where the deviation of the pressure derivative curve from the unit slope line become less than 5% was marked as the start of boundary dominated flow. Assuming the 5% deviation, the time at the end of transient flow was somewhat estimated optimistically, that the actual time at the end of transient flow might be slightly less than the estimated time. Similarly, the actual time at the start of boundary dominated flow might be slightly more than the estimated time at the start of boundary dominated flow.

The results from constant rate production case show that the conventional definition of the depth of investigation for linear flow most closely models the start of boundary dominated flow instead of the end of transient flow. The estimated time at the end of boundary dominated flow is ~0.4 in dimensionless time units, and the corresponding value obtained from conventional definition of the depth of investigation for linear flow constant rate production is 0.5. The depth of investigation expression presented by Clarkson (2014) also shows similar result (i.e. 0.5). This observation is also supported by the normalized volume of investigation values as shown in Table V.9. Normalized volume of investigation values determined at the time at the end of transient flow are in the ranges 0.89 – 0.99 whereas normalized volume of investigation values at the start of boundary dominated flow are in the ranges of ~0.96 – 0.97.

Constant pressure production cases were analyzed by plotting production data using actual time and material balance time. The results show that the conventional definition of the depth of investigation for linear flow more closely models the actual time at the start of boundary dominated flow obtained from material balance time plots. Whereas, the time obtained from Clarkson's equation for constant pressure production more closely models the actual time at the end of transient linear flow (TLF) obtained from actual time plots. However, the time obtained from conventional definition of depth of investigation for constant rate production condition (material balance time used for constant pressure production) more closely models the material balance time at the start of boundary dominated flow obtained from material balance time plots.

CHAPTER VI

OUTLIERS DETECTION

6.1. Introduction

Field data often contain large noise due to multiple shut-ins and operational issues resulting in poor data quality and decision making. Presence of large number of outliers may significantly compromise our ability to infer results from the model fitted to the noisy data. To fix this problem, field engineers often manually remove outliers based on their subjective judgement. This may introduce significant statistical bias in their results.

Therefore, we aim to implement a popular published outlier detection technique, i.e., Angle Based Outlier Detection (ABOD) as presented by Kriegel et al. (2008) for objective identification of outliers and their removal from production data. Kriegel et al. (2008) presented this method for outlier detection in high dimensional data, however, this method has been found to be equally applicable for our case of two-dimensional pressure data.

6.2. The Concept and the Method

The basic idea behind the angle-based outlier detection method is that within a cluster of data points if a point is well inside the cluster, the angles it will make with other points in the data set will have high variability than the variability of the angles of a point outside of the cluster as shown in Fig. 6.2.1. Therefore, the measurement of the variance of the angles of a point that it makes with other points can be used to classify it as either an inlier or an outlier.
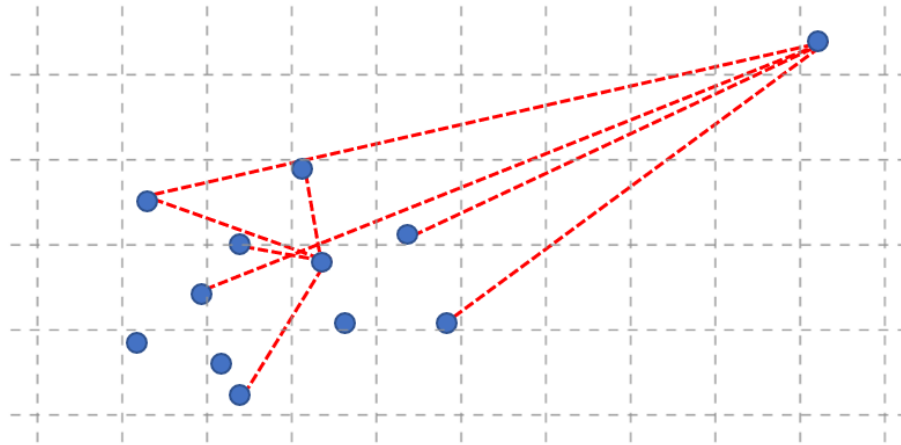
Fig. 6.2.1 – Difference in variation of angles for an inlier and an outlier

In this method, we calculate ABOF (angle-based outlier factor) for each point in the data set. To determine ABOF for our point of interest, we first calculate the scalar product of the difference vectors that our point of interest forms with any other two points in the data set, and we divide it by the magnitudes of the two vectors to obtain the cosine value of the angle between the vectors. This value is then normalized by dividing it again by the magnitudes of the vectors so that points that are far away from the point of concern are weighted less. This weighted cosine value is calculated for all possible pairs of the difference vectors that our point of interest forms and the variance of these values is the ABOF of the point. The ABOF is calculated for all the points in the data set and the points are ranked in increasing order of the ABOF. The first ranked point is the outermost point in the data and can be considered an outlier. Similarly, depending on the percentage of

noise in our data set, we can intuitively identify outliers from the ABOF ranked list of the data points. Here we list down some pros and cons of the fast ABOD method.

6.2.1. Pros

- Not a model-based approach – no assumptions on the distribution of outlier or inlier data points

- Works better than distance-based approaches for multi-dimensional data

6.2.2. Cons

- Scalability – $O(n^2 + nk^2)$ due to pairwise distance calculation between all points

- Subjective interpretation of the threshold value of ABOF

6.3. Application and Results

For the application of fast ABOD method, synthetic production data was used as shown in Fig. 6.3.1. I this data, random Gaussian noise was added. For this purpose, time series data was divided into n equal groups among which half of the groups were randomly selected. In those randomly selected groups of data, random Gaussian noise was added in 80% of the data points. Therefore, noise was added in almost 40% of the total number of data points as shown in Fig. 6.3.2.

We applied fast ABOD model on our synthetic data with noise to evaluate its performance. A Python code was used to run the model thru a series of values of k and $ABOF_{threshold}$. $ABOF_{threshold}$ is an arbitrary value based on that a user can decide about a point being an

inlier or an outlier. A relatively lower value will declare less points as outliers and a higher

value would result in high number of detected outliers. For minimum mean absolute error

(MAE), the best value of $ABOF_{threshold} = 1.18e - 17$ (which shows ~44% of points as

outliers) and a minimum number of $k = 5$ nearest neighbors was selected.
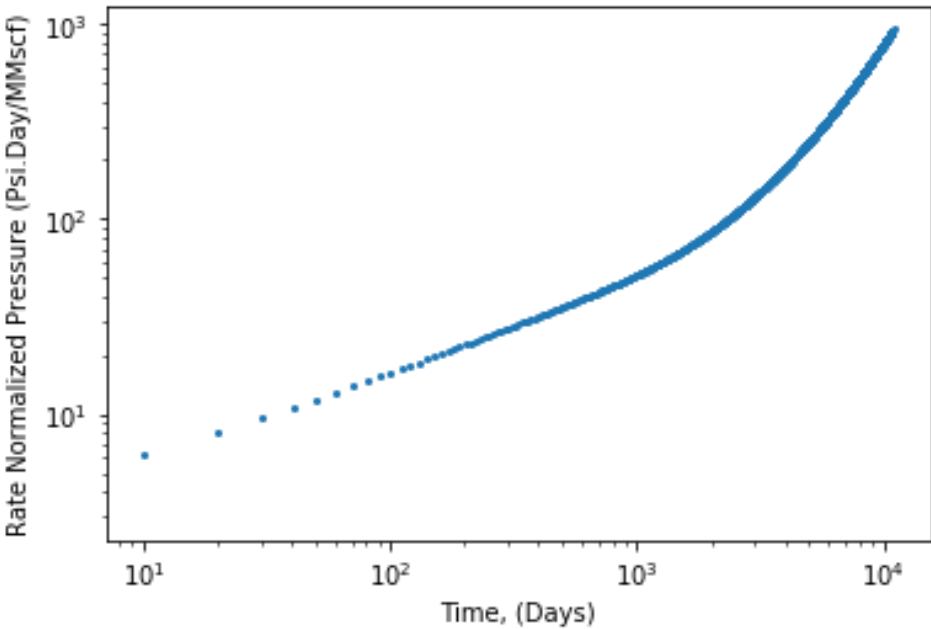
Fig. 6.3.1 – Synthetic production data
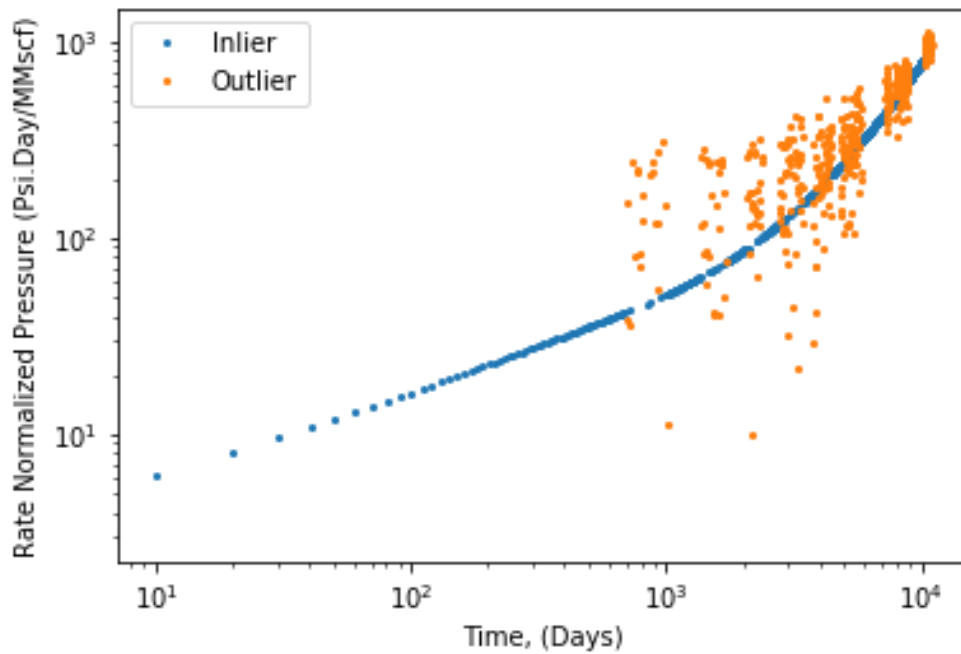
Fig. 6.3.2 – Synthetic production data with random noise

Fig. 6.3.3 shows plot of the synthetic data with noise after application of Fast ABOD algorithm. It shows four categories of data, i.e. True Positive (TP), True Negative (TN), False Positive (FP) and False Negative (FN). True Positive are those which contained noise and are correctly identified as outliers by the algorithm. Similarly, True Negative are those points which were correctly identified as inliers. False Negative are those points which are outliers but wrongly identified as inliers whereas False Positive are those data points which are inliers and are wrongly identified as outliers.

The results of this method show that 97% outliers were successfully detected out of actual number of outliers in the data, while the rest of the 3% were falsely predicted inliers.

68

Among actual inliers in the data, 89% of the points were detected correctly whereas the remaining 11% were falsely predicted. These results and the optimal values of fast ABOD parameters i.e. $ABOF_{threshold}$ and k, are summarized in Fig. 6.3.3 and the a plot of Angle Based Outlier Factors (ABOF) of all data points is shown in Fig. 6.3.5 .
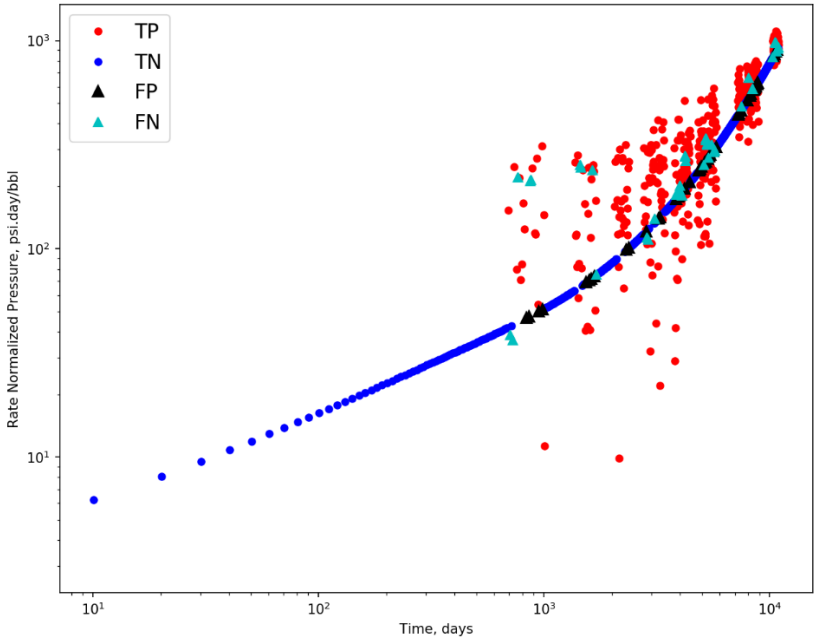
Fig. 6.3.3 – Fast ABOD results

Parameters	Value
k	5
ABOF	5.4e-16

		Truth	
		Outlier	Inlier
Prediction	Outlier	$TP \approx 97\%$	$FP \approx 11\%$	$P^* = 108\%$
Prediction	Inlier	$FN \approx 3\%$	$TN \approx 89\%$	$N^* = 92\%$
		$P = 100\%$	$N = 100\%$

Fig. 6.3.4 – Model parameters and truth table
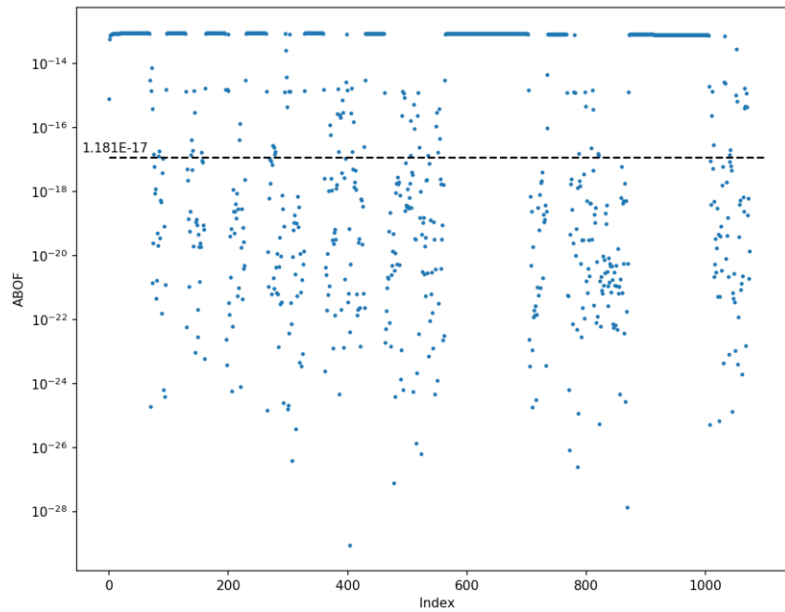
Fig. 6.3.5 – Angle Based Outlier Factor (ABOF)

70

Now that we have applied and evaluated FastABOD algorithm using synthetic data, we will use this method for outlier's identification and removal from actual field data. The clean data might then be used for calculation of Bourdet derivatives. Fig. 6.3.6 shows the results. Data points colored red are those which are identified as outliers whereas data points which are colored blue are identified as inliers by the algorithm. We can see that the algorithm has successfully identified 'obvious' outliers while keeping the overall trend of the data.

We have also compared the drawdown and derivative curves for three cases i.e. actual data (no points removed), with 30% data removed, and with 50% data removed. And for each case we have used three different Bourdet's smoothening parameter values i.e. 0.1, 0.3 and 0.5. The results are shown in Fig. 6.3.7 through Fig. 6.3.15. FastABOD algorithm works effectively in removing outliers as can be seen from the figures with increasing number of outliers removed. However, removing higher percentage of points from the data or using large values of Bourdet's smoothening parameter might affect the shape of the derivative curve.
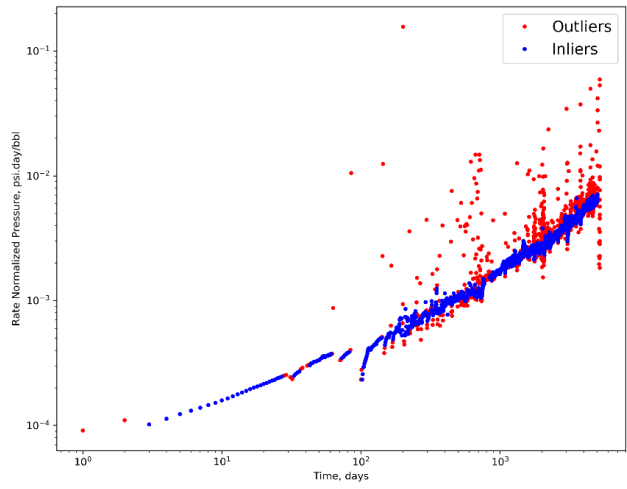
Fig. 6.3.6 – Identification of outliers using actual field data
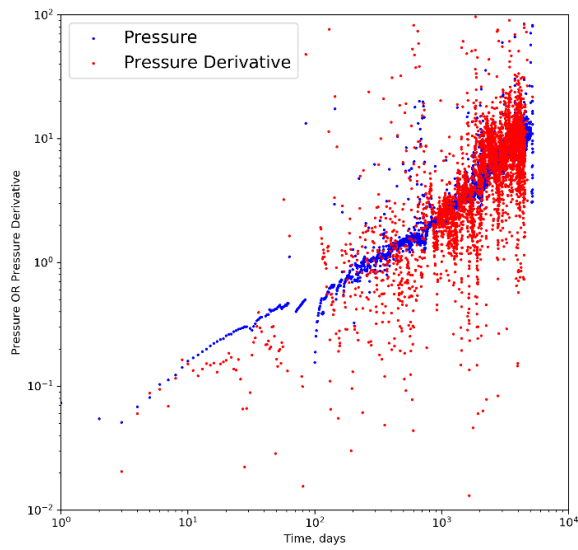
Fig. 6.3.7 – Pressure and pressure derivative of actual data with $L = 0.1$
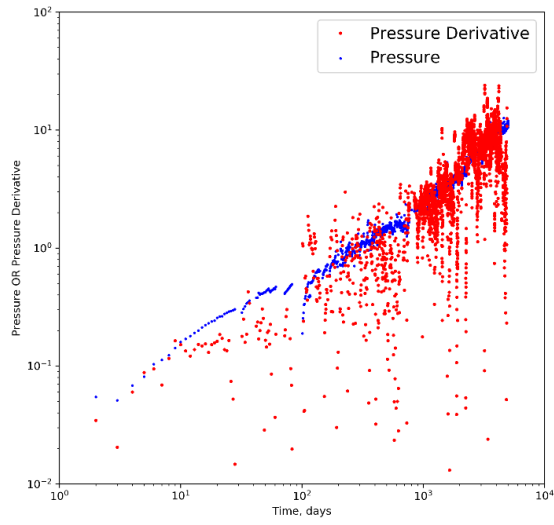
Fig. 6.3.8 – Pressure and pressure derivative of actual data with $L = 0.3$
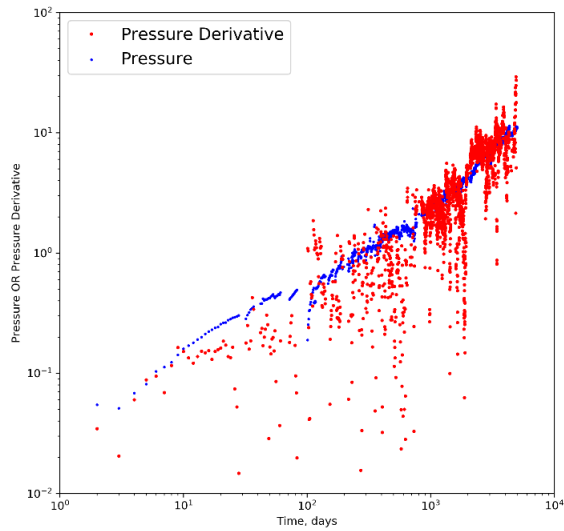
Fig. 6.3.9 – Pressure and pressure derivative of actual data with $L = 0.5$

73
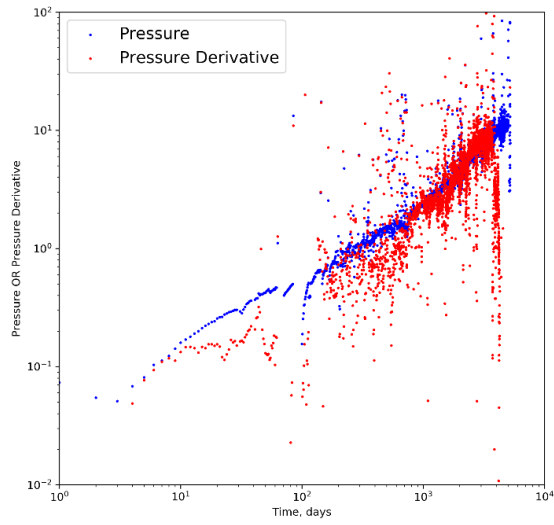
Fig. 6.3.10 – Pressure and pressure derivative with 30% data removed with $L = 0.1$
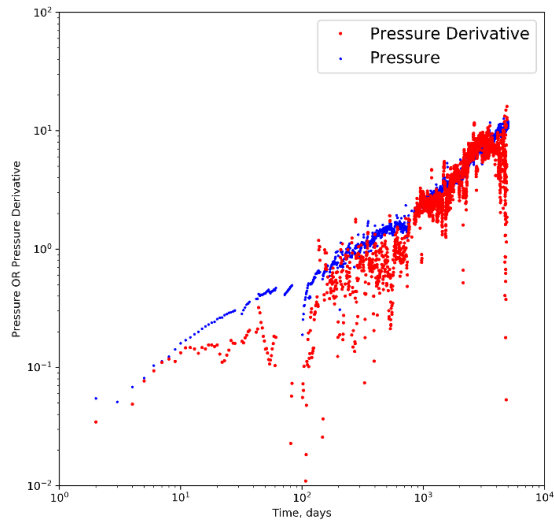
Fig. 6.3.11 – Pressure and pressure derivative with 30% data removed with $L = 0.3$

74
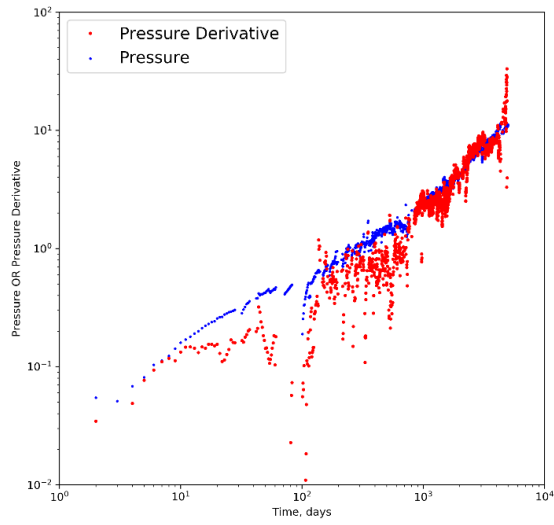
Fig. 6.3.12 – Pressure and pressure derivative with 30% data removed with $L = 0.5$
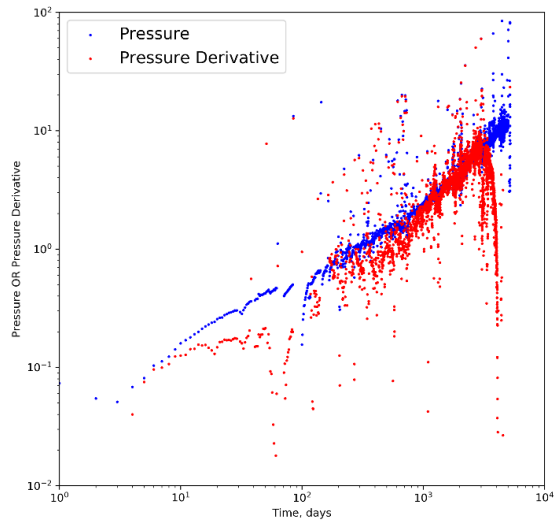
Fig. 6.3.13 – Pressure and pressure derivative with 50% data removed with $L = 0.1$
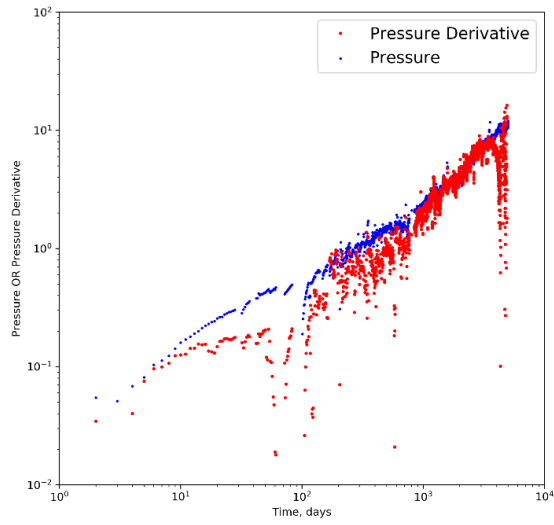
Fig. 6.3.14 – Pressure and pressure derivative with 50% data removed with $L = 0.3$
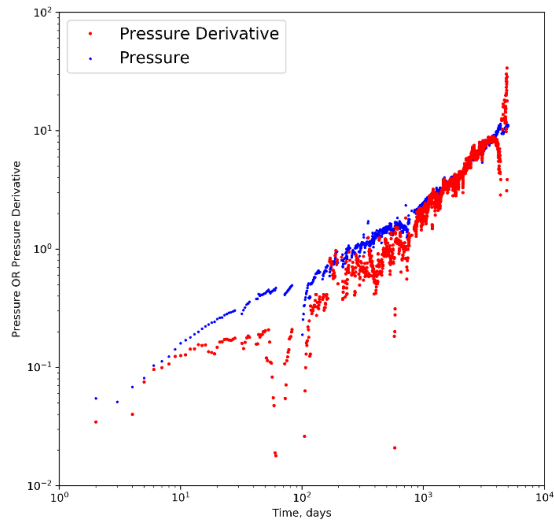
Fig. 6.3.15 – Pressure and pressure derivative with 50% data removed with $L = 0.5$

76

6.4. Discussion

In this chapter, we presented the results of an outlier detection method, i.e. ABOD, using synthetic production data. We applied a modified form of Angle Based Outlier Detection method i.e. *Fast ABOD* to synthetic production data with random gaussian noise added to known data points. Therefore, we already had the knowledge which data points contained noise and which points did not contain noise. Thus, we were able to evaluate the performance of the outlier detection method. Fig. 6.3.4 shows a summary of model parameters used and the truth table of production data. About 108% data points were identified as outliers i.e. 8% (P^*) outliers were over-predicted. Among them, 97% were those points which actually contained some noise, whereas, 7% of the points were wrongly identified as outliers. Similarly, 92% of data points were identified as inliers i.e. 8% (N^*) inliers were under-predicted. Among them, about 89% data points were those which actually did not contain any noise, whereas, only 3% data points were wrongly identified as inliers. These results show that angle based outlier detection method is quite useful in detection of outliers in production data.

CHAPTER VII

SUMMARY & CONCLUSIONS

Following is the summary and conclusions of this work:

1. Shape factors for pseudo-steady state equation were calculated for linear flow in rectangular shaped drainage areas of different aspect ratios i.e. $2x_f/S_f$. For more practical purposes where $2x_f/S_f < 0.5$, shape factor values were found to be changing drastically for small changes in aspect ratio. Therefore, care should be taken while selecting shape factor values for such cases.

2. Times at the end of transient flow and at the start of boundary dominated flow for various drainage area configurations were estimated from Bourdet pressure derivatives using synthetic production data for constant rate production and constant pressure production cases. For constant rate production cases, pressure derivatives were obtained using actual time while for constant pressure production cases derivatives were obtained using actual time and material balance time. The plots of pressure derivatives for all cases can be found in APPENDIX C.

3. For vertical wells in rectangular drainage areas (i.e. radial flow case), the time at the end of transient radial flow was found to be comparable with the conventional definition of radius of investigation for the time to reach the nearest boundary irrespective of the inner boundary condition at the well i.e. constant rate production or constant pressure production.

4. For horizontal wells with vertical fractures in rectangular drainage areas (i.e. linear flow case), the times at the end of transient flow and at the start of boundary dominated flow were different for constant rate production and constant pressure production cases. For constant rate production, the estimated time at the start of the boundary dominated flow was close to that obtained from existing analytical definitions. For constant pressure production, production data from each was plotted using actual time and material balance time. The time at the end of transient linear flow obtained from actual time plot was comparable to the time presented by Clarkson (2014) for constant pressure production, whereas, the material balance time at the start of boundary dominated flow obtained from material balance time plots was comparable to the time obtained from conventional definition of depth of investigation for constant rate production. However, the corresponding actual time at the start of boundary dominated flow obtained from material balance time plots was found to be comparable with the time from conventional definition of depth of investigation for constant pressure production.

5. Angle Based Outlier Detection (ABOD) method was evaluated using synthetic production data with synthetic random gaussian noise. The method has been found to be effective in objective identification and removal of outliers from production data.

NOMENCLATURE

a_{iD}	dimensionless distance of ith image well
A_d	drainage Area, ft^2.
A_f	fracture flow area, ft^2.
ABOD	angle-based outlier detection
ABOF	angle-based outlier factor
B	formation volume factor, bbl./STB
B_i	initial formation volume factor, bbl./STB
BDF	boundary dominated flow
c_t	total compressibility, psi^{-1}
C_A	drainage area shape factor
CPP	constant pressure production
CRP	constant rate production
ERF	end of radial flow
FN	false negative
FP	false positive
h	reservoir thickness, ft.
k	permeability, md
l	length of reservoir, ft.
l_i	depth of investigation, ft.
MAE	mean absolute error
MBT	material balance time
$(MBT)_{AD}$	dimensionless material balance time based on drainage area
$(MBT)_{S_fD}$	dimensionless material balance time based on fracture spacing
N_p	total oil produced, STB
NVOI	normalized volume of investigation
p	pressure, psia
p_D	dimensionless pressure
p'_D	dimensionless pressure derivative

p_i	initial pressure, psia
p_w	wellbore pressure, psia
p_{wD}	dimensionless pressure-drop at the wellbore
p_{wf}	flowing bottom-hole pressure, psia
$\bar{p}$	average pressure, psia
p^*	shut-in pressure extrapolated to infinite shut-in time on a semi-log plot of pressure vs. $[\Delta t/(t + \Delta t)]$
PSS	pseudo steady state
q	oil flowrate, STB/D
q_D	dimensionless flowrate
r	radius, ft.
r_D	dimensionless radius
r_i	radius of investigation, ft.
r_w	wellbore radius, ft.
s	skin factor, dimensionless
S	instantaneous source function
S_f	fracture spacing, ft.
t	time, hours
t_D	dimensionless time
t_{DA}	dimensionless time based on drainage area
t_{Dxf}	dimensionless time based on x_f
$t_{S_f D}$	dimensionless time based on fracture spacing
TLF	transient linear flow
TN	true negative
TP	true positive
TRF	transient radial flow
V_{bi}	investigated bulk volume, ft^3
V_{pi}	investigated pore volume, ft^3
w	width of reservoir, ft.

x	distance from fracture
x_f	fracture half-length, ft.
x_D	dimensionless distance from fracture
x_{iD}	dimensionless distance of ith image well
X	time function change
y_e	distance from fracture to reservoir boundary, ft.
γ	Euler's constant (0.5772156649…)
Δp	pressure change, psi
η	hydraulic diffusivity, md-psi/cp
λ	interporosity flow coefficient, dimensionless
μ	fluid viscosity, cp
π	pi constant, i.e. ratio of circumference to the diameter of a circle (3.14159…)
ϕ	porosity, fraction
ω	storativity ratio, dimensionless

REFERENCES

Aguilera, R. (2006, December 1). Radius and Linear Distance of Investigation and Interconnected Pore Volume in Naturally Fractured Reservoirs. Petroleum Society of Canada. doi:10.2118/06-12-04

Anderson, D. M., & Mattar, L. (2007, July 1). An Improved Pseudo-Time for Gas Reservoirs with Significant Transient Flow. Petroleum Society of Canada. doi:10.2118/07-07-05

Ayoub, J. A., Bourdet, D. P., & Chauvel, Y. L. (1988, September 1). Impulse Testing. Society of Petroleum Engineers. doi:10.2118/15911-PA

Behmanesh, H., Tabatabaie, S. H., Heidari Sureshjani, M., & Clarkson, C. R. (2014, April 1). Modification of the Transient Linear Flow Distance of Investigation Calculation for Use in Hydraulic Fracture Property Determination. Society of Petroleum Engineers. doi:10.2118/168981-MS

Brons, F., & Miller, W. C. (1961, August 1). A Simple Method for Correcting Spot Pressure Readings. Society of Petroleum Engineers. doi:10.2118/1610-G-PA

Carslaw, H. S., & Jaeger, J. C. (1992). Conduction of heat in solids (No. BOOK). Clarendon press.

Datta-Gupta, A., Xie, J., Gupta, N., King, M. J., & Lee, W. J. (2011, July 1). Radius of Investigation and its Generalization to Unconventional Reservoirs. Society of Petroleum Engineers. doi:10.2118/0711-0052-JPT

Dietz, D. N. (1965, August 1). Determination of Average Reservoir Pressure from Build-Up Surveys. Society of Petroleum Engineers. doi:10.2118/1156-PA

Earlougher, R. C. (1968, May 1). The Use of Interpolation to Obtain Shape Factors for Pressure Buildup Calculations. Society of Petroleum Engineers. doi:10.2118/2115-PA

Earlougher, R. C., Ramey, H. J., Miller, F. G., & Mueller, T. D. (1968, February 1). Pressure Distributions in Rectangular Reservoirs. Society of Petroleum Engineers. doi:10.2118/1956-PA

Ehlig-Economides, C. A. (1992, January 1). Computation of Test Area of Investigation in Nonradial Geometries. Society of Petroleum Engineers. doi:10.2118/25020-MS

Gringarten, A. C., Bourdet, D. P., Landel, P. A., & Kniazeff, V. J. (1979, January 1). A Comparison Between Different Skin And Wellbore Storage Type-Curves For Early-Time Transient Analysis. Society of Petroleum Engineers. doi:10.2118/8205-MS

Horner, D. R. (1951, January 1). Pressure Build-up in Wells. World Petroleum Congress.

Hsieh, B. Z., Chilingar, G. V. & Lin, Z. S. (2007). Propagation of Radius of Investigation from Producing Well. Energy Sources, Part A, 29:5, 403-417. doi:10.1080/15567030601003759

Jha, H. S. (2016). Inclusion of Fracture Skin in Duong's Model of Rate-Decline Analysis For Fracture-Dominated Shale Reservoirs. doi:https://hdl.handle.net/10657/5418

Jha, H. S., & Lee, W. J. (2017, July 24). Modifications for Fracture Damage and Changing Pressure Drawdown to Improve Accuracy of Duong Decline Model. Unconventional Resources Technology Conference. doi:10.15530/URTEC-2017-2697591

Jha, H. S., & Lee, W. J. (2017, July 24). Problems with Application of Material Balance Time to Transient Flow Data in Diagnostic Plots. Unconventional Resources Technology Conference. doi:10.15530/URTEC-2017-2697627

Kutasov, I. M., & Hejri, S. (1984, January 1). Drainage radius of a well produced at constant Bottomhole Pressure in an infinite acting reservoir. Society of Petroleum Engineers. doi:NA

Lee, J., Rollins, J. B., & Spivey, J. P. (2003). Pressure transient testing. Richardson, Tex.: Henry L. Doherty Memorial Fund of AIME, Society of Petroleum Engineers.

Lee, W.J. 1982. Well Testing, second edition, SPE textbook series Volume 1. Society of Petroleum Engineers of AIME

Lord Kelvin (Sir William Thorns on): Mathematical and Physical Papers, Cambridge at the University Press (1884) Vol. II, 41

Matthews, C. S. and Russell, D. G.: *Pressure Buildup and Flow Tests in Wells,* Monograph Series, Society of Petroleum Engineers of AIME, Dallas (1967) 1, 110.

Matthews, C. S., Brons, F., & Hazebroek, P. (1954, December 1). A Method for Determination of Average Pressure in a Bounded Reservoir. Society of Petroleum Engineers. doi:10.2118/296-G

Newman, A. B. (1936). Heating and cooling rectangular and cylindrical solids. Industrial & Engineering Chemistry, 28(5), 545-548.

Nisle, R. G. (1958, December 1). The Effect of Partial Penetration on Pressure Build-Up in Oil Wells. Society of Petroleum Engineers. doi:10.2118/971-G

Oliver, D. S. (1990, September 1). The Averaging Process in Permeability Estimation from Well-Test Data. Society of Petroleum Engineers. doi:10.2118/19845-PA

Palacio, J. C., & Blasingame, T. A. (1993, January 1). Decline-Curve Analysis With Type Curves - Analysis of Gas Well Production Data. Society of Petroleum Engineers. doi:10.2118/25909-MS

Peaceman, D. W. (1990, January 1). Recalculation Of Dietz Shape Factor For Rectangles. Society of Petroleum Engineers.

Ramakrishnan, T.S., Prange, M.D. & Kuchuk, F.J. Radius of Investigation in Pressure Transient Testing. Transport in Porous Media 131, 783–804 (2020). doi: https://doi.org/10.1007/s11242-019-01367-y

Sobbi, F. A., & Badakhshan, A. (1994, January 1). Radius of Investigation For Well Tests In Dual Porosity Reservoirs. Petroleum Society of Canada. doi:10.2118/94-16

Spivey, J.P., Lee, W.J., & Sheikh, H.M.U. (2020). Transient Volume of Investigation: Definition, Theory, and Applications. Society of Petroleum Engineers. doi:10.2118/201414-PA

Tabatabaie, S. H., Pooladi-Darvish, M., & Mattar, L. (2017, October 9). Distance of Investigation for Unconventional Reservoirs Could be Misleading. Society of Petroleum Engineers. doi:10.2118/187077-MS

Tek, M. R., Grove, M. L., & Poettmann, F. H. (1957, December 1). Method for Predicting the Back-Pressure Behavior of Low Permeability Natural Gas Wells. Society of Petroleum Engineers. doi:10.2118/770-G

Theory and Practice of the Testing of Gas Wells, third edition. 1975. Energy Resources Conservation Board, Calgary, Alberta, Canada.

Xie, J., Yang, C., Gupta, N., King, M. J., & Datta-Gupta, A. (2015, August 1). Depth of Investigation and Depletion in Unconventional Reservoirs With Fast-Marching Methods. Society of Petroleum Engineers. doi:10.2118/154532-PA

APPENDIX A DIMENSIONLESS VARIABLES

A-1 Dimensionless Variables for Radial Flow

Radial flow of a slightly compressible liquid flow through an isotropic homogeneous reservoir is represented by:

$$\frac{1}{r}\frac{\partial}{\partial r}\left(r\frac{\partial p}{\partial r}\right) = \frac{\phi\mu c_t}{0.0002637k}\frac{\partial p}{\partial t} \tag{A.1}$$

From Darcy's law, we can write inner boundary condition for constant rate production case as:

$$\left(\frac{\partial p}{\partial r}\right)_{r=r_w} = -\frac{141.2qB\mu}{kh} \tag{A.2}$$

Here we define dimensionless variables as:

$$p_D = \frac{kh}{141.2qB\mu}(p_i - p) \tag{A.3}$$

$$t_D = \frac{0.0002637kt}{\phi\mu c_t r_w^2} \tag{A.4}$$

$$r_D = \frac{r}{r_w} \tag{A.5}$$

Differentiating equation (A.3) with respect to dimensionless distance r_D using chain rule,

$$\frac{\partial p_D}{\partial r_D} = \frac{\partial p_D}{\partial r} * \frac{\partial r}{\partial r_D} \tag{A.6}$$

Or,

$$\frac{\partial p_D}{\partial r_D} = \frac{\partial}{\partial r}\left[\frac{kh}{141.2qB\mu}(p_i - p)\right] * \frac{\partial}{\partial r_D}[r_D r_w]$$

(A.7)

Or,

$$\frac{\partial p_D}{\partial r_D} = \left[-\frac{kh}{141.2qB\mu}\right]\frac{\partial p}{\partial r} * r_w$$

(A.8)

At $r = r_w$, or, $r_D = 1$,

$$\left(\frac{\partial p_D}{\partial r_D}\right)_{r_D=1} = \left[-\frac{kh}{141.2qB\mu}\right]\left(\frac{\partial p}{\partial r}\right)_{r=r_W}$$

(A.9)

Substituting equation (A.2)

$$\left(\frac{\partial p_D}{\partial r_D}\right)_{r_D=1} = \left[-\frac{kh}{141.2qB\mu}\right]\left[-\frac{141.2qB\mu}{kh}\right]$$

(A.10)

Or,

$$\left(\frac{\partial p_D}{\partial r_D}\right)_{r_D=1} = 1$$

(A.11)

which is the inner boundary condition in the dimensionless form.

Now, substituting dimensionless variables into equation (A.1).

$$\frac{1}{r_D r_w} \frac{\partial}{\partial (r_D r_w)} \left((r_D r_w) \frac{\partial \left(-\frac{141.2qB\mu}{kh} p_D + p_i \right)}{\partial (r_D r_w)} \right)$$

$$= \frac{\phi \mu c_t}{0.0002637k} \frac{\partial \left[-\frac{141.2qB\mu}{kh} p_D + p_i \right]}{\partial \left[\frac{\phi \mu c_t r_w^2}{0.0002637k} t_D \right]}$$

(A.12)

Or,

$$\frac{1}{r_w^2} \frac{1}{r_D} \frac{\partial}{\partial r_D} \left(r_D \frac{\partial \left(-\frac{141.2qB\mu}{kh} p_D + p_i \right)}{\partial r_D} \right)$$

$$= \frac{\phi \mu c_t}{0.0002637k} \frac{\partial \left[-\frac{141.2qB\mu}{kh} p_D + p_i \right]}{\partial \left[\frac{\phi \mu c_t r_w^2}{0.0002637k} t_D \right]}$$

(A.13)

Since, p_i is independent of time and space variables, its derivative would be zero. Also, taking out constant values from the derivatives.

$$\left(-\frac{141.2qB\mu}{kh} \right) \left(\frac{1}{r_w^2} \right) \frac{1}{r_D} \frac{\partial}{\partial r_D} \left(r_D \frac{\partial p_D}{\partial r_D} \right)$$

$$= \frac{\phi \mu c_t}{0.0002637k} \left(\frac{0.0002637kt}{\phi \mu c_t r_w^2} \right) \left(-\frac{141.2qB\mu}{kh} \right) \frac{\partial p_D}{\partial t_D}$$

(A.14)

Or,

$$\frac{1}{r_D} \frac{\partial}{\partial r_D} \left(r_D \frac{\partial p_D}{\partial r_D} \right) = \frac{\partial p_D}{\partial t_D}$$

(A.15)

Equation (A.15) is the partial differential equation for radial flow in terms of dimensionless variables.

88

A-2 Dimensionless Variables for Linear Flow

Linear flow of a slightly compressible liquid flow through an isotropic homogeneous reservoir is represented by:

$$\frac{\partial^2 p}{dx^2} = \frac{\phi \mu c_t}{0.0002637 k} \frac{\partial p}{\partial t} \tag{A.16}$$

From Darcy's law, we can write inner boundary condition for constant rate production case as:

$$\left(\frac{\partial p}{\partial x}\right)_{x=0} = -\frac{2\pi(141.2)qB\mu}{kA_f} \tag{A.17}$$

Or,

$$\left(\frac{\partial p}{\partial x}\right)_{x=0} = -\frac{887.2201 qB\mu}{kA_f} \tag{A.18}$$

Here we define dimensionless variables as:

$$p_D = \frac{k\sqrt{A_f}}{2\pi(141.2)qB\mu}(p_i - p) = \frac{k\sqrt{A_f}}{887.2201 qB\mu}(p_i - p) \tag{A.19}$$

$$t_D = \frac{0.0002637 kt}{\phi \mu c_t A} \tag{A.20}$$

$$x_D = \frac{x}{\sqrt{A_f}} \tag{A.21}$$

Differentiating equation (A.19) with respect to dimensionless distance x_D using chain rule,

$$\frac{\partial p_D}{\partial x_D} = \frac{\partial p_D}{\partial x} * \frac{\partial x}{\partial x_D} \qquad (A.22)$$

Or,

$$\frac{\partial p_D}{\partial x_D} = \frac{\partial}{\partial x}\left[\frac{k\sqrt{A_f}}{887.2201qB\mu}(p_i - p)\right] * \frac{\partial}{\partial x_D}\left[x_D\sqrt{A_f}\right] \qquad (A.23)$$

Or,

$$\frac{\partial p_D}{\partial x_D} = \left[-\frac{k\sqrt{A_f}}{887.2201qB\mu}\right]\frac{\partial p}{\partial x} * \sqrt{A_f} \qquad (A.24)$$

At $x = 0$, or, $x_D = 0$,

$$\left(\frac{\partial p_D}{\partial x_D}\right)_{x_D=0} = \left[-\frac{kA_f}{887.2201qB\mu}\right]\left(\frac{\partial p}{\partial x}\right)_{x=0} \qquad (A.25)$$

Substituting equation (A.18)

$$\left(\frac{\partial p_D}{\partial x_D}\right)_{x_D=0} = \left[-\frac{kA_f}{887.2201qB\mu}\right]\left[-\frac{887.2201qB\mu}{kA_f}\right] \qquad (A.26)$$

Or,

$$\left(\frac{\partial p_D}{\partial x_D}\right)_{x_D=0} = 1 \qquad (A.27)$$

which is the inner boundary condition in the dimensionless form.

Now, substituting dimensionless variables into equation (A.16).

$$\frac{\partial^2\left[-\dfrac{887.2201qB\mu}{k\sqrt{A_f}}p_D + p_i\right]}{d\left(x_D\sqrt{A_f}\right)^2} = \frac{\phi\mu c_t}{0.0002637k}\frac{\partial\left[-\dfrac{887.2201qB\mu}{k\sqrt{A_f}}p_D + p_i\right]}{\partial\left[\dfrac{\phi\mu c_t A}{0.0002637k}t_D\right]} \tag{A.28}$$

Or,

$$\left[-\frac{887.2201qB\mu}{k\sqrt{A_f}} * \frac{1}{A_f}\right]\frac{\partial^2 p_D}{dx_D{}^2}$$
$$= \frac{\phi\mu c_t}{0.0002637k}\left[-\frac{887.2201qB\mu}{k\sqrt{A_f}} * \frac{0.0002637k}{\phi\mu c_t A}\right]\frac{\partial p_D}{\partial t_D} \tag{A.29}$$

Or,

$$\frac{\partial^2 p_D}{dx_D{}^2} = \frac{\partial p_D}{\partial t_D} \tag{A.30}$$

Equation (A.30) is the partial differential equation for linear flow in terms of dimensionless variables.

Laplace domain solution of equation (A.30) for constant rate production condition is:

$$p_D(x_D, s) = \frac{1}{s\sqrt{s}}e^{-x_D\sqrt{s}} \tag{A.31}$$

From Roberts and Kaufman: Table of Laplace Transforms, Section 2, Equation 3.2.22, page 247:

$$\frac{1}{s\sqrt{s}}e^{-a\sqrt{s}} = 2\sqrt{\frac{t}{\pi}}e^{-\frac{a^2}{4t}} - a * erfc\left(\frac{a}{2\sqrt{t}}\right) \tag{A.32}$$

Therefore, equation (A.31) can be written in time domain as:

$$p_D(x_D, t_D) = 2\sqrt{\frac{t_D}{\pi}}\, e^{-\frac{x_D^2}{4t_D}} - x_D * erfc\left(\frac{x_D}{2\sqrt{t_D}}\right) \tag{A.33}$$

For $x_D = 0$,

$$p_D(0, t_D) = 2\sqrt{\frac{t_D}{\pi}} \tag{A.34}$$

Now substituting values of dimensionless pressure and dimensionless time:

$$\frac{k\sqrt{A_f}}{887.2201qB\mu}(p_i - p_{wf}) = \frac{2}{\sqrt{\pi}}\sqrt{\frac{0.0002637kt}{\phi\mu c_t A}} \tag{A.35}$$

Or, after simplification:

$$p_i - p_{wf} = 16.2564\frac{qB}{A_f}\left(\frac{\mu t}{k\phi c_t}\right)^{\frac{1}{2}} \tag{A.36}$$

Or, after substituting $A_f = 4x_f h$:

$$p_i - p_{wf} = 4.0641\frac{qB}{x_f h}\left(\frac{\mu t}{k\phi c_t}\right)^{\frac{1}{2}} \tag{A.37}$$

Now for constant rate production, we know the following constant pressure-constant rate convolution identity in Laplace domain:

$$p_D q_D = \frac{1}{s^2} \tag{A.38}$$

Or,

$$q_D = \frac{1}{p_D s^2} \tag{A.39}$$

Substituting equation (A.31) into equation (A.39):

$$q_D(x_D, s) = \frac{s\sqrt{s}\,1}{e^{-x_D\sqrt{s}}} * \frac{1}{s^2} \tag{A.40}$$

Or,

$$q_D(x_D, s) = \frac{e^{-(-x_D)\sqrt{s}}}{\sqrt{s}} \tag{A.41}$$

Equation (A.41) is the constant flowing bottom hole pressure solution of the partial differential equation in Laplace domain. From Roberts and Kaufman: Table of Laplace Transforms, Section 2, Equation 3.2.16, page 246:

$$\frac{e^{-x_D\sqrt{s}}}{\sqrt{s}} = \frac{e^{-\frac{a^2}{4t}}}{(\pi t)^{1/2}} \tag{A.42}$$

Therefore, equation (A.41) can be written in time domain as:

$$q_D(x_D, t_D) = \frac{e^{-\frac{x_D^2}{4t_D}}}{\sqrt{\pi t_D}} \tag{A.43}$$

Or at $x_D = 0$,

$$q_D(0, t_D) = \frac{1}{\sqrt{\pi t_D}} \tag{A.44}$$

Or,

$$\frac{1}{q_D} = \sqrt{\pi t_D}$$

(A.45)

Here we define dimensionless flow rate as:

$$q_D = \frac{2\pi(141.2)qB\mu}{k\sqrt{A_f}(p_i - p_{wf})} = \frac{887.2201qB\mu}{k\sqrt{A_f}(p_i - p_{wf})}$$

(A.46)

Now substituting dimensionless rate and dimensionless time into equation (A.45):

$$\frac{k\sqrt{A_f}(p_i - p_{wf})}{887.2201qB\mu} = \sqrt{\pi}\sqrt{\frac{0.0002637kt}{\phi\mu c_t A}}$$

(A.47)

Or, after simplification

$$\frac{p_i - p_{wf}}{q} = 25.53546\frac{B}{A_f}\left(\frac{\mu t}{k\phi c_t}\right)^{\frac{1}{2}}$$

(A.48)

Or, after substituting $A_f = 4x_f h$:

$$\frac{p_i - p_{wf}}{q} = 6.38386\frac{B}{x_f h}\left(\frac{\mu t}{k\phi c_t}\right)^{\frac{1}{2}}$$

(A.49)

APPENDIX B GRAPHS FOR SHAPE FACTORS
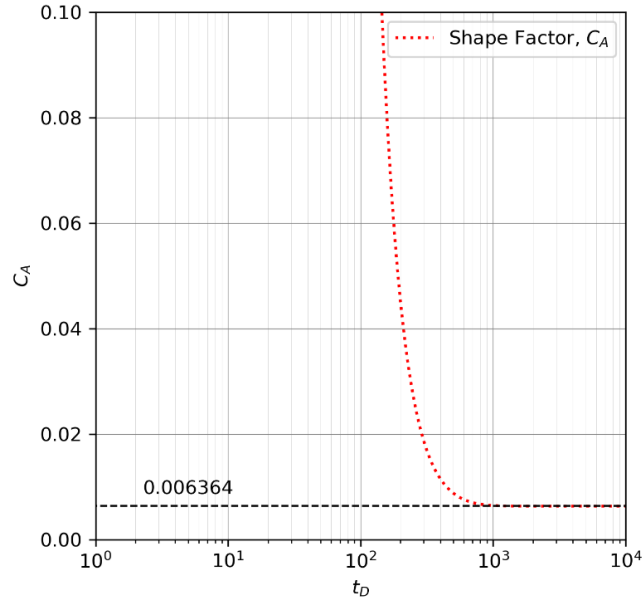
Fig. B.1 – Calculated shape factor, C_A for $2x_f : S_f = 1:10$
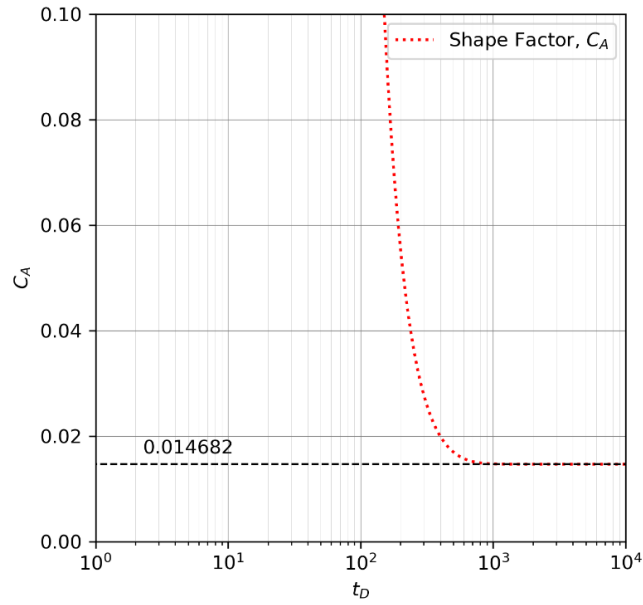
Fig. B.2 – Calculated shape factor, C_A for $2x_f : S_f = 1:9$
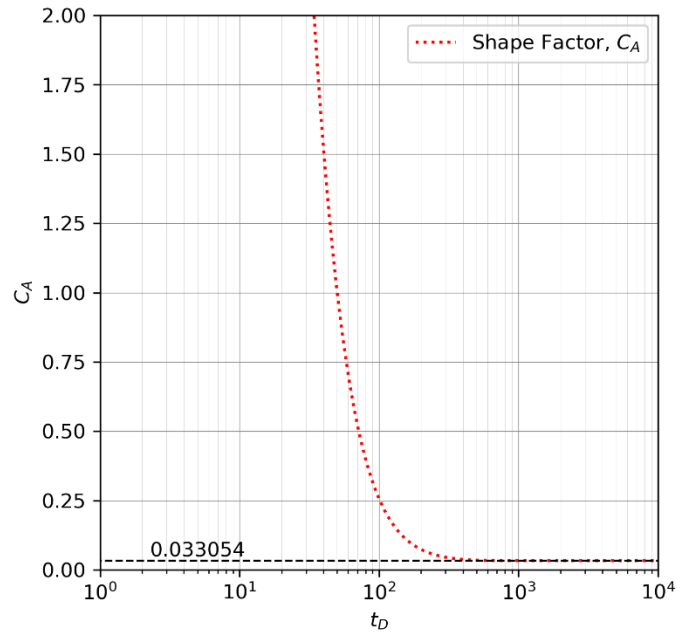
Fig. B.3 – Calculated shape factor, C_A for $2x_f : S_f = 1:8$
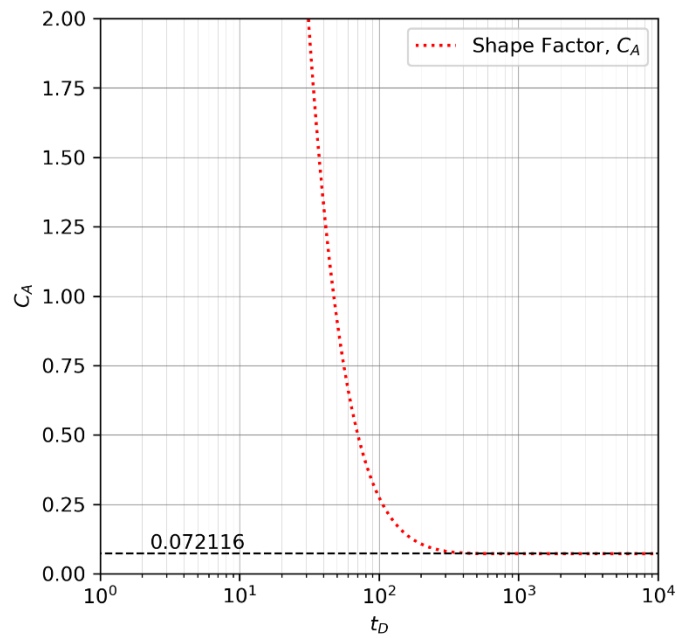
Fig. B.4 – Calculated shape factor, C_A for $2x_f : S_f = 1:7$
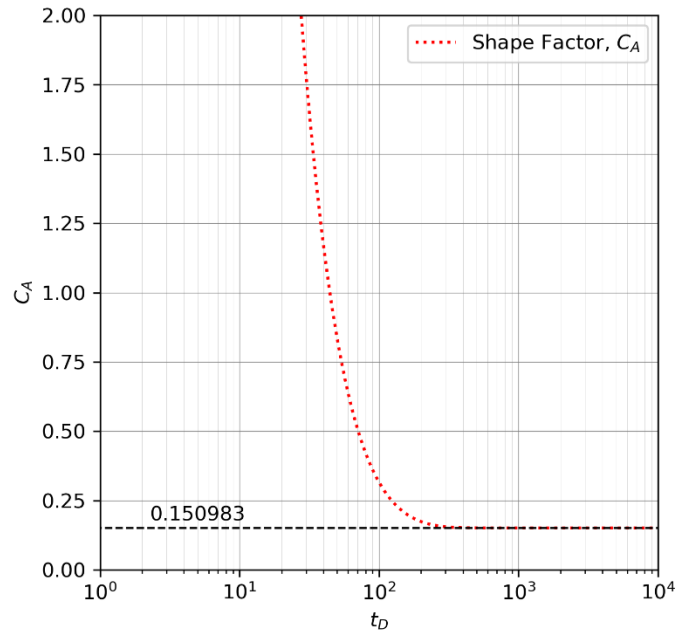
Fig. B.5 – Calculated shape factor, C_A for $2x_f : S_f = 1:6$
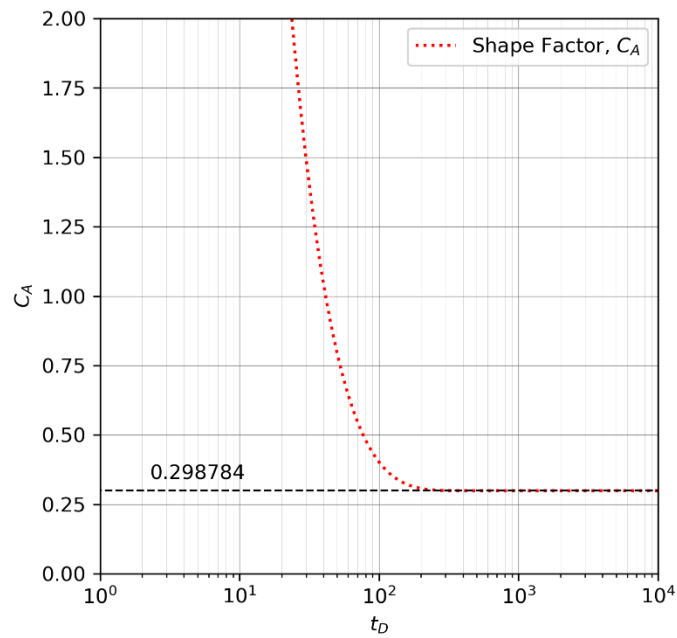
Fig. B.6 – Calculated shape factor, C_A for $2x_f : S_f = 1:5$
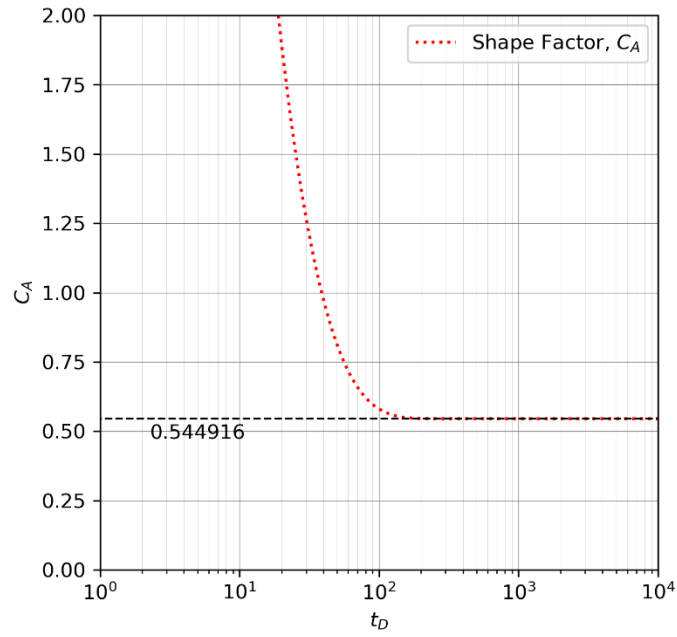
Fig. B.7 – Calculated shape factor, C_A for $2x_f : S_f = 1:4$
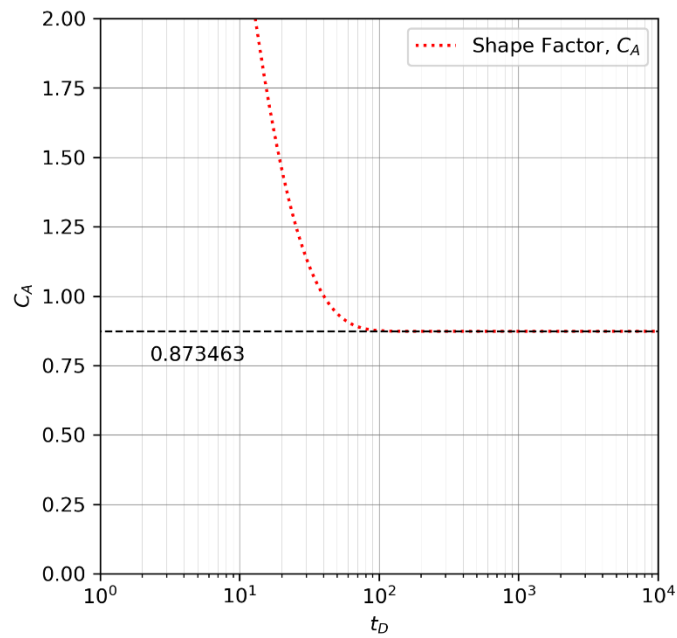
Fig. B.8 – Calculated shape factor, C_A for $2x_f : S_f = 1:3$

98
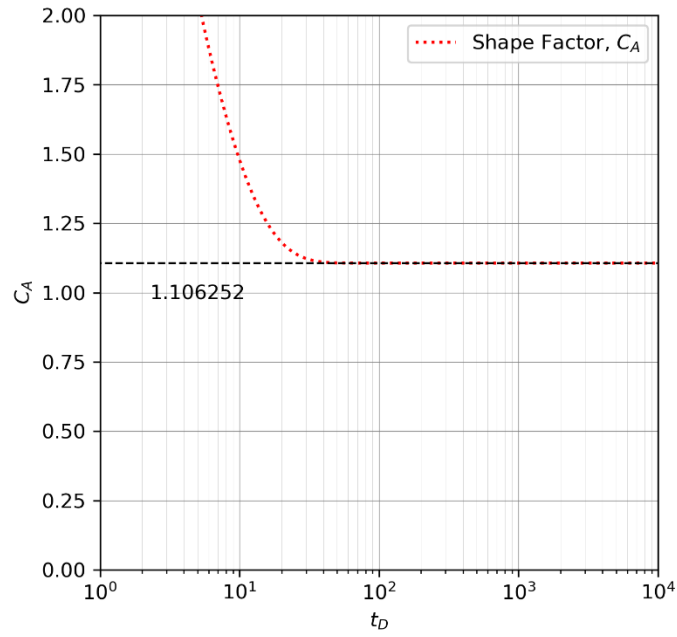
Fig. B.9 – Calculated shape factor, C_A for $2x_f : S_f = 1:2$
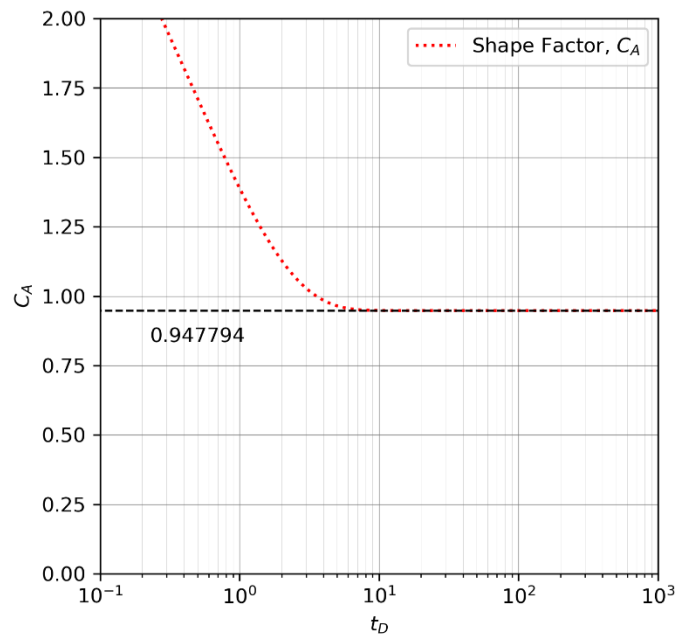
Fig. B.10 – Calculated shape factor, C_A for $2x_f : S_f = 1:1.2$
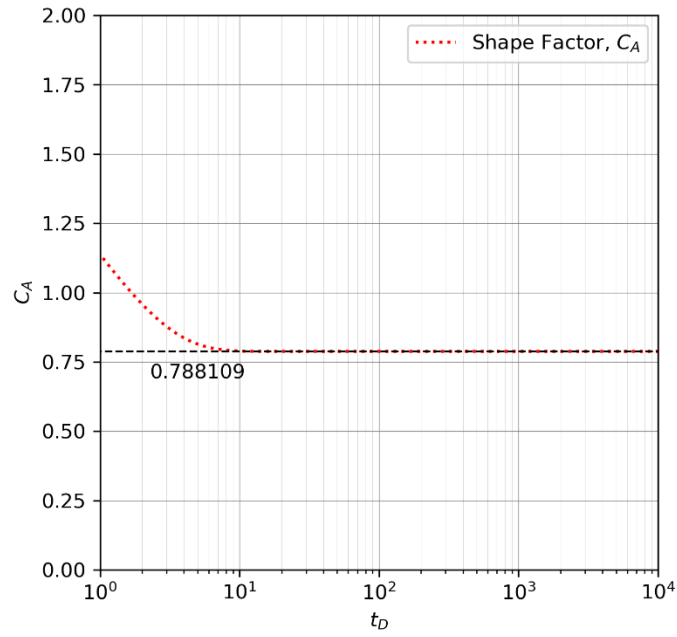
Fig. B.11 – Calculated shape factor, C_A for $2x_f : S_f = 1:1$
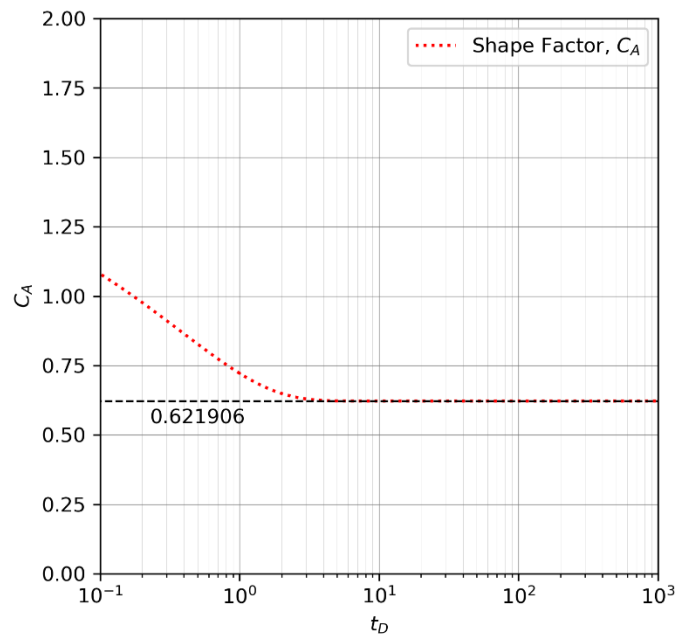
Fig. B.12 – Calculated shape factor, C_A for $2x_f : S_f = 1.25:1$

100
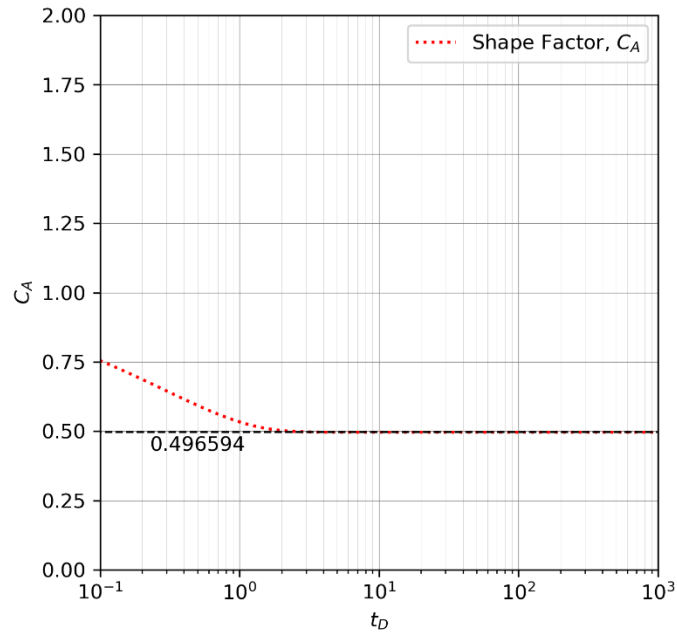
Fig. B.13 – Calculated shape factor, C_A for $2x_f : S_f = 1.5 : 1$
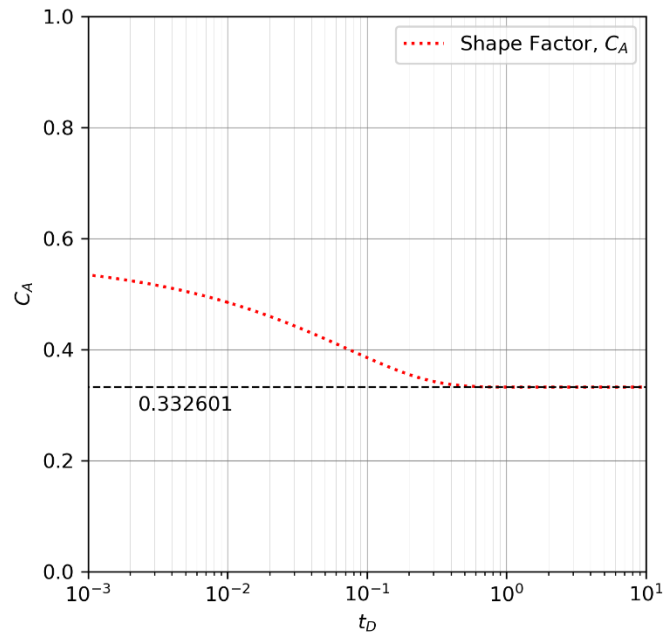
Fig. B.14 – Calculated shape factor, C_A for $2x_f : S_f = 2 : 1$
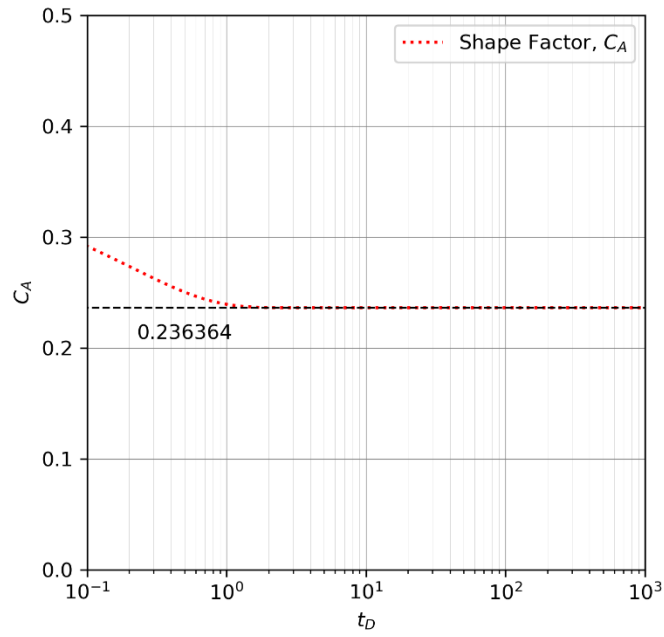
Fig. B.15 – Calculated shape factor, C_A for $2x_f : S_f = 2.5 : 1$
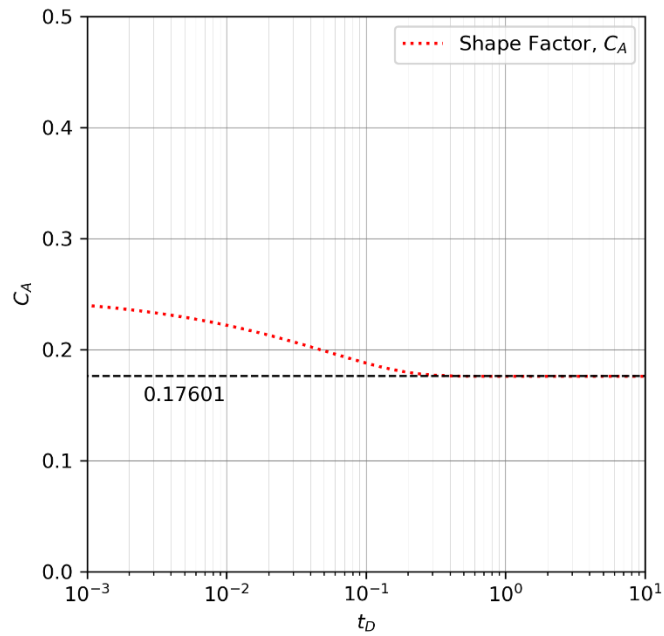
Fig. B.16 – Calculated shape factor, C_A for $2x_f : S_f = 3 : 1$
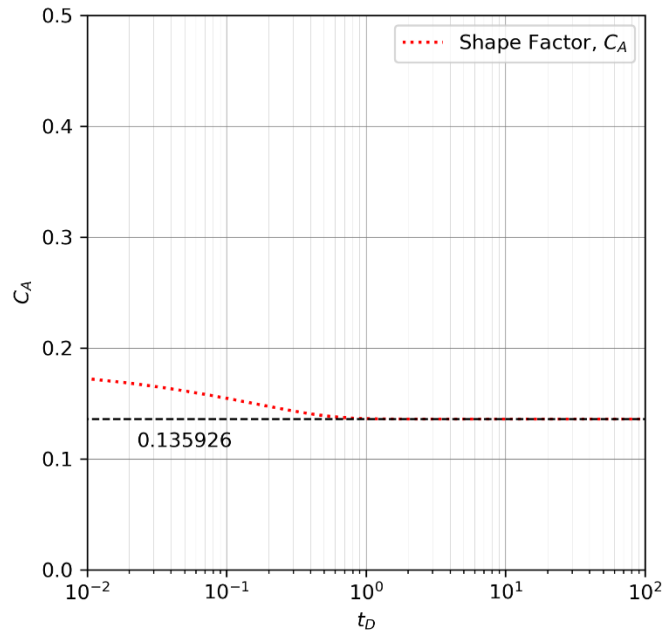
Fig. B.17 – Calculated shape factor, C_A for $2x_f : S_f = 3.5 : 1$
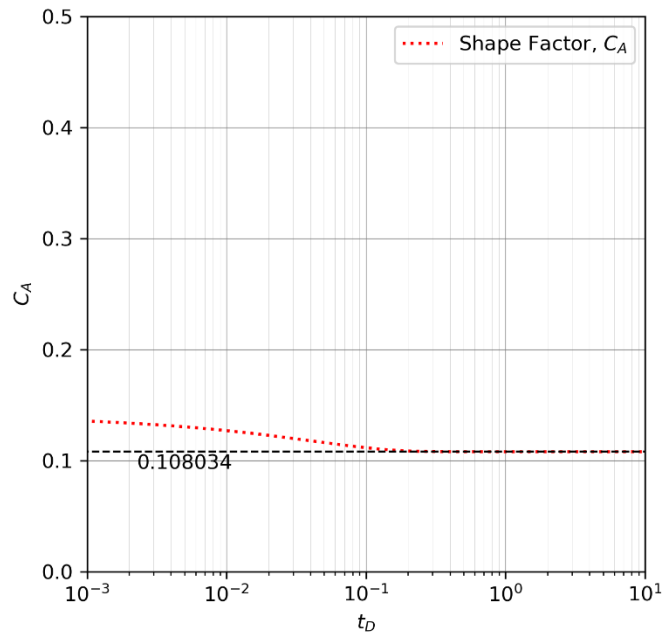
Fig. B.18 – Calculated shape factor, C_A for $2x_f : S_f = 4 : 1$
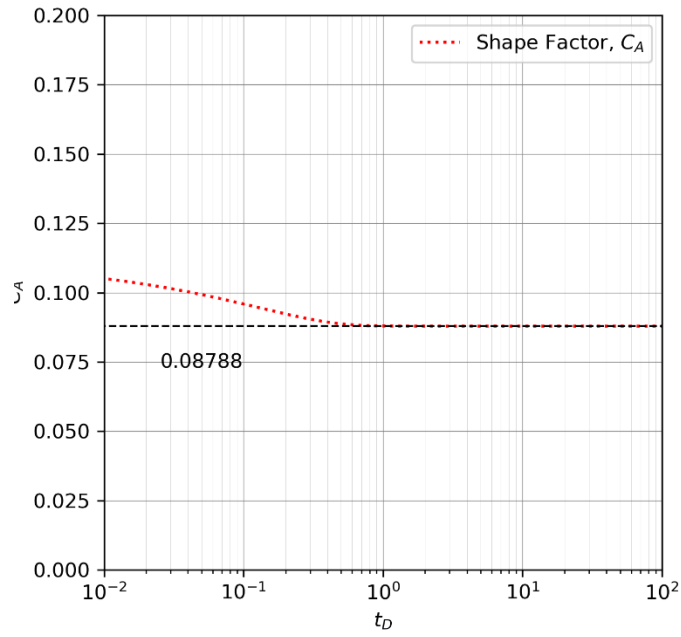
Fig. B.19 – Calculated shape factor, C_A for $2x_f : S_f = 4.5 : 1$
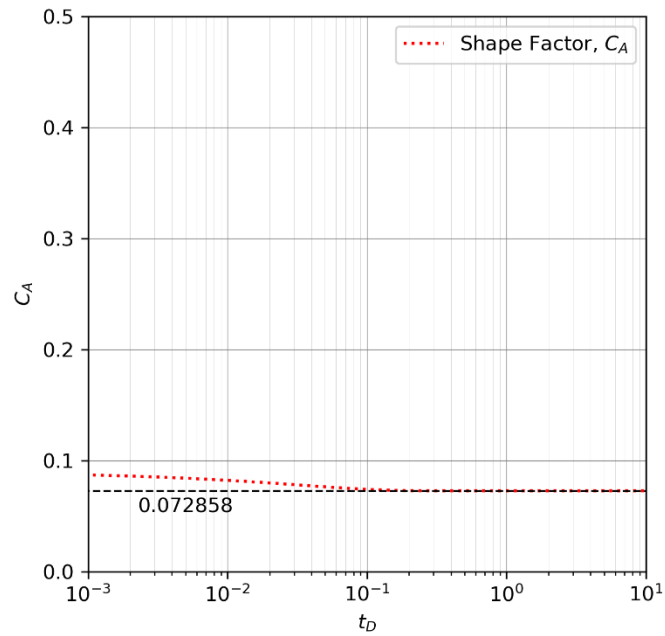
Fig. B.20 – Calculated shape factor, C_A for $2x_f : S_f = 5 : 1$

APPENDIX C PRESSURE DERIVATIVE PLOTS

C-1 Constant Rate Production from Vertical Wells – p_D $vs.$ t_{AD} plots
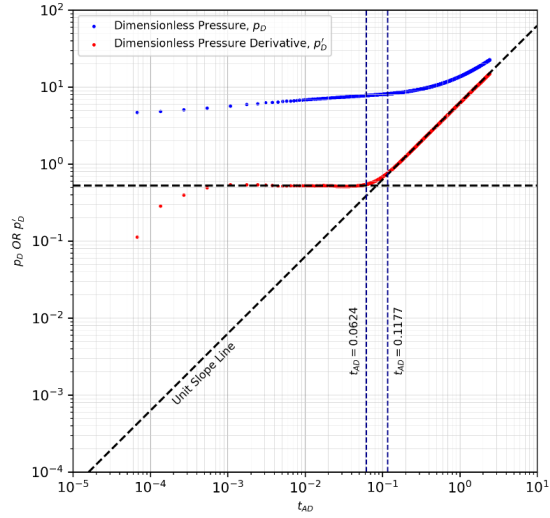

Fig. C.1 – p_D vs. t_{AD} (1x1 CRP case)
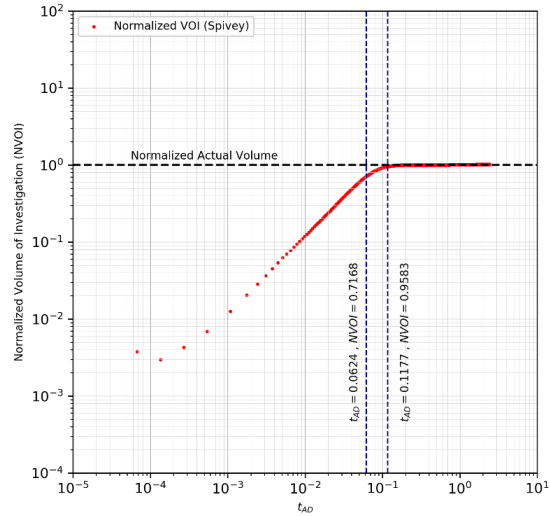
Fig. C.2 – Normalized Volume of Investigation vs. t_{AD} (1x1 CRP case)
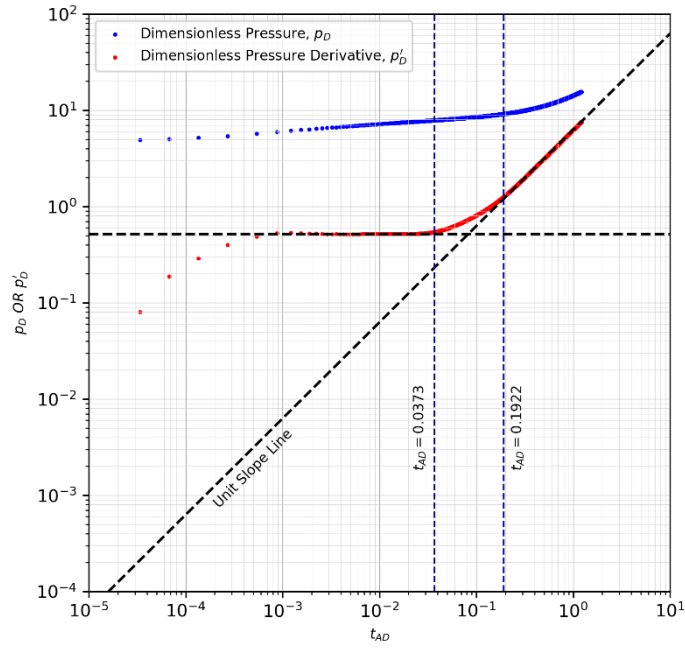
Fig. C.3 – p_D vs. t_{AD} (1x2 CRP case)
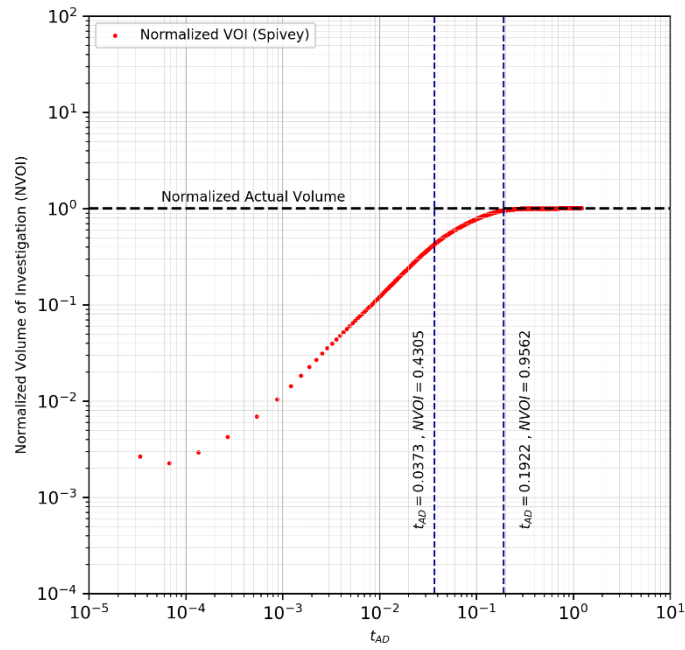
Fig. C.4 – Normalized Volume of Investigation vs. t_{AD} (1x2 CRP case)

106
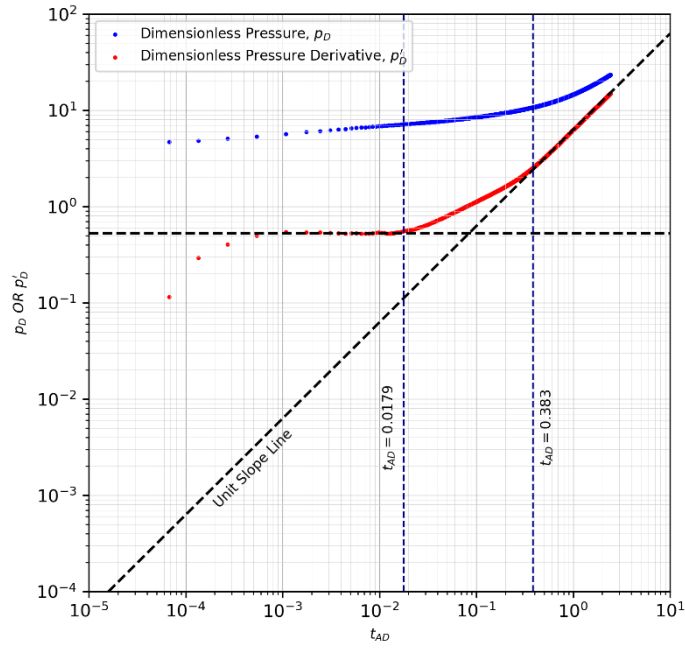
Fig. C.5 – p_D vs. t_{AD} (1x4 CRP case)
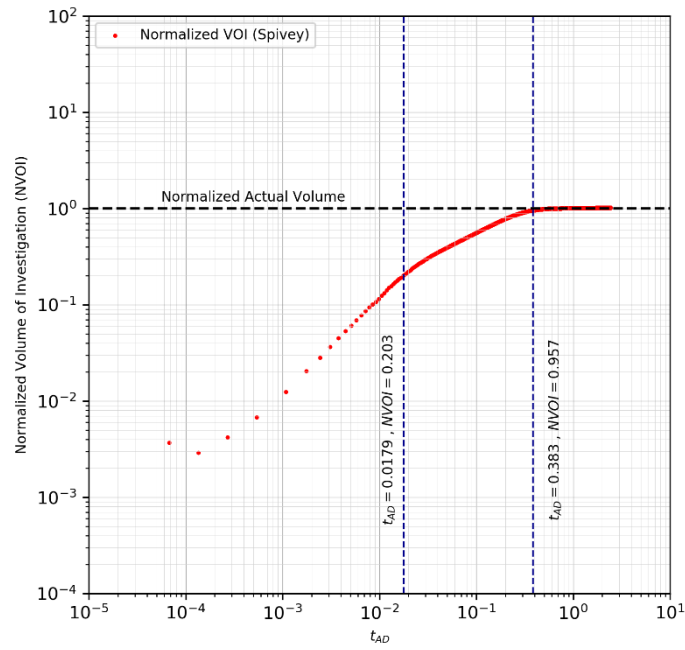
Fig. C.6 – Normalized Volume of Investigation vs. t_{AD} (1x4 CRP case)

107
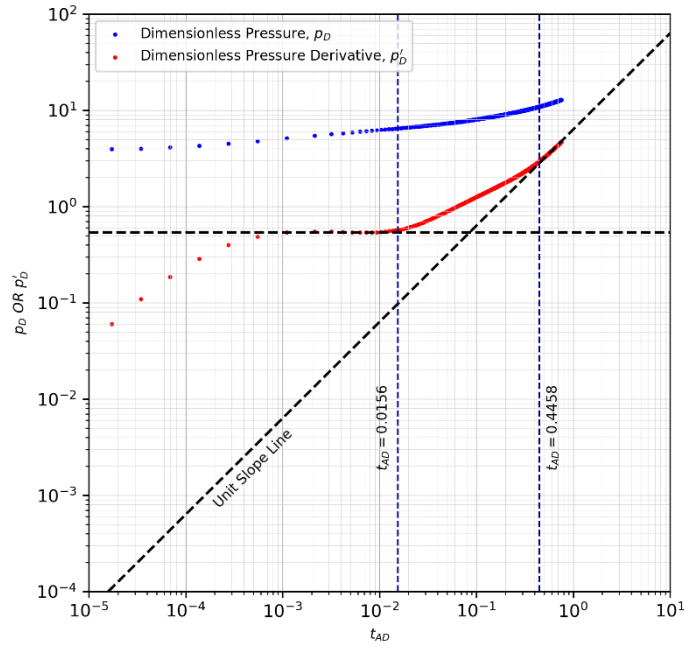
Fig. C.7 – p_D vs. t_{AD} (1x5 CRP case)
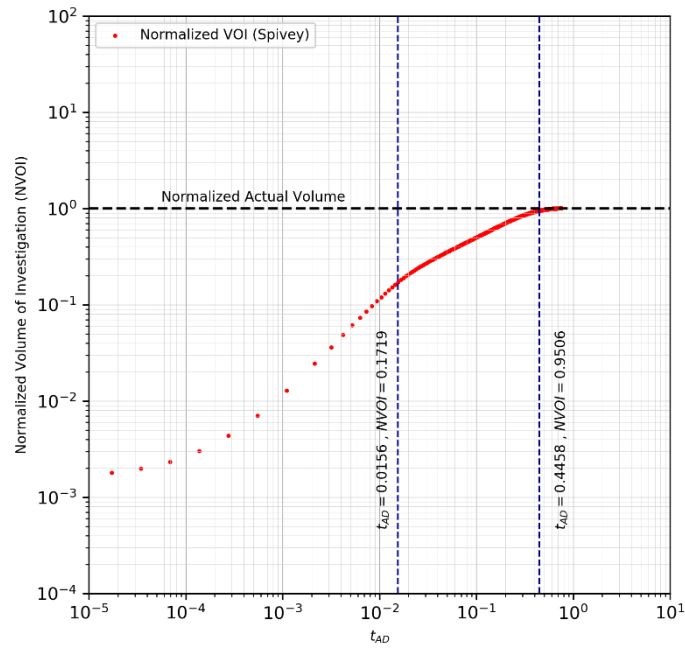
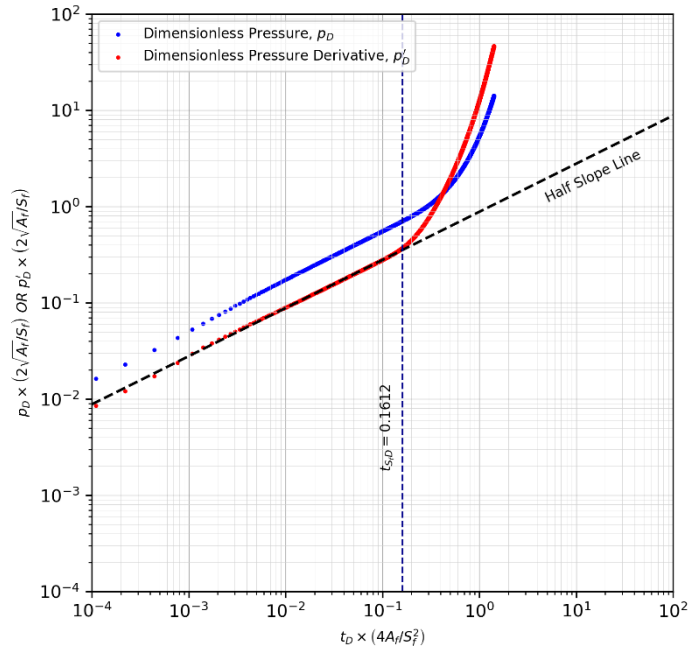Fig. C.8 – Normalized Volume of Investigation vs. t_{AD} (1x5 CRP case)

C-2 Constant Pressure Production from Vertical Wells – p_D $vs.$ t_{AD} plots
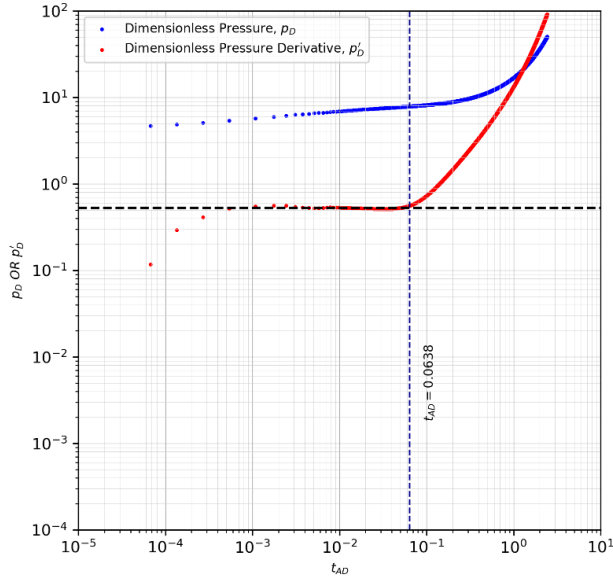
Fig. C.9 – $(1/q_D)$ vs. t_{AD} (1x1 CPP case)
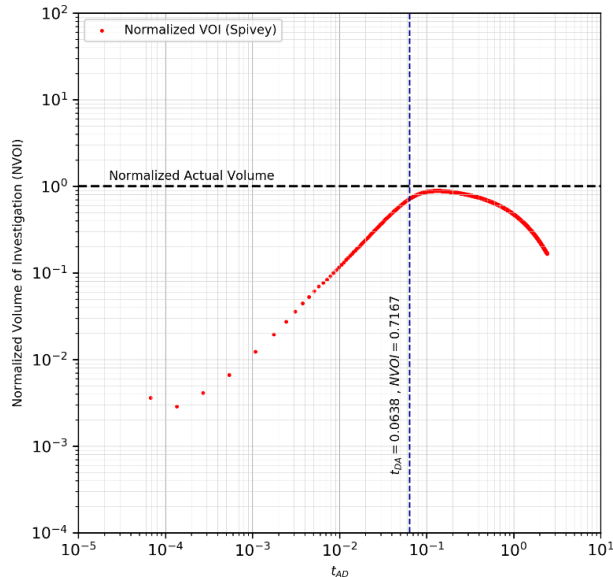
Fig. C.10 – Normalized Volume of Investigation vs. t_{AD} (1x1 CPP case)
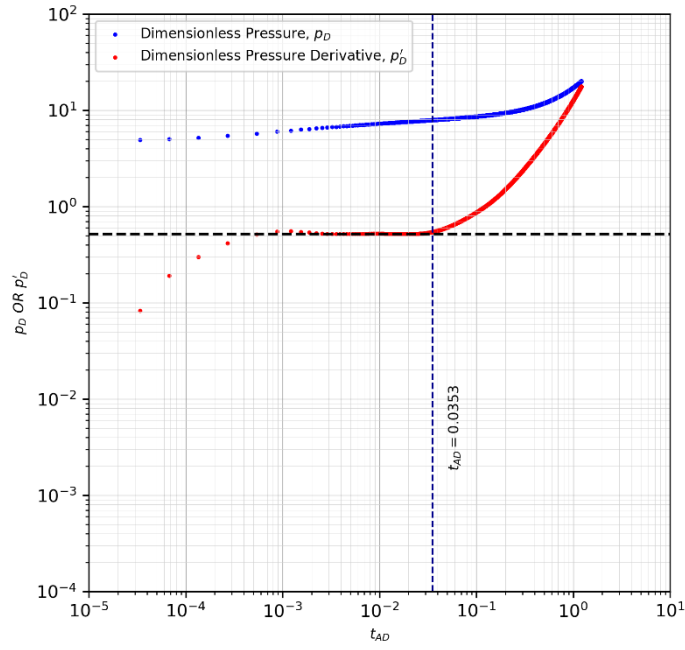
Fig. C.11 – p_D vs. t_{AD} (1x2 CPP case)
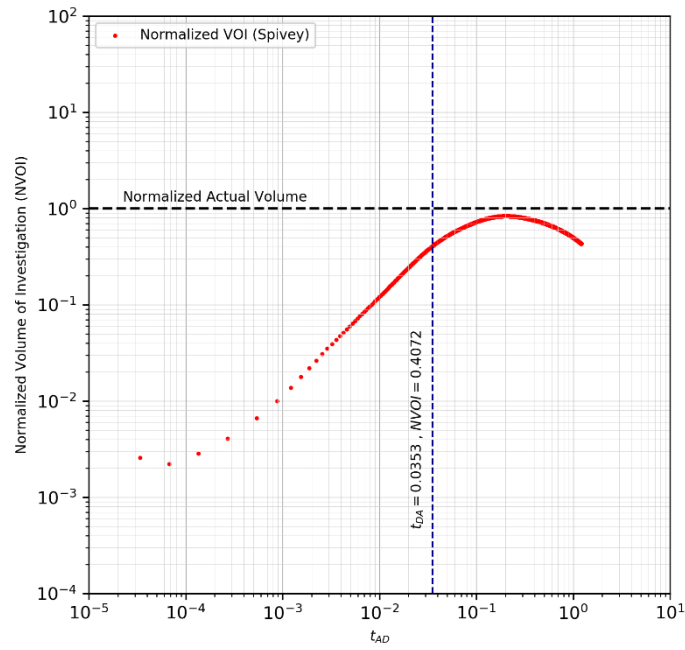
Fig. C.12 – Normalized Volume of Investigation vs. t_{AD} (1x2 CPP case)

110
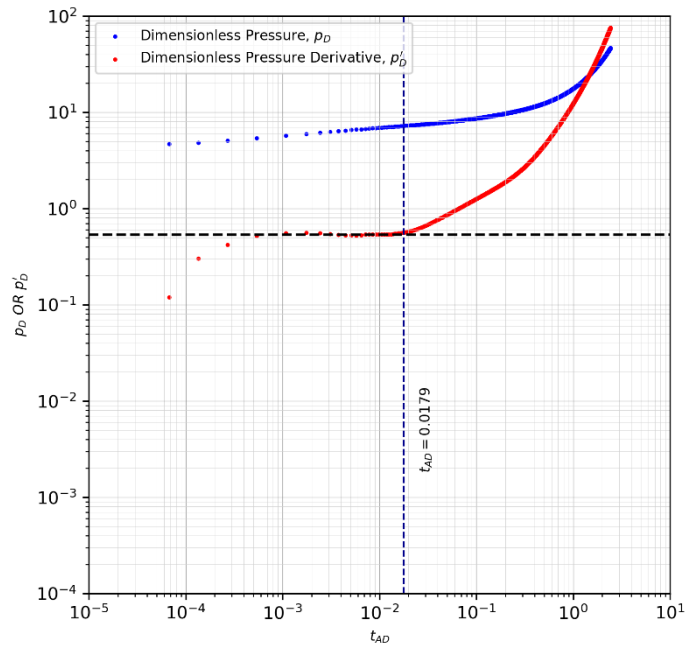
Fig. C.13-p_D vs. t_{AD} (1x4 CPP case)
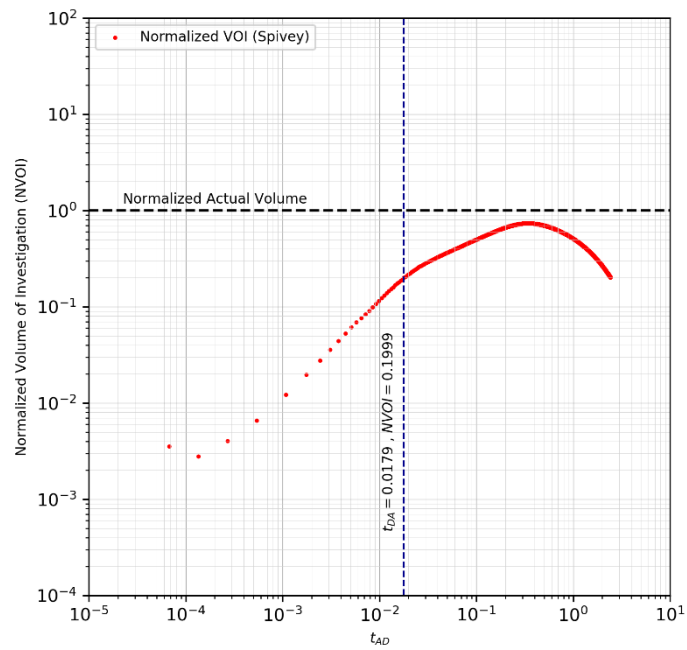
Fig. C.14 – Normalized Volume of Investigation vs. t_{AD} (1x4 CPP case)
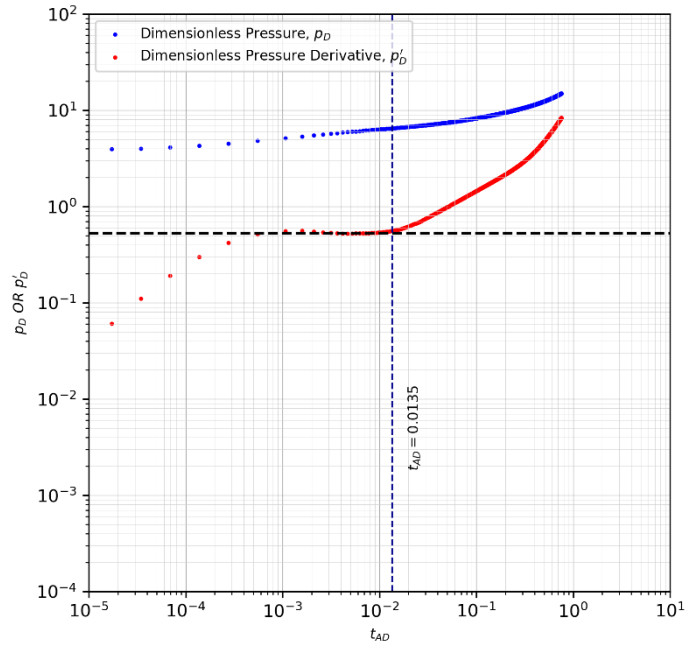
Fig. C.15 – p_D vs. t_{AD} (1x5 CPP case)
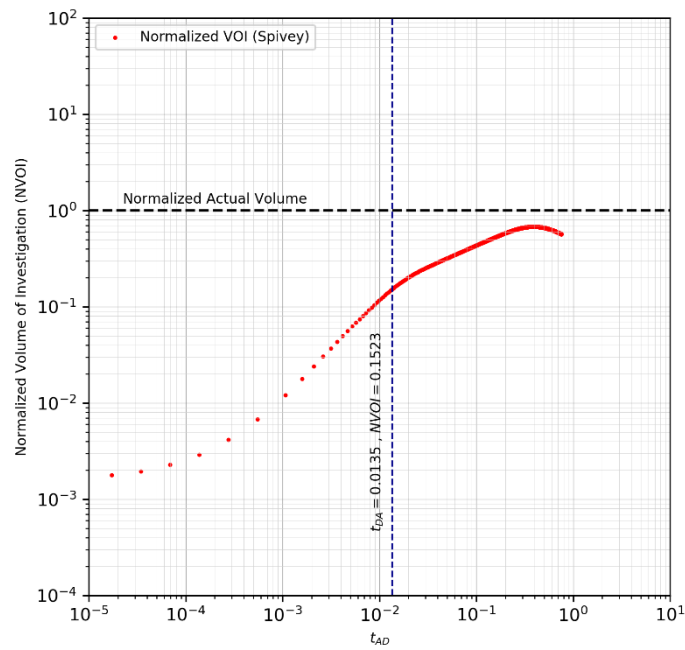
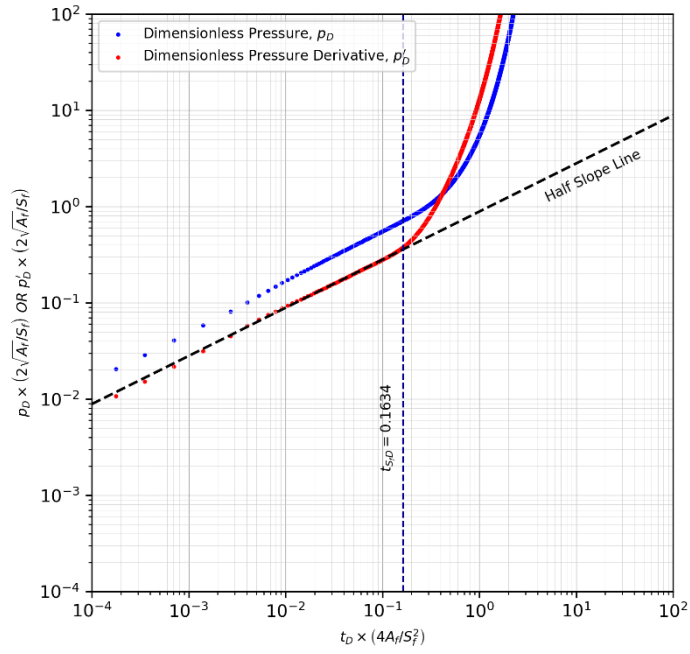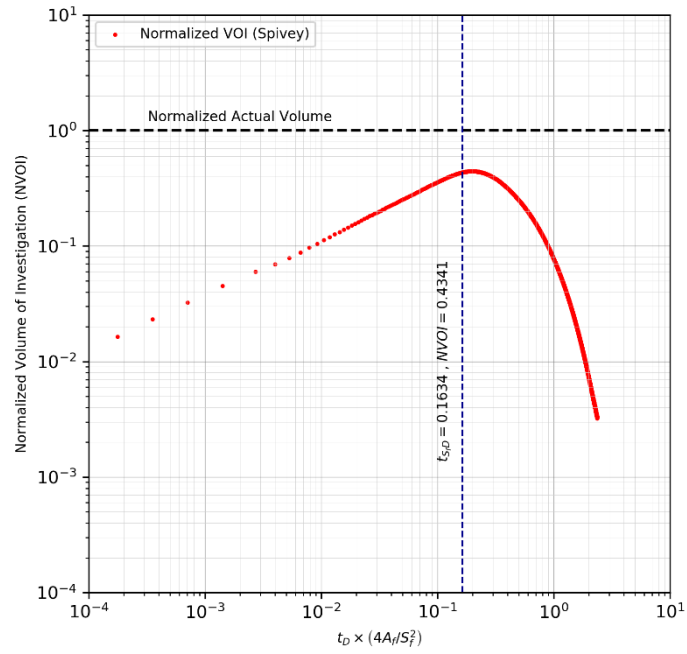Fig. C.16 – Normalized Volume of Investigation vs. t_{AD} (1x5 CPP case)

C-3 Constant Pressure Production from Vertical Wells – p_D $vs.$ $(MBT)_{AD}$ plots
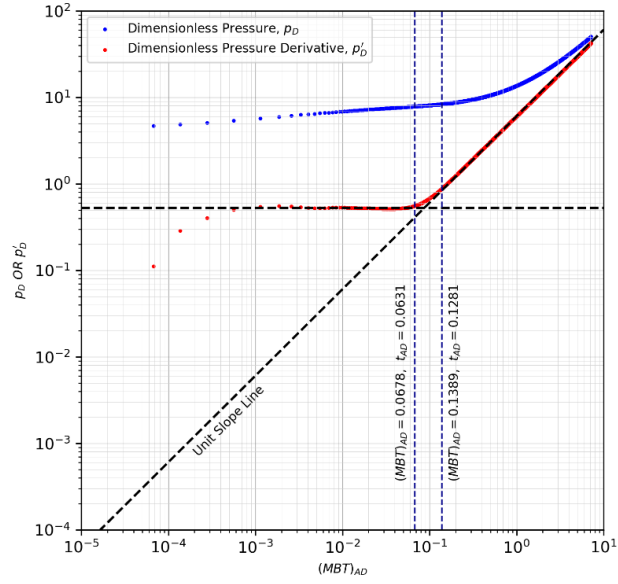
Fig. C.17 – p_D vs. $(MBT)_{AD}$ (1x1 CPP case)
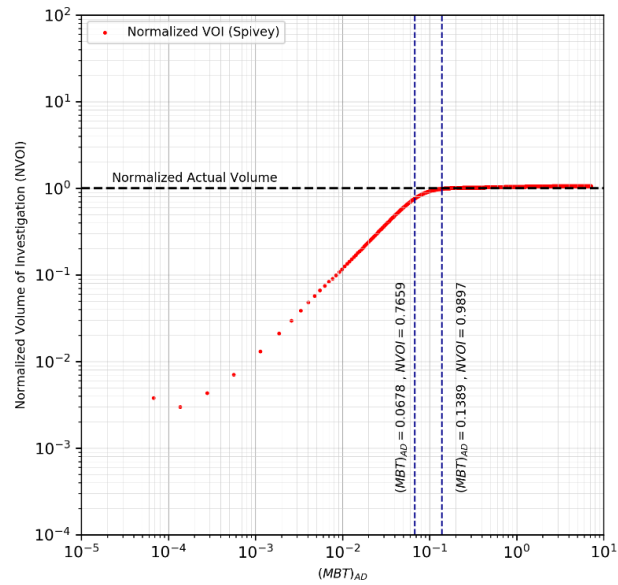
Fig. C.18 – Normalized Volume of Investigation vs. $(MBT)_{AD}$ (1x1 CPP case)
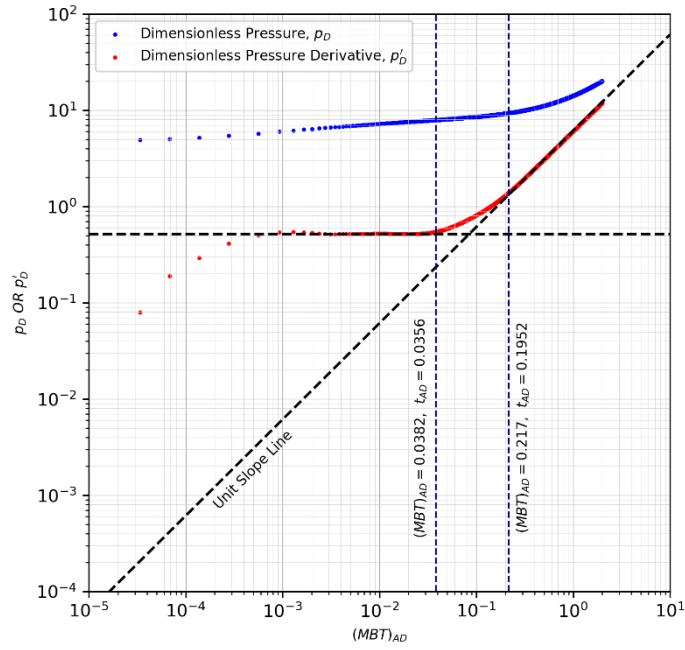
Fig. C.19 – p_D vs. $(MBT)_{AD}$ (1x2 CPP case)
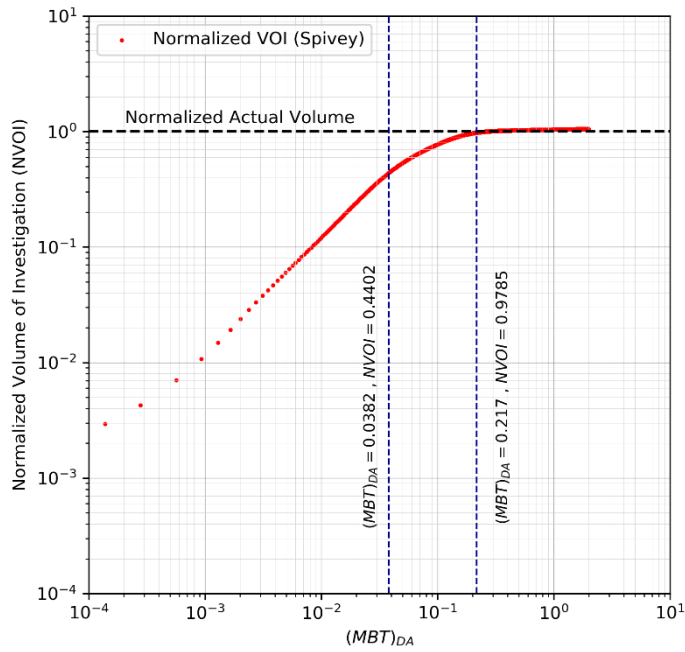
Fig. C.20 – Normalized Volume of Investigation vs. $(MBT)_{AD}$ (1x2 CPP case)

114
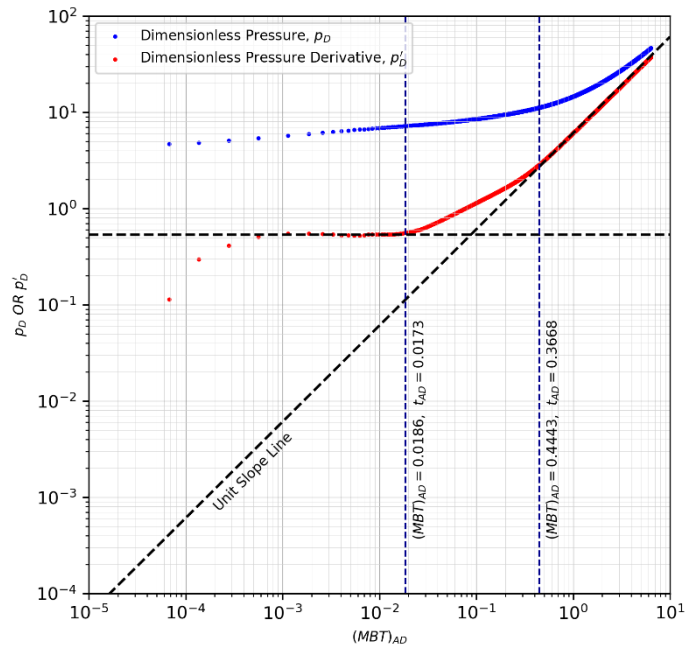
Fig. C.21 – p_D vs. $(MBT)_{AD}$ (1x4 CPP case)
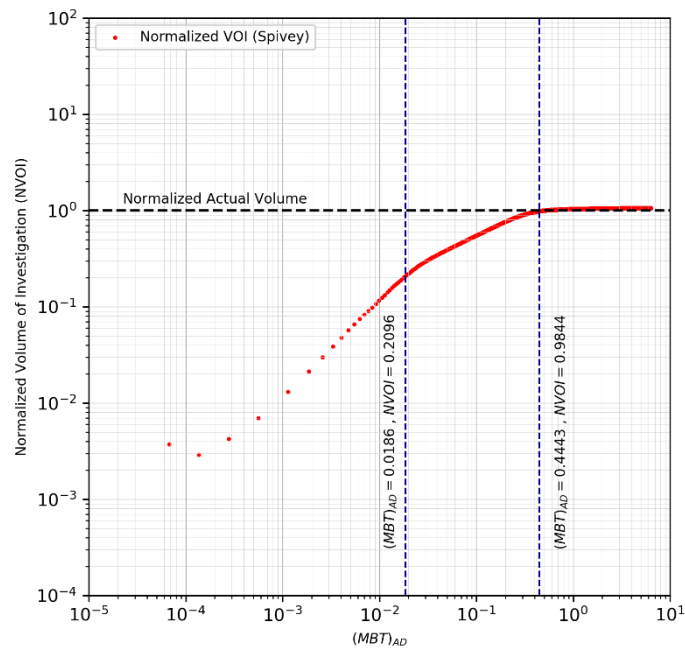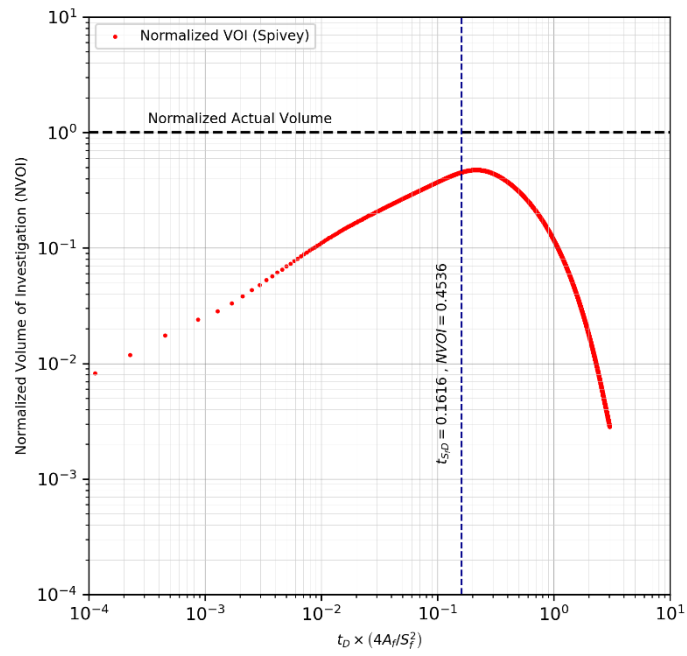

Fig. C.22 – Normalized Volume of Investigation vs. $(MBT)_{AD}$ (1x4 CPP case)
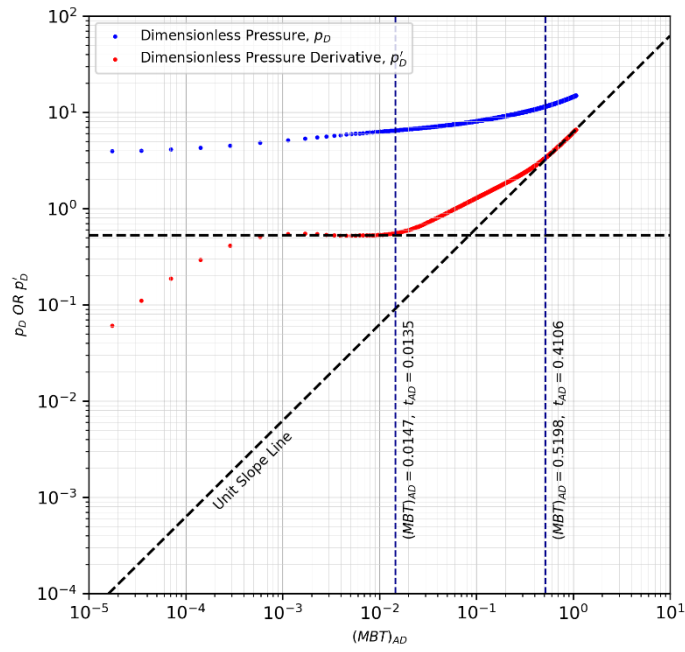
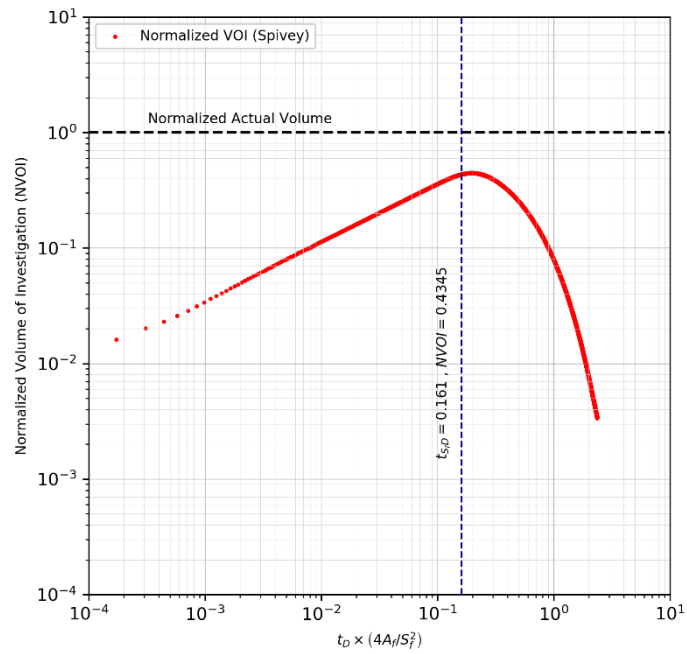Fig. C.23 – p_D vs. $(MBT)_{AD}$ (1x5 CPP case)
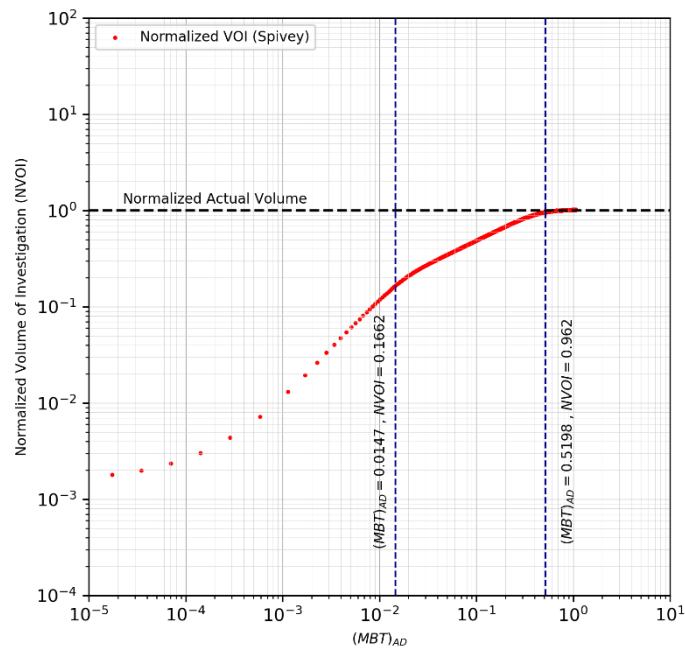
Fig. C.24 – Normalized Volume of Investigation vs. $(MBT)_{AD}$ (1x5 CPP case)

C-4 Constant Rate Production from Horizontal Wells – p_D $vs.$ t_{S_fD} plots
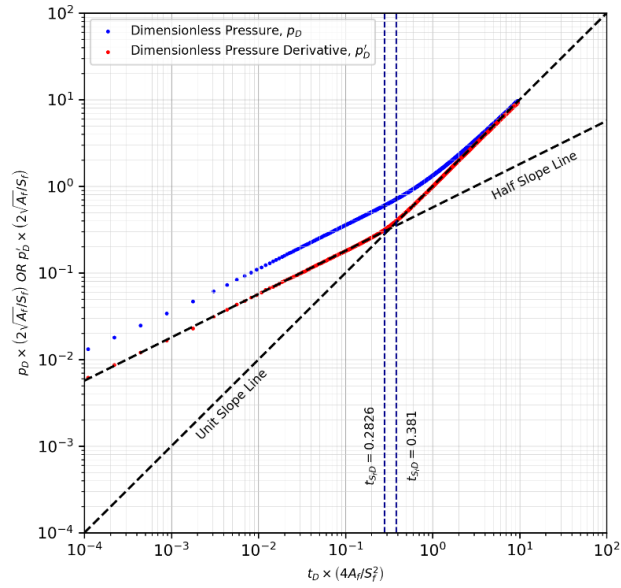
Fig. C.25 – p_D vs. t_{S_fD} (1x2 CRP case)
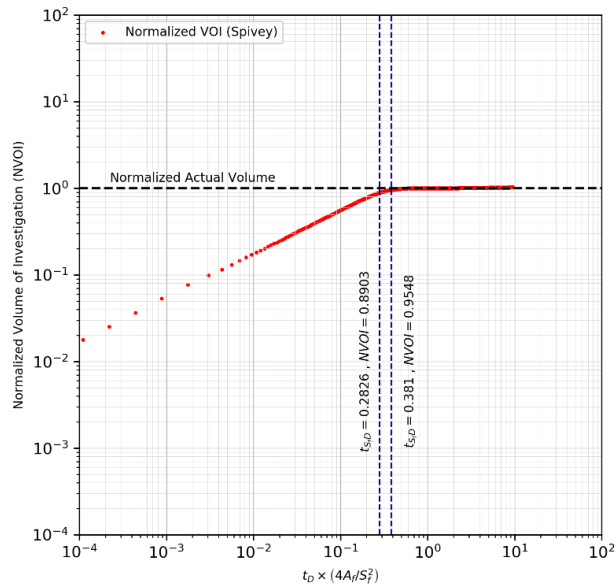
Fig. C.26 – Normalized Volume of Investigation vs. t_{S_fD} (1x2 CRP case)
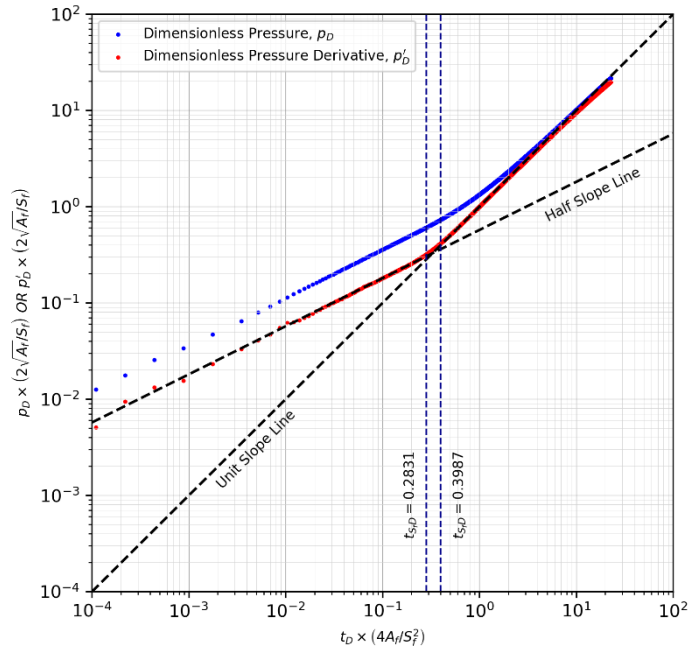
Fig. C.27 – p_D vs. $t_{S_f D}$ (1x1 CRP case)
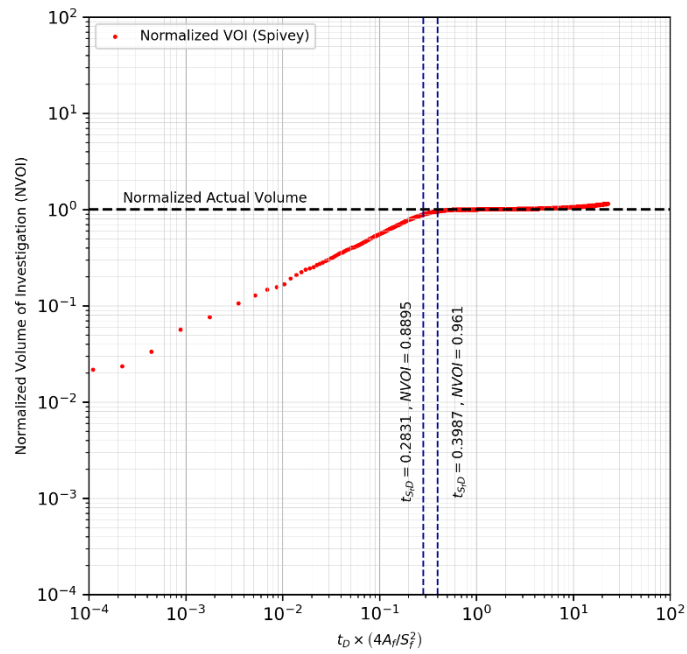
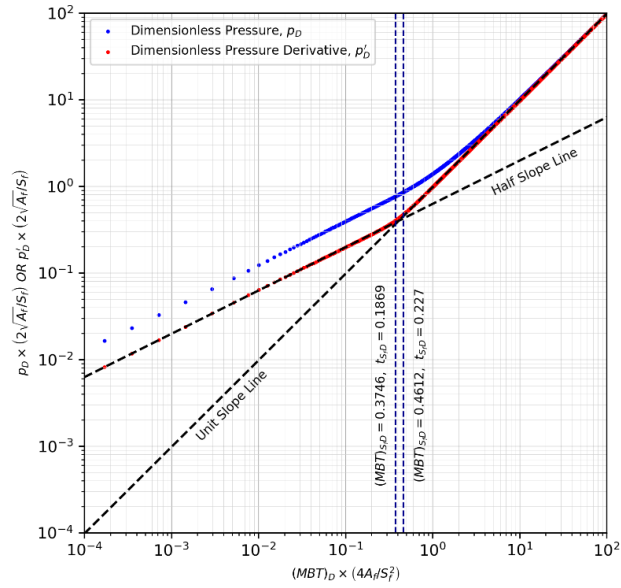Fig. C.28 – Normalized Volume of Investigation vs. $t_{S_f D}$ (1x1 CRP case)

118
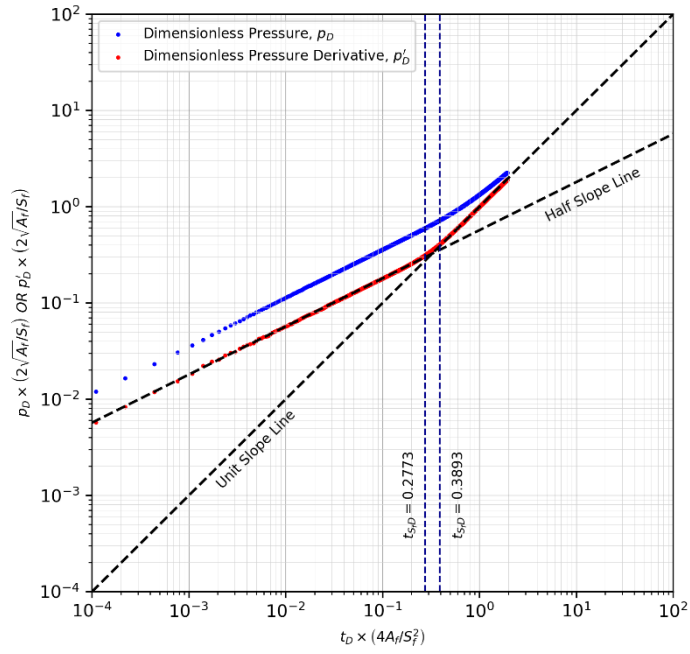
Fig. C.29 – p_D vs. $t_{S_f D}$ (2x1 CRP case)
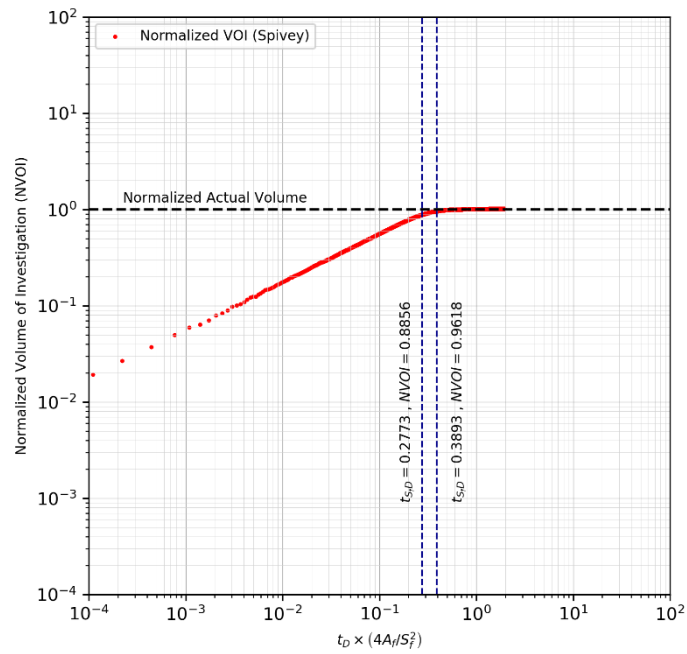
Fig. C.30 – Normalized Volume of Investigation vs. $t_{S_f D}$ (2x1 CRP case)
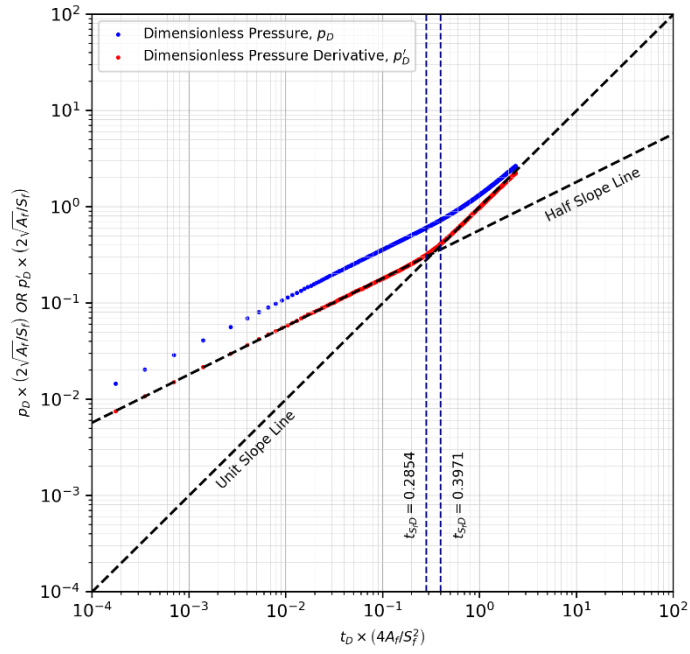
Fig. C.31 – p_D vs. t_{S_fD} (4x1 CRP case)
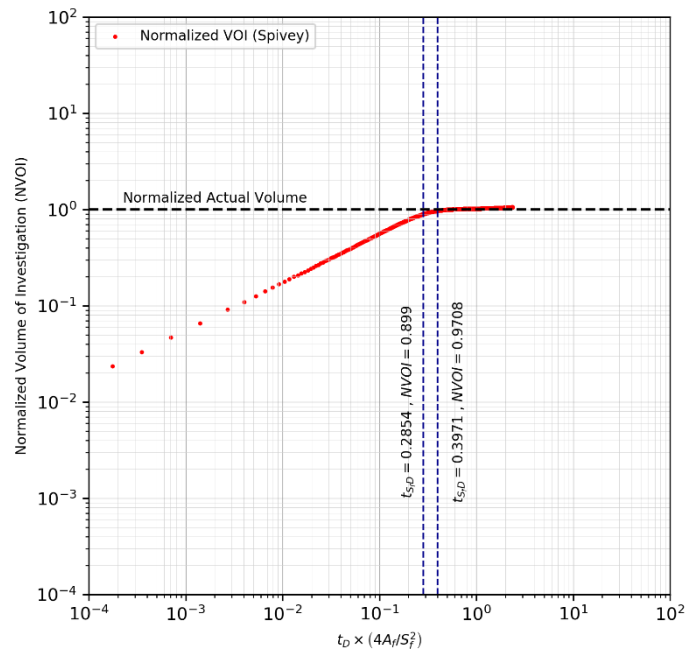
Fig. C.32 – Normalized Volume of Investigation vs. t_{S_fD} (4x1 CRP case)
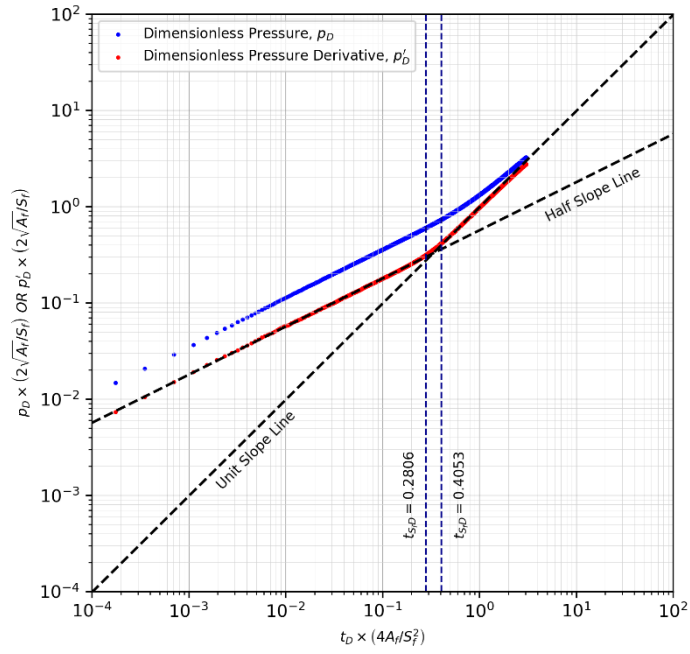
Fig. C.33 – p_D vs. t_{S_fD} (5x1 CRP case)
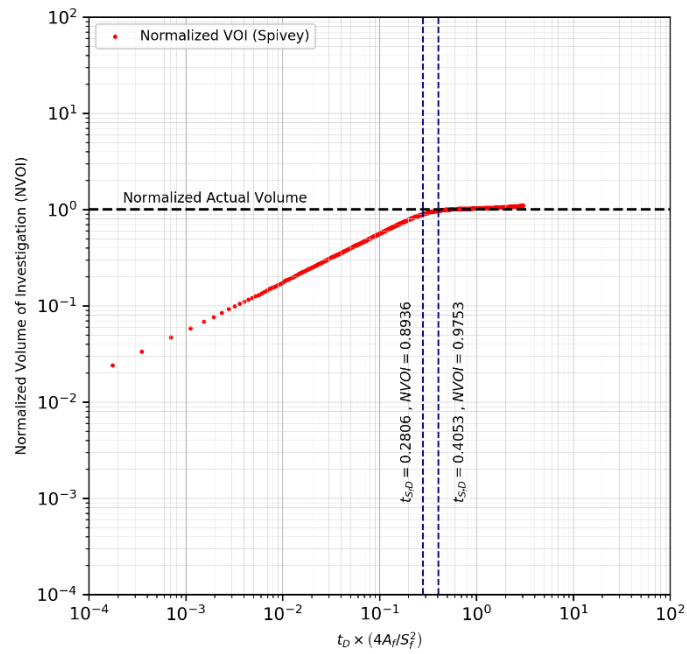
Fig. C.34 – Normalized Volume of Investigation vs. t_{S_fD} (5x1 CRP case)

121
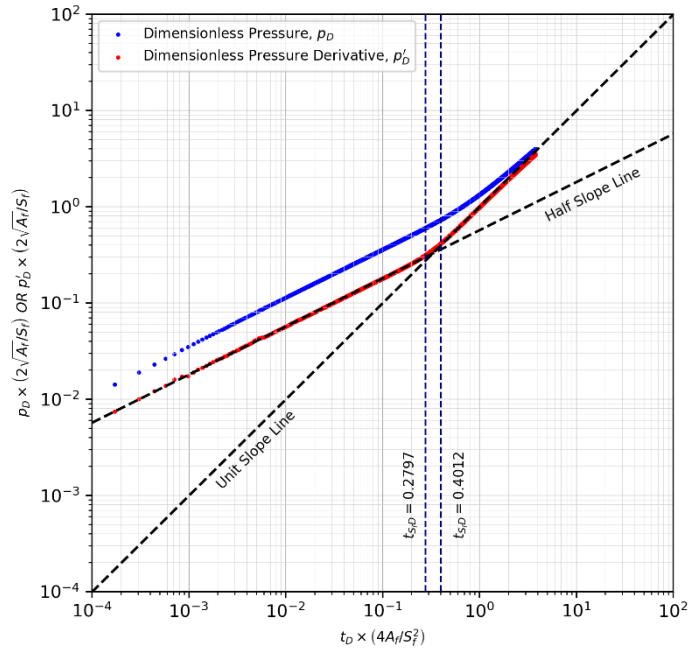
Fig. C.35 – p_D vs. t_{S_fD} (8x1 CRP case)
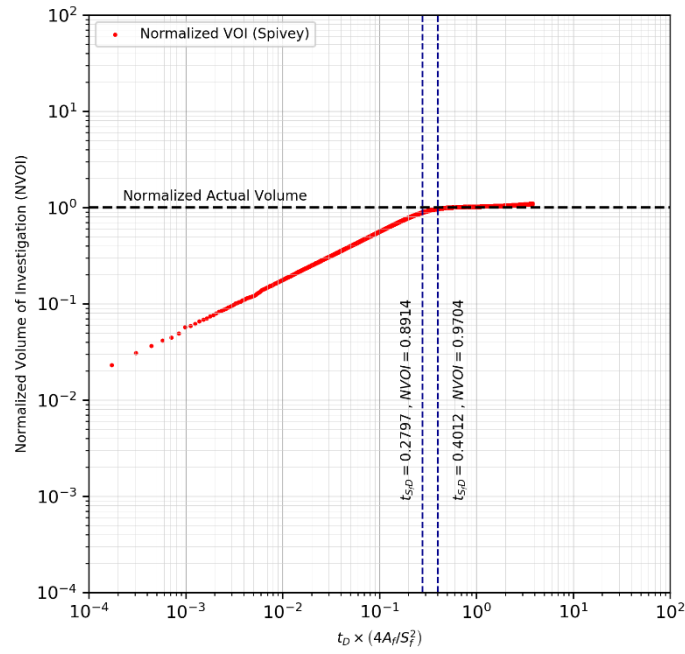
Fig. C.36 – Normalized Volume of Investigation vs. t_{S_fD} (8x1 CRP case)

C-5 Constant Pressure Production from Horizontal Wells – p_D $vs.$ t_{S_fD} plots
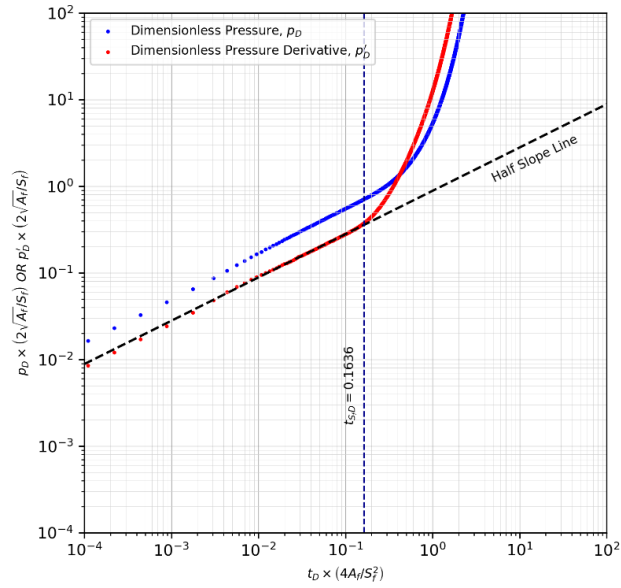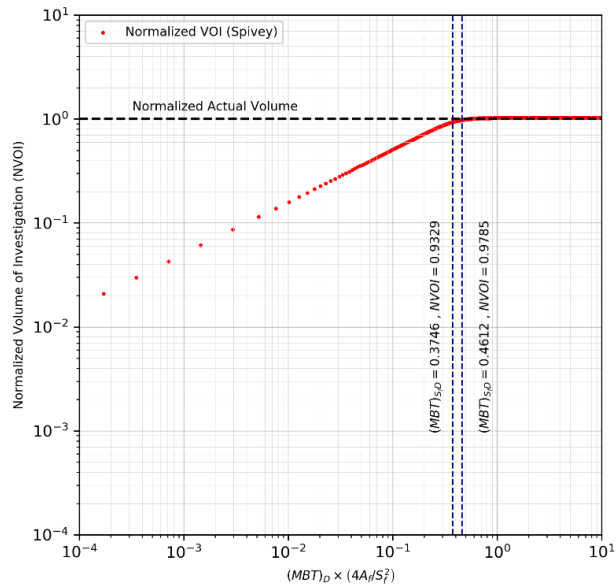

Fig. C.37 – p_D vs. t_{S_fD} (1x2 CPP case)
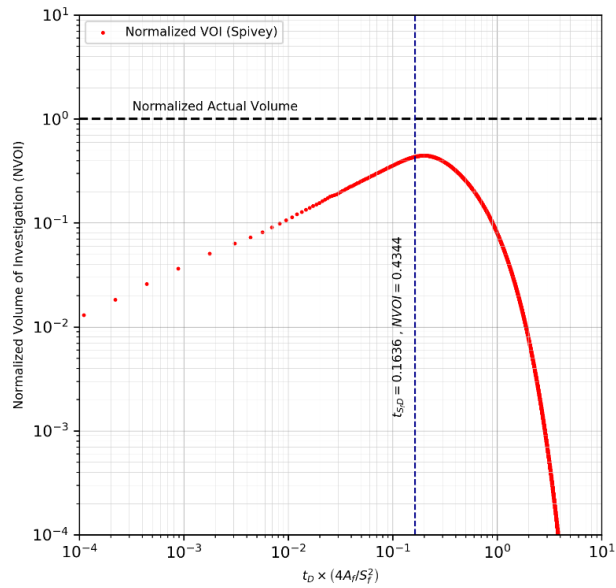
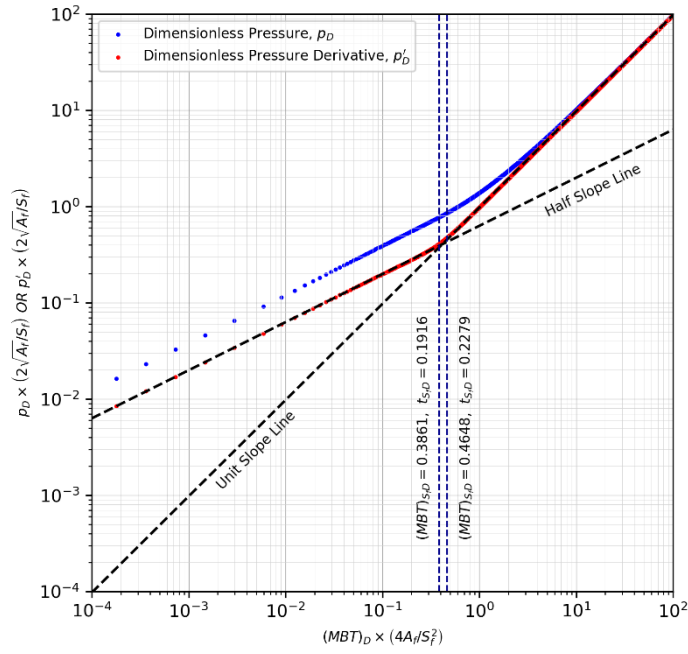Fig. C.38 – Normalized Volume of Investigation vs. t_{S_fD} (1x2 CPP case)
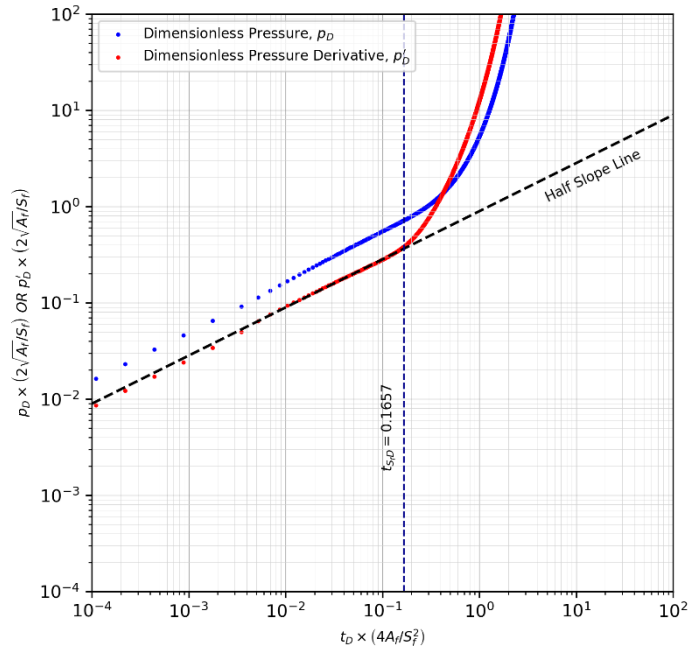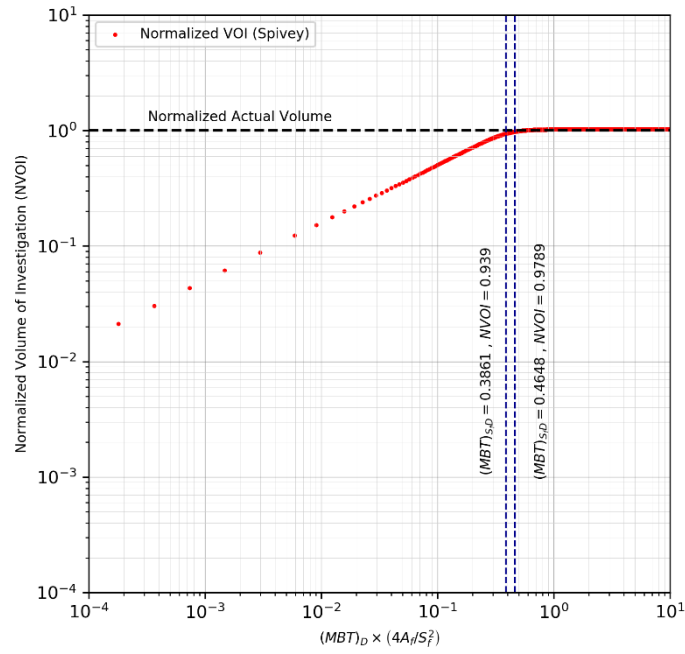
Fig. C.39 – p_D vs. t_{S_fD} (1x1 CPP case)
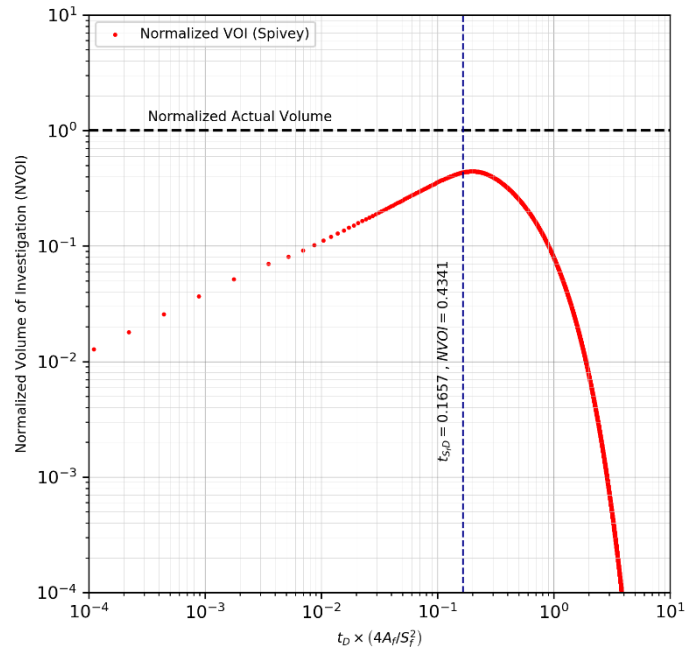
Fig. C.40 – Normalized Volume of Investigation vs. t_{S_fD} (1x1 CPP case)

Fig. C.41 – p_D vs. t_{S_fD} (2x1 CPP case)
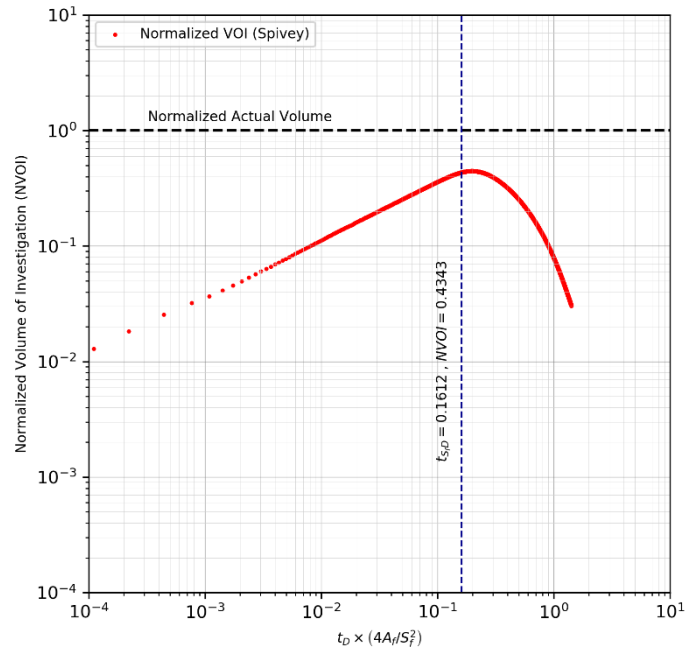
Fig. C.42 – Normalized Volume of Investigation vs. t_{S_fD} (2x1 CPP case)

125
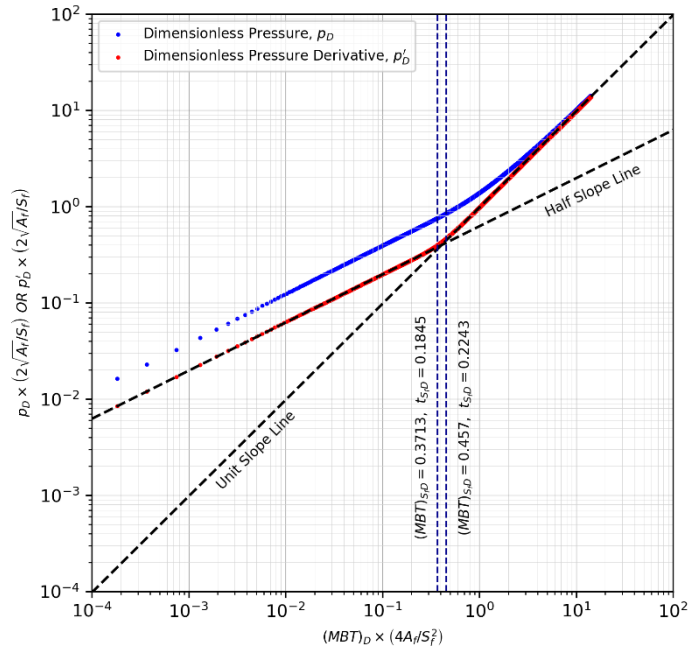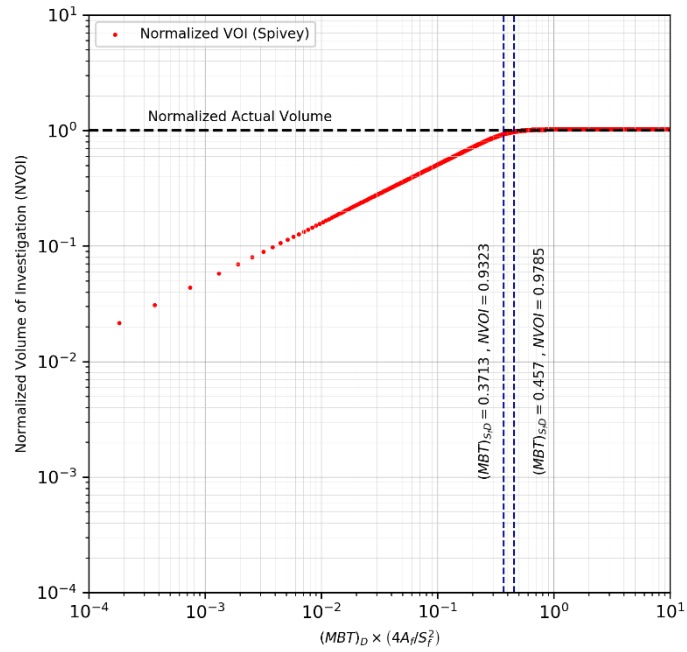
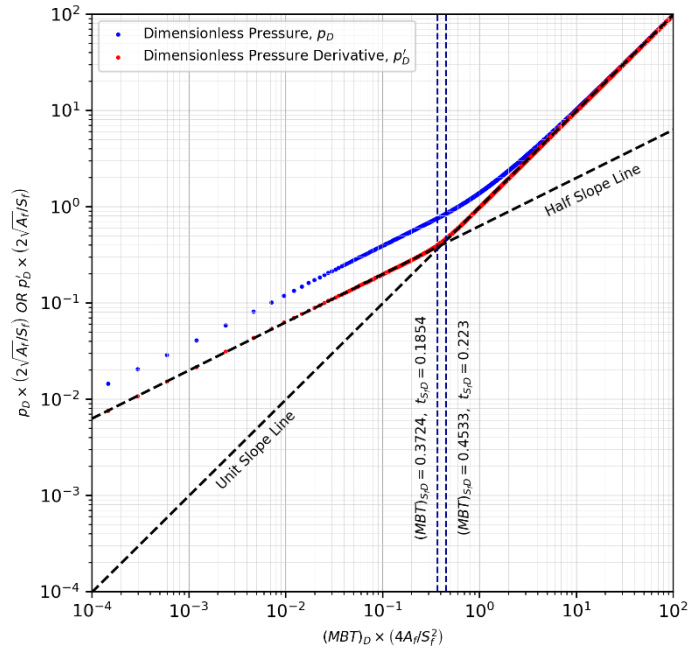Fig. C.43 – p_D vs. t_{S_fD} (4x1 CPP case)

Fig. C.44 – Normalized Volume of Investigation vs. t_{S_fD} (4x1 CPP case)
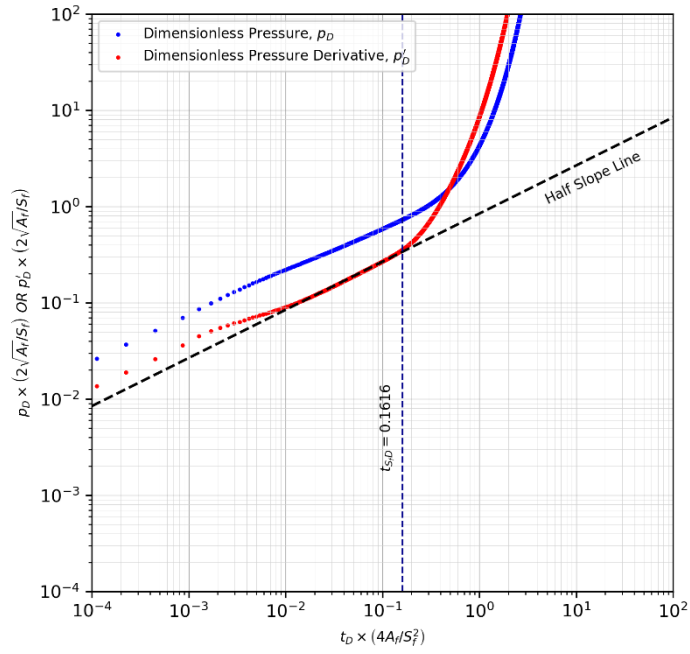
Fig. C.45 – p_D vs. t_{S_fD} (5x1 CPP case)

Fig. C.46 – Normalized Volume of Investigation vs. t_{S_fD} (5x1 CPP case)
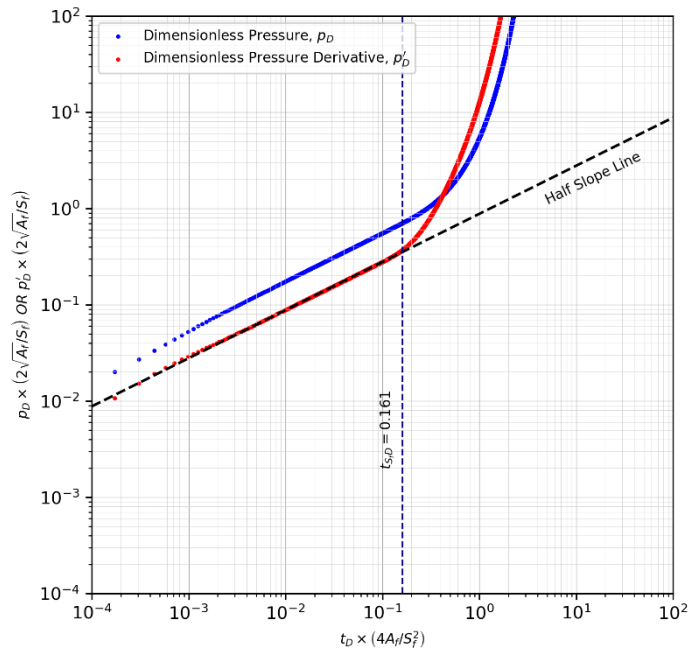
Fig. C.47 – p_D vs. $t_{S_f D}$ (8x1 CPP case)

Fig. C.48 – Normalized Volume of Investigation vs. $t_{S_f D}$ (8x1 CPP case)

C-6 Constant Pressure Production from Horizontal Wells – p_D $vs.$ $(MBT)_{S_fD}$ plots

Fig. C.49 – p_D vs. $(MBT)_{S_fD}$ (1x2 CPP case)

Fig. C.50 – Normalized Volume of Investigation vs. $(MBT)_{S_fD}$ (1x2 CPP case)

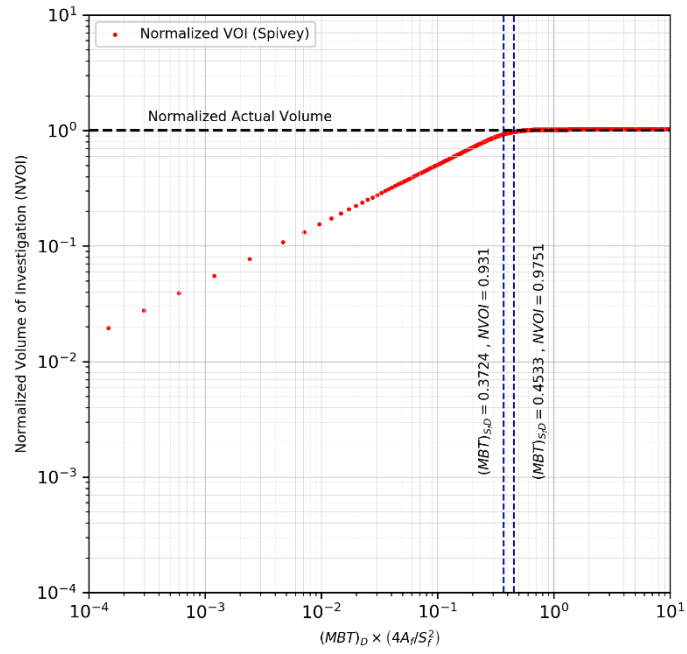Fig. C.51 – p_D vs. $(MBT)_{S_fD}$ (1x1 CPP case)

Fig. C.52 – Normalized Volume of Investigation vs. $(MBT)_{S_fD}$ (1x1 CPP case)

Fig. C.53 – p_D vs. $(MBT)_{S_fD}$ (2x1 CPP case)

Fig. C.54 – Normalized Volume of Investigation vs. $(MBT)_{S_fD}$ (2x1 CPP case)

131

Fig. C.55 – p_D vs. $(MBT)_{S_fD}$ (4x1 CPP case)

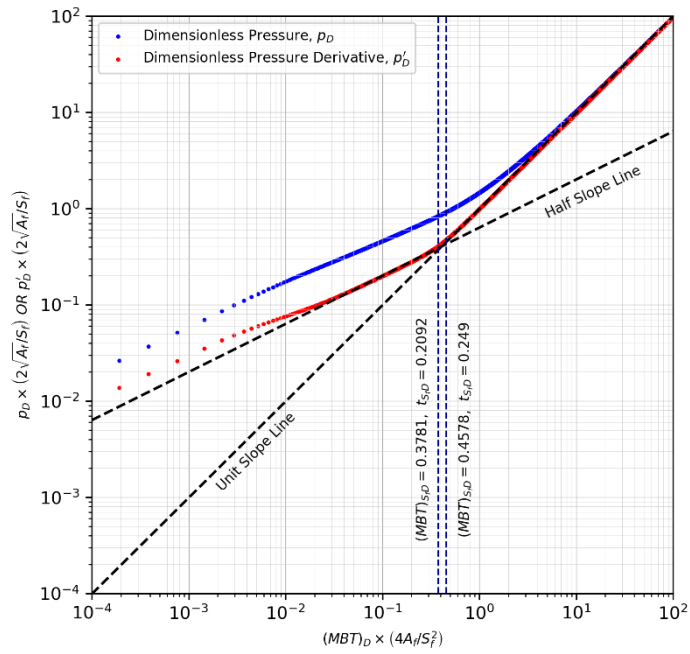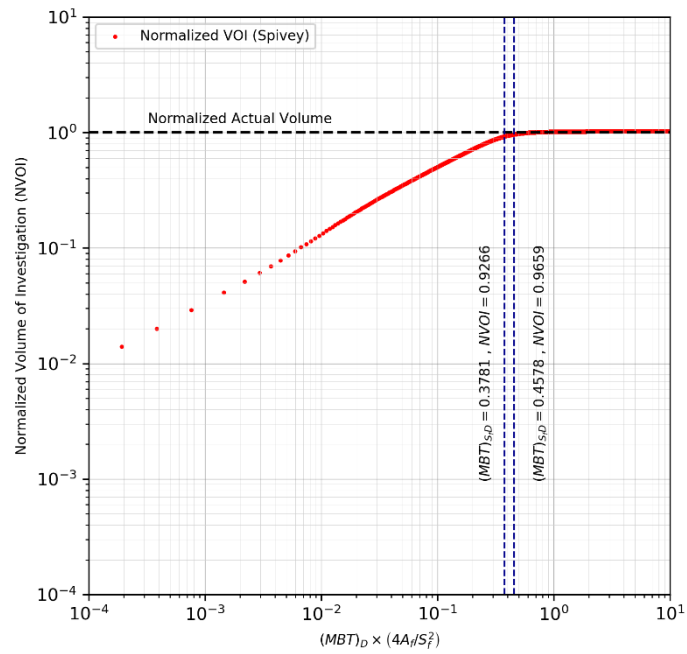Fig. C.56 – Normalized Volume of Investigation vs. $(MBT)_{S_fD}$ (4x1 CPP case)

Fig. C.57 – p_D vs. $(MBT)_{S_fD}$ (5x1 CPP case)

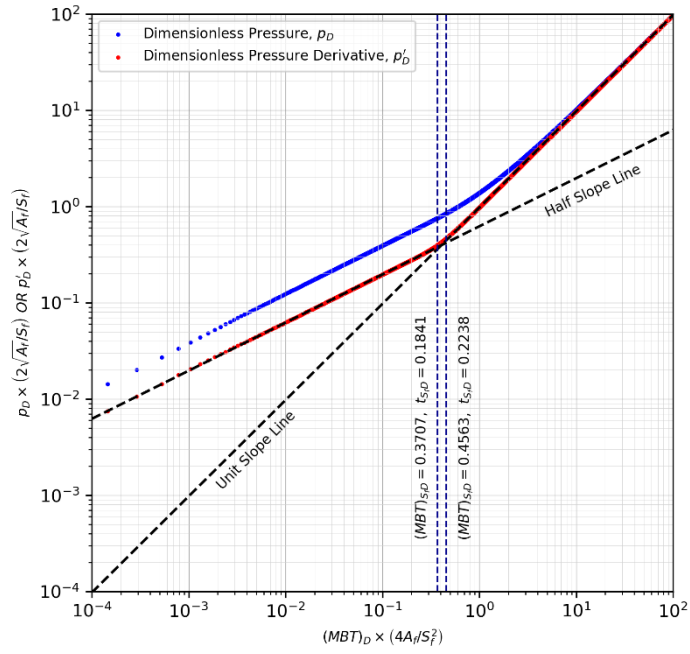Fig. C.58 – Normalized Volume of Investigation vs. $(MBT)_{S_fD}$ (5x1 CPP case)

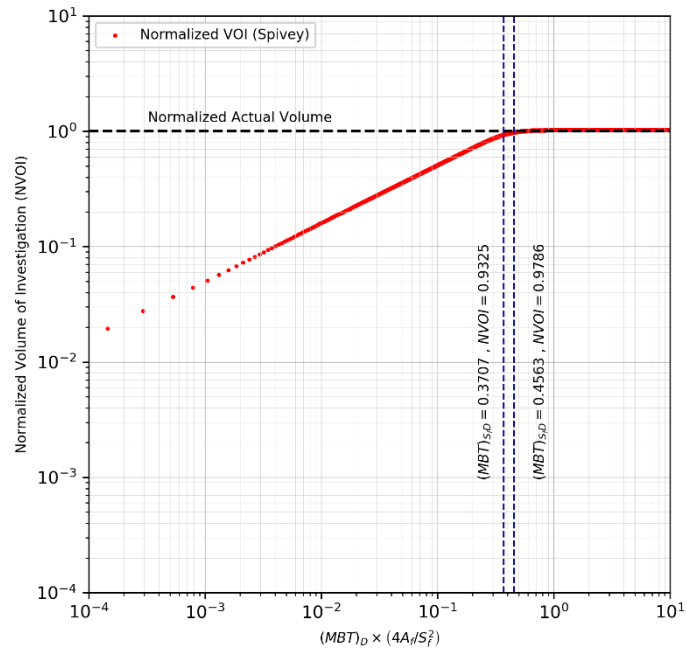Fig. C.59 – p_D vs. $(MBT)_{S_fD}$ (8x1 CPP case)

Fig. C.60 – Normalized Volume of Investigation vs. $(MBT)_{S_fD}$ (8x1 CPP case)